To the Graduate Council:

I am submitting herewith a thesis written by Balaji Ramamurthy entitled "Design of a Catalyst System with Periodic Flow Reversal for Lean Burn Natural Gas Engines." I have examined the final electronic copy of this thesis for form and content and recommend that it be accepted in partial fulfillment of the requirements for the degree of Master of Science, with a major in Mechanical Engineering.

David K. Irick
Major Professor

We have read this thesis
and recommend its acceptance:

Ke. Nguyen

Robert Wagner

Accepted for the Council:

Anne Mayhew
Vice Chancellor and
Dean of Graduate Studies

(Original signatures are on file with official student records.)

# DESIGN OF A CATALYST SYSTEM WITH PERIODIC FLOW REVERSAL FOR LEAN BURN NATURAL GAS ENGINES

**A**

**Thesis**

**Presented for the**

**Master of Science Degree**

**The University of Tennessee, Knoxville**

**Balaji Ramamurthy**

**May 2006**

Copyright © 2006 by Balaji Ramamurthy
All rights reserved.

# DEDICATION

This thesis is dedicated to my parents, especially to my mom, for giving me the gift of higher education, without which none of this would have been possible. They provided much needed and appreciated support throughout my educational journey. In addition, their love and encouragement gave me the strength I needed to complete enormous task of getting this Master of Science degree.

# ACKNOWLEDGEMENTS

My appreciation is due to many people who have helped me often, without knowing that they were doing so. I am forever grateful to my advisor, Dr. David Irick, for giving me the opportunity to work in this project. His guidance and assistance was paramount in helping me achieve my goals. I value his intelligence and ambition and will look to him as a role model throughout the rest of my career.

My special thanks goes to Dr. Naoumov for his constant guidance, which has been invaluable to me throughout the completion of this thesis. My sincere gratitude goes to Dr. Nguyen who is never in short of help in explaining concepts and answering my questions. I would also like to thank my committee member Dr. Robert Wagner, for serving on my committee and for his support and assistance. Thanks to the U.S. Department of Energy and the Advanced Reciprocating Engine Systems (ARES) program for their financial support and to Dr. Ming Zheng for obtaining funding for this project.

Special thanks to the Mechanical, Aerospace and Biomedical Engineering Department's shop personnel Danny Graham, Gary Hatmaker and Dennis Higdon, especially Danny Graham and Gary Hatmaker, for their patience, enthusiasm, and support in the fabrication of the FWSDV. This work would not have been complete without their help.

I also thank all of my friends for their constant support, especially Hariharan and John Miller, who provided valuable feedback on my thesis. Finally, I would like to thank almighty for being with me through out the success in my life.

# ABSTRACT

The objective of this research is to accomplish methane conversion from lean burn natural gas engines. As methane conversion requires high temperatures, the concept of PFR (Periodic Flow Reversal) is used. The PFR is a heat trap that performs active heat recovery in addition to the heat retention capability of monolith solids. Cyclically alternating the direction of exhaust flow produces a thermal wave along the center of the catalyst thereby elevating the temperature above the engine exhaust temperature. The PFR loop is developed connecting catalyst canisters with a Four-Way Single Diversion Valve (FWSDV) using a set of pipes and pipe connectors. Two oxidation catalysts are used to develop exothermic reactions, which would increase the temperature further. The FWSDV is the main control device, which performs the switching of exhaust gases through the monolith reactor. It is designed and fabricated in the University of Tennessee. Gas dynamics and thermodynamics calculations determine the optimal dimensions and allowable leakage of the exhaust gases through the FWSDV. Special techniques have been implemented in the design to provide minimal leakage and several schemes are employed to minimize the valve size and to make the system compact and low cost. Actuator for FWSDV has been sized, which rotates the rotor assembly of the valve, thereby switching the direction of the exhaust gas flow. The Switching time, Gas Hourly Space Velocity (GHSV) and exhaust temperature are major factors in achieving methane conversion. Recommendations for supplemental fuel injections are given for further research as this would result in significant reduction of methane.

# TABLE OF CONTENTS

**CHAPTERS** **PAGES**


**1. INTRODUCTION** ……....1

1.1 Mission of ARES Program …….1

1.2 Alternative Fuel for DP Application ……..1

1.3 Lean Burn Natural Gas Engines …….2

**2. BACKGROUND REVIEW** ……....4

2.1 Need for Using Natural Gas as a Fuel. ……...4

2.2 Regulated Emissions.....……...5

2.2.1 Unburned Hydrocarbon Emissions……..……....5

2.2.2 Oxides of Nitrogen……..7

2.2.3 Carbon Monoxide…….…..9

2.2.4 Particulate Matter…….. 10

2.3 Emission from Natural Gas and Need for Methane Emission Abatement……...11

2.4 Methods Of Reducing Methane Emissions……12

2.4.1 Methane Emission Abatement Using Three-Way Catalyst……...13

2.4.2 Methane Oxidation Using Nobel Catalyst…….…17

2.4.3 Methane Oxidation Using Reverse Flow Catalytic Converter…..21

2.4.4 Experiments Using Bench Flow Reactor...……25

2.4.5 Few Other Common Methods……28

2.5 Problem Statement and Research Objective……..29

**3. CONCEPTUAL DESIGN AND CALCULATIONS**……..…….30

3.1 Conceptual Design of Reverse Flow Catalytic Converter…….30
3.2 Four – Way Single Diversion Valve Conceptual Schematic and Operation …….34
3.2.1 Unidirectional Rotation……..……...35
3.2.2 Multidirectional Rotation……..……....40
3.3 Calculations……43
3.3.1 Calculation for Catalyst Dimensions…….……43
3.3.2 Residence Time for the Peak Power Condition…….....44
3.3.3 Residence Time for the Peak Torque Condition……46
3.4 Dimensions for the Rotor's and Stator's Openings……...…47
3.5 Permissible Leakage Bypassing the Catalysts…….…..51
3.6 Maximum Momentum Acted Against Valve's Partition…….…..56

**4 ACTUAL DESIGN OF PFR MECHANISM WITH THE FWSDV**…….....59

4.1 Detailed Schematic and Specification of Periodic Flow Reversal Mechanism……..…59
4.1.1 Design of Catalyst Canisters……...60
4.1.2 Design of Flanges and Pipe Reducers……62
4.2 Design of Four-Way Single Diversion Valve……... 65
4.2.1 Description of the Outer Cylinder……..66
4.2.2 Description of the Inner Cylinder……..66
4.2.3 Description of the Inner Cap……..71
4.2.4 Stainless Steel Shaft…...……71
4.2.5 Rectangular Block……..73
4.2.6 Description of the Outer Cap...……..74
4.2.7 Description of the Stainless Steel Flange…….…74

4.3 Actuator for the FWSDV……...79

4.3.1 Description and Operation of Rotation Control Mechanism…….79

5 **CONCLUSION AND RECOMMENDATIONS.**……..82

5.1 Conclusion…….82

5.2 Recommendations for Further Research……....83

**BIBLIOGRAPHY**..……..84

**APPENDIX**……...89

**VITA**……..…….110

# LIST OF TABLES

**TABLE** **PAGE**

2.1 Catalytic oxidation of methane over supported Pt and Pd catalyst…….……..20

2.2 Exhaust gas properties for three cases….……..22

3.1 Exhaust gas properties of C 8.3 Gas Plus Engine…….44

3.2 Tier 4 Emission standards for engines up to 560 kW……...52

# LIST OF FIGURES

**FIGURE** **PAGE**


2.1 Emission from a SI engine as a function of equivalence ratio……..6

2.2 Conversion efficiency of Pt/Rh-based three-way catalyst in the gasoline engine emission……..13

2.3 Conversion efficiency of Pt/Rh-based three-way catalyst in the CNG engine emission……..14

2.4 Conversion efficiency of Pd-based three-way catalyst for the mixture model gas……..15

2.5 Experimental set-up for catalytic activity evaluation……18

2.6 Methane conversion as a function of inlet temperature……19

2.7 Experimental set up of reverse flow reactor……..21

2.8 Development of the middle reactor temperature $T_3$ and $T_4$ with reverse flow cycling……...23

2.9 HC and CO conversion with reverse flow cycling……....24

2.10 Comparison between the unidirectional operation and the reverse flow operation……25

2.11 Methane conversion at a reactor furnace temperature of 450 °C, GHSV of 40,000 $hr^{-1}$, and a ST of 10s……..26

2.12 Temperature profiles across the catalyst length at various times at a reactor furnace temperature of 450 °C, GHSV of 40,000 $hr^{-1}$…….……..26

2.13 Effects of switching time on $CH_4$ conversion with GHSV as a parameter at a temperature of 400 °C……..…….27

3.1 The reverse flow catalytic converter concept.…….……..31

3.2 Temperature profile across the length of the catalyst……33

3.3 Four-Way Single valve system: (a) forward mode; (b) reverse mode……. 33

3.4 FWSDV conceptual schematic with unidirectional rotation……36

3.5 Flow rate/rotation diagram for FWSDV with unidirectional rotation……...37
3.6 Temperature profile across the catalyst at a reactor furnace temperature of 400 °C, a GHSV of 20,000 $hr^{-1}$, and a ST of 10s at various experimental run times……...……39
3.7 Temperature profile across the catalyst at various times during an experimental run at a reactor furnace temperature of 400 °C, GHSV of 20,000 $hr^{-1}$, and a ST of 30s…….…….39
3.8 FWSDV conceptual schematic with multidirectional rotation……..41
3.9 Flow rate/rotation diagram for FWSDV with multidirectional rotation…….…...42
3.10 Thermodynamic data for the combustion mixture…….49
3.11 Uniform distributed load of simply supported beam…….57
4.1 Schematic of the loop…….60
4.2 Catalyst canister…….61
4.3 Male flange……63
4.4 Female flange…….63
4.5 Pipe reducer (cone)……64
4.6 Sectional view of assembly……64
4.7 Diverter valve assembly…….65
4.8 Outer cylinder……...…….68
4.9 Inner cylinder…….....69
4.10 Sectional view of the valve assembly..……..70
4.11 Inner cap…….……72
4.12 Stainless steel shaft……73
4.13 Rectangular Block..……...75
4.14 Outer cap……76
4.15 Stainless steel flange……..77
4.16 Catalyst system with the FWSDV…….78
4.17 Schematic diagram of the motion control mechanism…….…..80
4.18 Schematic of valve-actuator assembly……...81

## APPENDIX FIGURES

**FIGURE** **PAGE**


A-1 Valve Assembly...……..……90

A-2 Sectional View of Outer Cylinder.....…...91

A-3 Sectional View of Inner Cylinder...……...92

A-4 Diverter Plate…….93

A-5 Sectional View of Inner Cap.....…...94

A-6 Sectional View of Outer Cap…….…...95

A-7 Sectional View of Stainless Steel Flange……...96

A-8 Copper Gasket…….……..…….97

A-9 Stainless Steel Washer.....….....98

A-10 Sectional View of Valve Housing….…….……..…….99

A-11 Exhaust Pipe…….…...100

A-12 Sectional View of Assembly with Valve Housing...…….……..……101

A-13 Rectangular Block in 2D and 3D…….……...…….102

A-14 Sleeve.....…...103

A-15 Stainless Steel Shaft in 2D….....104

A-16 Catalyst System Assembly.....…....105

A-17 Sectional View of Male Flange…….……..……106

A-18 Sectional View of Female Flange….……..….107

A-19 Sectional View of Stainless Steel Gasket.....…...108

A-20 Sectional View of Copper Gasket….....109

# LIST OF SYMBOLS

$\mu$……Molecular mass

$\rho$……..density

$\sigma_b$……bending stress

$\sigma_y$……yield stress

$\Phi$……..diameter

a……..velocity of sound

A……..area

$Al_20_3$……aluminum oxide

C……carbon atom

$C_3H_6$……...propylene

$C_3H_8$……..propane

$CH_4$……..methane

CO……..carbon monoxide

$CO_2$……carbon dioxide

F……force

gms/min……...grams/ minute

H……hydrogen atom

$H_2O$……water

$H_2S$……...hydrogen sulphide

HC……hydro carbon

I……moment of inertia

ID……....inner diameter

$K_1$……experimental constant

$K_{co}$……..rate constant

m……mass flow rate

M……molecule

n……..number of moles

$N_2O$……...nitrous oxide

NO……..….nitric oxide

$NO_2$…….…nitrogen dioxide

$NO_x$……...oxides of nitrogen

$O_2$……..oxygen

OD…….outer diameter

P……..pressure

Pd……..palladium

PdO……...palladium oxide

Pp……...partial pressure

$psi_a$……..pound per square inch in absolute value

$psi_g$……..pound per square inch in gauge value

Pt/Rh……platinum- rhodium

Pt…….....platinum

R……....hydro carbon radical

R……..universal gas constant

$SO_x$…….oxides of sulphur

SV……space velocity

hr…….hour

T…….....temperature

t……thickness

$T_1$,$T_2$,$T_3$,$T_4$…….reactor temperatures

THC…….total hydro carbon

$TiO_2$……anatase

$T_{or}$……..original residence time

$T_{rs}$…….standard residence time

$v_{exh}$…….exhaust gas velocity

$v_{op}$…… …….velocity of gas through perforated openings

V……volume

W…….unit load

y…….….distance from the reference axis

$\gamma$……gamma

## LIST OF ABBREVIATION

AF…….Air-to-fuel ratio
BFR…….Bench flow reactor
CARB…….California air resources board
CC……Catalytic converter
CNG…….Compressed natural gas
DER……...Distributed energy resource
DOE……....Department of energy
DP…….Distributed power
EGR…….Exhaust recirculation system
EPA……..Environmental protection agency
EPS……Exhaust pipe system
FWSDV…….Four way single diversion valve
GHSV……..Gas hourly space velocity
LNC…….Lean NOx catalyst
LNT……..Lean NOx traps
NGV……....Natural gas vehicle
NMHC……Non-methane hydrocarbon
PFR…….Periodic flow reversal
RCM…….Rotation control mechanism
RFC…….Reverse flow catalyst
RFR……..Reverse flow reactor
SCR……...Selective catalytic reduction
SFI……..Supplemental fuel injection
SI…….Spark ignition
WOT…….……...Wide open throttle

# CHAPTER 1

# INTRODUCTION

## 1.1 Mission of ARES Program

The new millennium needs a high standard engine technology to meet the ever-increasing demands for more energy and stricter environmental regulations. The U.S. Department of Energy (DOE) is currently developing advanced natural gas reciprocating engine systems for Distributed Energy Resource (DER) applications in industries and other utility settings. DER refers to local energy systems that generate electric, thermal or mechanical energy. The natural gas reciprocating engines have various advantages in terms of environmental benefits and fuel efficiencies. Established U.S. engine manufacturers have entered into a cooperative program called an Advanced Reciprocating Engine System (ARES), which over the next several years, will bring forth a new generation of highly advanced, natural gas engines to meet future needs. Several universities are also involved in the research activities, developing models and prototypes for this project. The mission of this program is to lead a national effort to design, develop, test and demonstrate a new generation of reciprocating engine systems for Distributed Power (DP) applications that are cleaner, more affordable, reliable and efficient than products that are commercially available today.

## 1.2 Alternative Fuel for DP Application

Reciprocating engine systems are available in different combinations and the most familiar combination used in DP application is the reciprocating, spark-ignited, four-stroke gasoline engine. Environmental concerns and depletion in petroleum resources have forced researchers to concentrate on finding alternatives to conventional petroleum fuels. Another problem with petroleum is the emission of pollutants such as carbon dioxide ($CO_2$), nitrogen oxides ($NO_x$), carbon monoxide (CO), hydrocarbons (HC),

Particulate Matter (PM), Lead, Sulfur and other traces of Volatile Organic Compounds (VOC). In order to decrease these pollutants, alternative fuels such as natural gas are being considered.

### 1.3 Lean Burn Natural Gas Engines

Natural gas is a mixture of simple hydrocarbon components primarily methane. Natural gas is thought to be a major energy source of the future due to its clean burning nature and eventual availability from the renewable sources. Natural gas engines are commanding more attention as interest grows in on-site power production equipment that is efficient and more environmentally friendly. In response to this interest, manufacturers have introduced natural gas engines which feature new "lean burn" technology. Lean-burn engines use an air-fuel (AF) mixture with much more air than is required in stoichiometric mixture, to burn all of the fuel. The extra air dilutes the mixture and reduces the flame temperature, thus reducing engine-out $NO_x$ emissions, as well as exhaust temperatures. Lean burn engines also have greater fuel efficiency due to its inherently lower engine knock tendency and higher compression ratios.

Nitrogen oxide emissions from lean burn engines are lower than stoichiometric due to cooler combustion resulting from high AF ratios. Although $NO_x$ production is lower in a lean burn than in a rich burn and stoichiometric condition, it does not meet the stringent emission target of 0.1 gm/hp-hr of $NO_x$ aftertreatment challenge of lean burn engines **[1]**. The addition of secondary chemical supply (urea) and the control of urea dosage make the system much complex when using Selective Catalytic Reduction (SCR) method. The leading de-$NO_x$ contender used to reduce the $NO_x$ contents is by using Lean $NO_x$ Traps (LNT). LNT has demonstrated high $NO_x$ conversion efficiencies, approaching 91 – 97 %, and experimental results demonstrate the potential for LNT technology to reach the ARES targeted of 0.1 gm/hp-hr $NO_x$ rating for Lean Burn (LB) natural gas engines **[1].** Due to excess oxygen availability in lean burn engines, the CO

level is very low, the combustion process is more efficient, and more power is produced from the same amount of fuel. But the main ingredient present in the natural gas is methane, which is typically up to 99% of the total volume. Other constituents may include non-methane hydrocarbons such as ethane, propane and butane and in other cases, traces of hydrocarbons as well as inert gases like nitrogen, helium, carbon dioxide and hydrogen sulfide. Since methane is highly stable, it is highly difficult to reduce at ordinary temperatures.

The aim of this research is to explore several possible ways and to use the most efficient technique for methane emission abatement from the lean burn natural gas engine exhaust system. The C-H bond in $CH_4$ is very strong and hence the disassociation of the bond requires large amount of energy. (The bond energy of C-H = 414 J/mol). The temperature of the exhaust gas from the engine is not sufficient to break the C-H bond, and hence catalytic converter with oxidation catalyst is used in the downstream of the LNT to enhance the temperature of the exhaust. In many cases feed pre-heating is not the viable option, and other methods of achieving a sufficiently high reactor temperature must be explored. With the combined use of Exhaust Gas Recirculation (EGR) and an oxidation catalytic converter, low emission operation has been extended to a larger region, from medium to full loads across all speeds. However, conventional converters exhibit poor conversion efficiency at low engine loads due to the low level of exhaust temperature. This leads to increased exhaust emissions during low load operations, especially for the non-reactive hydrocarbons, specifically, methane **[20].** In order to provide good conversion efficiencies for all engine loads, several techniques were investigated. This study focuses on a concept that has been successfully exploited in many applications, which is the "Reverse Flow Catalyst" (RFC). The reverse flow concept was first discussed by Frank-Kamenetski for "diffusion and heat exchange in chemical kinetics" **[8]** and has been revised later on by Matros and Bunimovich **[17]** for catalytic converter application.

# CHAPTER 2

# BACKGROUND REVIEW

This chapter discusses the advantages of natural gas as a fuel, exhaust emissions of different concentrations from the engine (regulated emissions) and possible ways of controlling them, the need for reducing methane emissions and methods for achieving the reduction. The drawbacks of previous methods are discussed and the solution is provided in the research objective, which could be implemented to provide good methane conversion from the exhaust of lean burn natural gas engines.

## 2.1 Need for Using Natural Gas as a Fuel

Natural gas is the cleanest burning alternative fuel available today. Because natural gas releases only few harmful byproducts compared to other conventional fuels, it has been recognized as an excellent fuel when used to generate electricity, heat homes and fuel industrial facilities. In addition to being a domestically abundant and secured source of energy, the use of natural gas also offers a number of environmental benefits over other sources of energy. It is an extremely important source of energy for reducing pollution and maintaining a clean and healthy environment. When natural gas is burned, it produces virtually no emissions of sulfur dioxide or particulate matter and far lower levels of "greenhouse" gases in the form of $CO_2$ and $NO_x$ than other traditional sources of energy like oil and coal **[21].** In addition, unlike oil, coal and nuclear processes, natural gas fueled processes produce virtually no solid waste and has much less impact on water quality. The inherent cleanliness of natural gas compared to other fuels, coupled with its high fuel efficiency, can help reducing emission of the air pollutants that produce smog and acid rain and that could exacerbate the "greenhouse" effect. Natural gas also has many advantages in various sectors such as consumer use, commercial markets, industrial markets, electric generation, vehicles, supply challenge and delivery systems.

Due to its many economic and environmental benefits, natural gas has become the fuel of choice for electricity generation **[21].** In the 1990s, there was a dramatic shift to natural gas for power generation. Large coal and nuclear generating plants were the clear choice of electric utility planners in the 1970s and 1980s, but a combination of economic, environmental and technological factors have resulted in a pronounced movement to natural gas **[21].** Composed primarily of methane, the main products of combustion of natural gas are carbon dioxide and water vapor. It is expressed by the following chemical equation:

$$CH_4\,[g] + 2\,O_2\,[g] \text{ -----> } CO_2\,[g] + 2\,H_2O\,[l] + 891 \text{ kJ / kmol.} \qquad (2.1)$$

Burning methane releases only carbon dioxide and water. Since natural gas is comprised mainly of methane, the combustion of natural gas releases fewer harmful byproducts such as $CO_2$ and $NO_x$ compared to particulates and various other gases such as sulfur dioxide, VOC, etc. from other fossil fuels.

## 2.2 Regulated Emissions

The principle emissions regulated by the U.S.EPA (United States Environmental Protection Agency) and CARB (California Air Resources Board) to reduce air pollution include non-reactive hydrocarbons, oxides of nitrogen, carbon monoxide, and particulate matter. Particulate matter emissions are the primary concern for diesel engines. The section follows focuses on the methods of reducing these emissions to provide pollutant free environment.

### 2.2.1 Unburned Hydrocarbon Emissions

Hydrocarbon emissions are the consequence of incomplete combustion of the hydrocarbon fuel, which means, hydrocarbon emissions occur when fuel molecules in the engine do not burn or burn only partially. The level of unburned hydrocarbon (HC) in the exhaust gases is generally specified in terms of total hydrocarbon concentration expressed in ppm of carbon atoms (C).

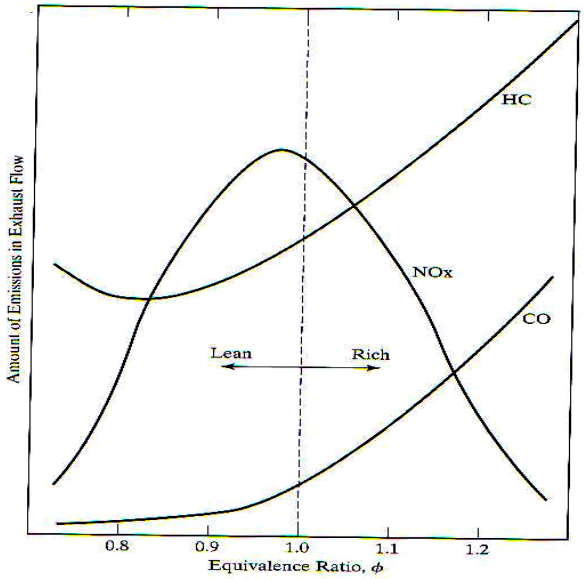


**Figure 2.1 Emissions from a SI engine as a function of equivalence ratio**

Figure 2.1 shows that hydrocarbon (HC) emission levels are a strong function of air-to-fuel (AF) ratio **[25].** With a fuel-rich mixture, there is not enough oxygen to react with all of the carbon, resulting in high levels of HC and CO in the exhaust gases. This is particularly true during engine start-up, when the air-fuel mixture is very rich. It is also true to a lesser extent during rapid acceleration under load. If AF ratio is too lean, poorer combustion occurs, again resulting in HC emissions. The extreme of poor combustion for a cycle is total misfire, which occurs when AF ratio is made more lean, approaching the lean limit of combustion.

There are several mechanisms that contribute to total HC emissions. Four possible HC emissions formation mechanisms for spark-ignition engines (where the fuel-air mixture is essentially premixed) have been proposed **[25]** and **[10]**: (1) flame quenching at the combustion chamber walls, leaving a layer of unburned fuel-air mixture adjacent to the wall; (2) the filling of crevice volumes with unburned mixture which, since the flame quenches at the crevice entrance, escapes the primary combustion process; (3) adsorption

of fuel vapor into oil layers on the cylinder wall during intake and compression, followed by desorption of fuel vapor into the cylinder during expansion and exhaust; (4) incomplete combustion in a fraction of the engine's operating cycles (either partial burning or complete misfire), occurring when combustion quality is poor (e.g., during engine transients when AF, EGR, and spark timing may not be adequately controlled). In addition, as deposit builds up on the combustion chamber walls, HC emissions increase. All these processes (except misfire) result in unburned hydrocarbons close to the combustion chamber walls, and not in the bulk of the cylinder gases. Thus, the distribution of HC in the exhaust gases would not be expected to be uniform.

When hydrocarbon emissions get into the atmosphere, they act as irritants and odorants; some are carcinogenic. All components except $CH_4$ react with atmospheric gases to form photochemical smog. There are several methods by which HC emissions could be avoided. As engine out HC emissions are dependent on AF ratio, maintaining AF ratio in the lean region is a primary method for controlling HC. An oxidizing or three-way catalyst can oxidize engine exhaust hydrocarbons to carbon dioxide and water under stoichiometric and lean operation. Engine designs that minimize crevice volumes and have lower compression ratios can also help reduce these emissions. The lower compression ratios reduce peak pressures, thus reducing the amount of fuel-air mixture that is forced into the crevice volumes.

### 2.2.2 Oxides of Nitrogen

Oxides of nitrogen (NO, $NO_2$, $N_2O_2$, etc.) are formed at the high combustion temperatures present in engines. Exhaust gases of an engine can have up to 2000 ppm of oxides of nitrogen. Most of this will be nitrogen oxide (NO), with a small amount of nitrogen dioxide ($NO_2$), and traces of other nitrogen-oxygen combinations. These are all grouped together as $NO_x$. $NO_x$ is a very undesirable emission, and regulations that restrict the allowable amount continue to become more stringent. Released $NO_x$ reacts

in the atmosphere to form ozone and is one of the major causes of photochemical smog **[25].**

$NO_x$ is created mostly from nitrogen in the air. Nitrogen can also be found in fuel blends, which may contain trace amounts of $NH_3$, NC, and HCN, but this would contribute only to a minor degree. The extended Zeldovich mechanism is given by **[25]**

$$O + N_2 ---> NO + N \tag{2.2}$$

$$N + O_2 ---> NO + O \tag{2.3}$$

$$N + OH ---> NO + H \tag{2.4}$$

NO can further react either with water or oxygen to form $NO_2$. At the very high temperatures that occur in the combustion chamber of an engine, some diatomic nitrogen ($N_2$) disassociates to form monatomic nitrogen (N), which is highly reactive:

$$N_2 \quad ---> 2\,N \tag{2.5}$$

The higher the combustion chamber reaction temperature, the more diatomic nitrogen, $N_2$, dissociates to monatomic nitrogen, N, and the more $NO_x$ will be formed. At low temperatures very little $NO_x$ is created.

Although maximum flame temperature will occur at a stoichiometric air-fuel ratio ($\varphi$ = 1), Figure 2.1 shows that maximum $NO_x$ is formed at a slightly lean equivalence ratio of about $\varphi$ = 0.95 **[25]**. At this condition, the flame temperature is still very high, and in addition, there is an excess of oxygen that can combine with the nitrogen to form various oxides. In addition to its dependence on temperature, the formation of $NO_x$

depends on pressure, AF ratio, and combustion time within the cylinder. Hence by controlling any of these parameters the formation of $NO_x$ can be reduced.

There are several ways for controlling $NO_x$, either by combustion process or with an exhaust aftertreatment system. In the combustion process, $NO_x$ can be controlled by retarding ignition timing or through the use of an exhaust gas recirculation (EGR) system. Reducing $NO_x$ through exhaust aftertreatment depends on the stoichiometry of engine operation. For engines that operate under stoichiometric air-fuel conditions, a typical three-way catalyst will reduce $NO_x$ emissions. However, lean burn engines present challenges in the aftertreatment of $NO_x$ emissions. Unlike hydrocarbons and carbon monoxide, which are removed through oxidation, $NO_x$ must be reduced in a fuel-rich environment. The three leading aftertreatment technologies for reducing $NO_x$ emissions from lean burn engines are Selective Catalytic Reduction (SCR), the lean-$NO_x$ catalyst (LNC) and lean $NO_x$ traps (LNT). Unlike SCR, which uses urea as a reducing agent, LNT uses the same fuel supplied to the engine as the reductant. LNT has demonstrated high reduction efficiencies in diesel application where diesel fuel is the reducing agent. It was also demonstrated that LNT was effective method in reducing $NO_x$ emissions from natural gas engines, and this method met the stringent emission target of 0.1 gm/hp-hr set by ARES **[1].**

### 2.2.3 Carbon Monoxide

Carbon monoxide is mainly due to incomplete combustion of a fuel. It is seen earlier in the Figure 2.1 that the carbon monoxide emissions are significant in the fuel rich region due to the insufficiency of oxygen **[25]**. When the engine is operated in the fuel rich region, there is not enough oxygen to convert all carbon to $CO_2$, some fuel does not get burned and some carbon ends up as CO. So, CO emission is a strong function of AF ratio and hence, avoiding fuel rich combustion is the one way of preventing CO

emissions. Three-Way catalyst is effective in reducing CO in lean and stoichiometric operation. Carbon monoxide is a colorless, odorless and poisonous gas that renders the blood incapable of transporting oxygen. This lack of oxygen can lead to headaches, dizziness, nausea and even death at high enough concentrations. As CO is not a concern for LB engines it has been dealt just briefly.

### 2.2.4 Particulate Matter

The exhaust from any engine may contain solid carbon soot particles that are generated in the fuel-rich zones within the cylinder during combustion. These are seen as exhaust smoke and cause an undesirable odorous pollution. Fine particulate matter ($2.5\ \mu m$) poses a significant risk to human health. These fine particulate matters, as they are small, get into the defenses of the respiratory system and then deposit themselves on the alveoli regions of the lungs. The significant health problems include premature death, respiratory problems, aggravated asthma, chronic bronchitis and decrease lung function.

Maximum density of particulate emissions occurs when the engine is under load at wide-open throttle (WOT). At this condition, maximum fuel is injected to supply maximum power, resulting in a rich mixture and poor fuel economy. This can be seen in the heavy exhaust smoke emitted when a truck or railroad locomotive accelerates up a hill or from a stop. Soot particles are clusters of solid carbon spheres with HC and traces of other components adsorbed on the surface. These carbon spheres are generated in the combustion chamber in the fuel-rich zones where there is not enough oxygen to convert all carbon to $CO_2$ **[25].**

$$C_xH_y + zO_2 --> aCO_2 + bH_2O + cCO + dC(s) \qquad (2.6)$$

Then, as turbulence and mass motion continue to mix the components in the combustion chamber, most of these carbon particles find sufficient oxygen to further react and are consumed to $CO_2$:

$$C(s) + O_2 --> CO_2 \quad (2.7)$$

Over 90% of carbon particles originally generated within an engine are thus consumed and never get exhausted.

Particles generation can be reduced by engine design and control of operating conditions, but quite often this will create other adverse results. If the combustion time is extended by combustion chamber design and timing control, particulate amounts in the exhaust can be reduced. Soot particles originally generated will have a greater time to be mixed with oxygen and combusted to $CO_2$. However, a longer combustion time means a high cylinder temperature and more $NO_x$ emissions. Engine management systems can be programmed to minimize $NO_x$, HC, CO, and particulate emissions by controlling ignition timing, injection pressure, injection timing, and/or valve timing. In most engines, exhaust particulate amounts cannot be reduced to acceptable levels solely by engine design and control. As discussed earlier, particulate matter emissions are discussed as a general pollutant regulations and it is not an issue for Lean Burn (LB) engines.

## 2.3 Emission from Natural Gas and Need for Methane Emission Abatement

Natural gas engines can operate under lean conditions so that the fuel efficiency can be increased compared to stoichiometric conditions. Under lean-burn conditions nitrogen oxides ($NO_x$) emissions of Compressed Natural Gas (CNG) engines are much reduced **[14].** This is due to cooler combustion resulting from the high AF ratios at which the lean engines operate. $CO_2$ emissions are also reduced because of the high H to C ratio of the methane molecule, which is the main component (85-95%) of natural gas. Because of the very low sulfur content of natural gas, $SO_x$ emissions are also very low. Even though natural gas is considered to be one of the most promising candidates for a clean substitute fuel, the presence of methane poses environmental problems. The hydrocarbon composition in the exhaust gases of lean-burn CNG engines reflects the

composition of natural gas in methane and non-methane hydrocarbons (NMHCs), typically 90-95% methane **[15].** Methane is a potent greenhouse gas, which is recognized to contribute more to global warming than carbon dioxide at equivalent emission rates, mainly due to its long lifetime. But calculating exactly how much more a molecule of methane contributes to climate change than a molecule of carbon dioxide is fraught with difficulties. While methane is much shorter–lived in the atmosphere than carbon dioxide, each methane molecule is much more efficient at trapping heat. The methane multiplier commonly used is known as the 100–year Global Warming Potential (GWP) and represents the impact after 100 years of a one–time pulse into the atmosphere of a ton of methane compared to one ton of $CO_2$. The UN's Intergovernmental Panel on Climate Change currently estimates methane's 100–year GWP as 21, meaning that a ton of methane in the atmosphere causes 21 times more warming than a ton of carbon dioxide **[12].**

## 2.4 Methods of Reducing Methane Emissions

The advantages of natural gas are partially offset by the emission of unburned methane. In light-duty application, the exhaust emissions from natural gas engines are much lower than that of gasoline engines. In addition, smog-producing gases, such as carbon monoxide and nitrogen oxides, are reduced by more than 90% and 60%, respectively, and carbon dioxide, a greenhouse gas, is reduced by 30%-40%. For heavy-duty and medium-duty applications, natural gas engines have demonstrated more than 90% reduction of CO and particulate matter and more than 50% reduction of $NO_x$ relative to commercial diesel engines **[6]**. At the same time the presence of methane in the natural gas poses environmental problems and methane oxidation proceeds much more slowly than oxidation of CO and NMHC because methane is highly stable and high energy is needed to break the C-H bond. There are many methods available for methane emission abatement from lean burn natural gas engines. Initial methods suggested were the use of three-way catalysts, the use of noble metal catalysts and also the process of reverse flow mechanism using catalytic converter **[26], [2]** and **[16].** A good conversion of methane could be achieved through the Periodic Flow Reversal (PFR), which was originally

patented by Cottrell in 1983. Various experiments were performed using this method for natural gas / diesel dual fuel engines where this method has proved to be the most effective method of reducing methane emission completely from the engine exhaust.

### 2.4.1 Methane Emission Abatement Using Three-Way Catalyst

One of the effective methods of abating methane emission is by using a catalyst, and experiments with three-way catalyst show good conversion of methane for both gasoline and CNG engines under stoichiometric condition **[26].** The conversion characteristics of three-way catalyst were studied and compared for both the gasoline engine emission and the CNG engine emission, which are shown through Figures 2.2 – 2.3 **[26].** A Pt/Rh-based three-way catalyst used for gasoline engines is employed as a test catalyst. A significant difference exists when comparing the conversion efficiency of the gasoline engine emission with that of the CNG engine emission. The HC conversion efficiency of gasoline engine emission increases in the lean mixture region, whereas it decreases considerably for the CNG engine emission. Furthermore, the HC conversion efficiency of the CNG emission is also low even in the excessively rich mixture region.

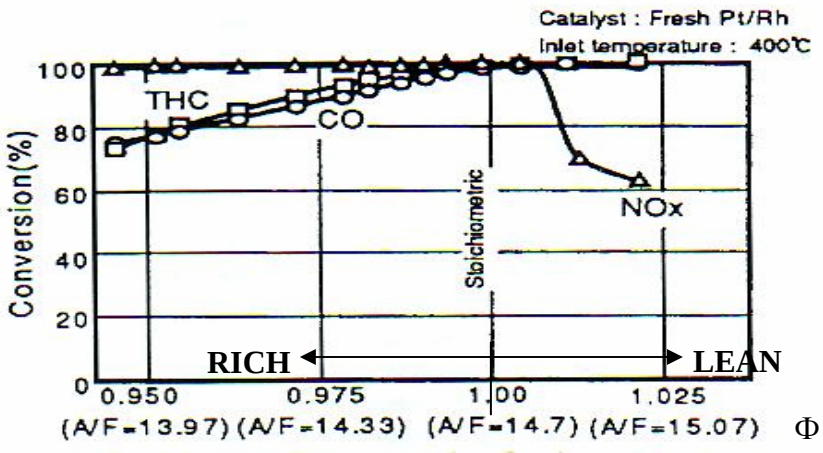


**Figure 2.2 Conversion efficiency of Pt/ Rh-based three-way catalyst in the gasoline engine emission**

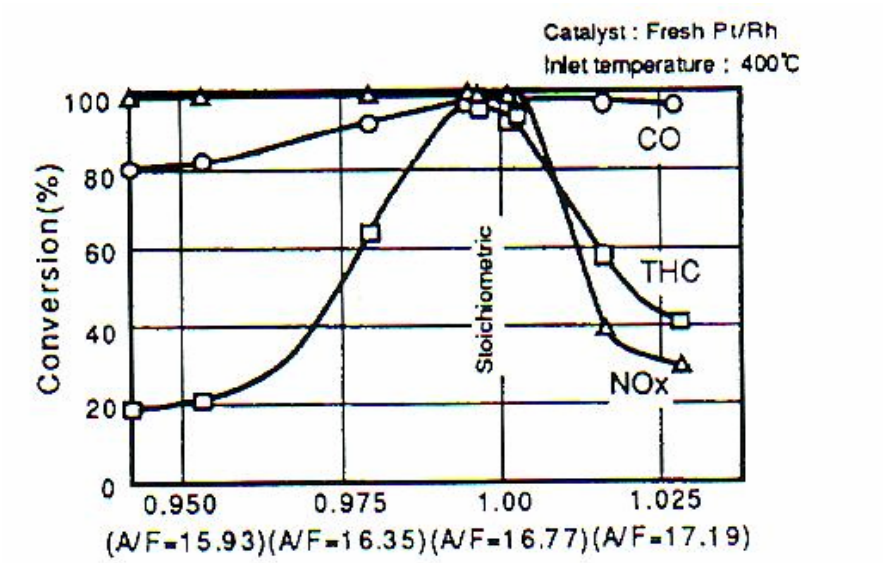


**Figure 2.3 Conversion efficiency of Pt / Rh-based three-way catalyst in the CNG engine emission**

The low conversion efficiency of HC for CNG is due to the fact that $CH_4$ is a highly stable molecule and the chemical reactions using Pt/Rh-based three-way catalyst are not sufficient to provide good conversion. A Pd-based three-way catalyst, which is increasingly used for gasoline engines, exhibits improved HC conversion efficiency for CNG engine in the excessively rich mixture region compared to the Pt/Rh-based catalyst. Figure 2.4 shows the conversion efficiency for the CNG engine emission by the Pd-based three-way catalysts **[26]**. Therefore, the Pd-based catalyst is considered to be an effective catalyst for CNG engines. At the same time, Pd-based catalyst also exhibits poor HC conversion efficiency in the lean-mixture region. Consequently, it is necessary to improve the HC emission characteristics in the lean-mixture region by improving the engine system or catalyst system. The conversion characteristics of each HC species in the lean mixture region was studied and it is considered that the reduction of the HC conversion efficiency in the lean-mixture region is caused by the low HC conversion efficiency for HCs of lower carbon numbers, mainly methane.

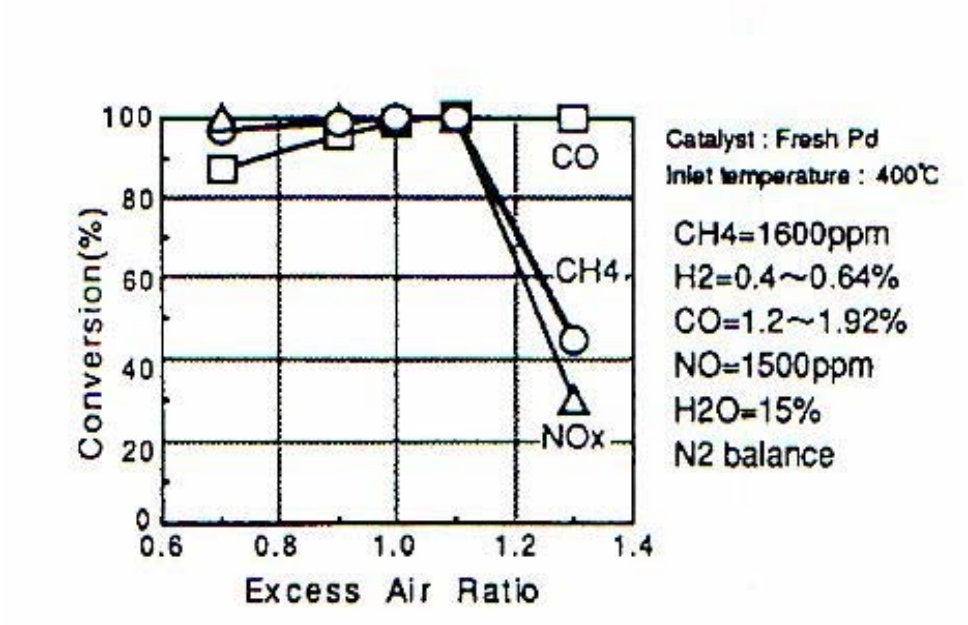


**Figure 2.4 Conversion efficiency of Pd-based three-way catalyst for the mixture model gas**

The cause of reduced conversion efficiency of methane in the lean-mixture region was analyzed by using model gas. The model gas is a gas mixture used in the experiment, which simulates the exhaust emission of the CNG engine. The model gas experiment was performed under the same condition of AF ratio and the same Pd-based three-way catalyst of the same specification as that employed in the CNG engine bench test was used as the test catalyst **[26].** Methane conversion efficiency is compared for both the simple model gas (reaction gas composed of methane and oxygen) and the mixture model gas (previously called as a model gas, a gas which simulates CNG engine emission). In the simple model gas, contrary to the mixture model gas, the conversion efficiency for methane increases in the lean-mixture region. The decrease in methane conversion for mixture model gas is found due to the adsorption of nitrogen oxide and water, especially $H_2O$ (because $H_2O$ is adsorbed instead of $CH_4$ due to poor absorbability of $CH_4$ and this adsorbed $H_2O$ inhibits the adsorption of $CH_4$) and increase in the conversion efficiency of methane in the region ranging from the stoichiometric ratio to the lean mixture was found

due to the influence of $H_2$ and CO. In a separate experiment, $H_2$ and CO are added into the simple model gas and the conversion efficiency of methane increases and this is caused by the accelerated $CH_4$ oxidizing reaction through the activation of the redox reaction by $H_2$ and CO with the oxygen adsorbing species on the surface of the catalyst **[26].** Influence of hydrocarbon species on the HC conversion efficiency was also studied. Comparing the conversion efficiency of propylene, propane and methane, all HCs show high conversion efficiency at the stoichiometric ratio. In the lean mixture region, on the other hand, the efficiency varied in the order as $C_3H_6 > C_3H_8 > CH_4$. This order is the same as that of the absorbability of these HCs on Pd. This is thought to be so because, unlike methane, propylene and propane are adsorbed on the catalyst surface without being inhibited by $H_2O$, and hence, can react on the catalyst easily. This reduction of HC conversion is not observed in the gasoline emission. This may be due to the fact that the major HC components of the gasoline emission are olefins and aromatic compounds, which have higher absorbability than methane.

Following conclusions were arrived based on these experimental studies.

- Pd-based three-way catalyst is considered to be promising when compared to Pt/Rh-based three-way catalysts for CNG engine because it can provide a higher HC conversion efficiency in the over-rich mixture region. However the conversion efficiency of both Pt/Rh and Pd-based catalysts decreases similarly in the lean-mixture region.
- The reduction of total hydrocarbon (THC) conversion efficiency in the lean-mixture region is mainly caused by the decrease in conversion efficiency of methane.
- The reduction of conversion efficiency for methane in the lean-mixture region is assumed to be caused by the inhibition of methane adsorption by the adsorption of $H_2O$ or NO.

Based on the above conclusions, methane emission abatement using three-way catalysts does not seem to be the promising method of achieving good methane

conversion for lean burn natural gas engine. Hence there is a need for further research to improve $CH_4$ conversion in the lean mixture region.

### 2.4.2 Methane Oxidation Using Noble Catalyst

Experiment using noble metal catalysts compares the activities of different catalysts. The activities of Pt, Pd and Pt + Pd catalysts supported on $\gamma$-$Al_2O_3$ and Ti$O_2$ (anatase) were compared for the complete oxidation of methane. It was found that Pt is less active than Pd when deposited on Ti$O_2$ and more active when deposited on $\gamma$-$Al_2O_3$. However, when combined, the Pt +Pd mixture exhibits more active than either metal individually, when supported on $\gamma$-$Al_2O_3$. In order to compare the performance of catalysts, experiments were conducted with $CH_4$/ air mixture with 300 ppmv of $CH_4$. The reason for using 300 ppmv of $CH_4$ is to avoid VOC emissions **[2].** $Pt/Al_2O_3$ catalysts are superior to $Pd/Al_2O_3$ in fuel-rich mixtures, while the latter is superior in oxygen-rich atmospheres **[3].** Pd on $\gamma-Al_2O_3$ stabilized by lanthanum was very effective, and deactivation was mostly correlated with the transformation of PdO to Pd metal **[7].** The experimental set up for the catalytic activation is shown in Figure 2.5 **[2]**, which consists of a fixed bench scale adiabatic reactor with stainless steel tube to hold the catalyst. Thermocouples were used to measure the gas temperatures both at the inlet and the outlet of the catalyst. Furnaces were used to preheat the catalyst section. The reaction was carried out at a Gas Hourly Space Velocity (GHSV) of 21,000 $hr^{-1}$.

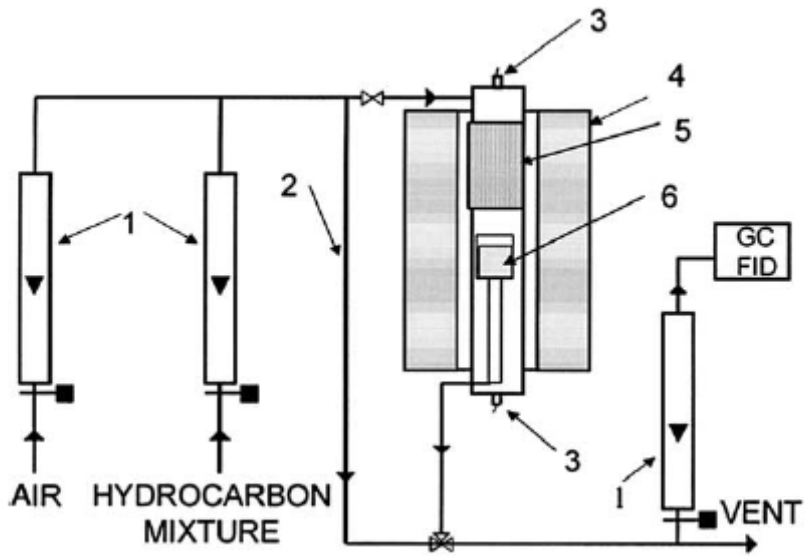


**Figure 2.5 Experimental set-up for catalytic activity evaluation**
**(1) Flow meters, (2) bypass, (3) thermocouples, (4) furnaces, (5) reactor and (6) catalyst bed**

The experimental result shows that both the Pt-Pd catalysts were more active, and achieved complete conversion of methane at significantly lower temperatures [$420\,°C$ for Pt (0.1 wt. %) - Pd (0.2 wt. %) $/TiO_2$, $320\,°C$ for Pt (0.2 wt. %) - Pd (0.3 wt. %)/ $TiO_2$] than the catalysts having a single metal, where the rates of increase of conversion with temperature above $400\,°C$, were quite slow **[2].** Of the two single metal catalysts, the Pd/$TiO_2$ is more active than the Pt/$TiO_2$ at all temperatures, however both required temperatures above $600\,°C$ for complete conversion. Figure 2.6 shows the conversion of methane as a function of inlet temperature for the $Al_2O_3$ -supported catalysts.

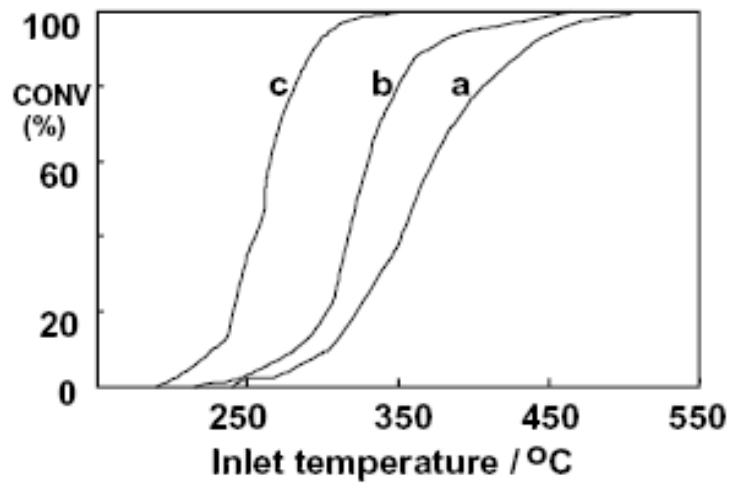


**Figure 2.6 Methane conversion as a function of inlet temperature (a) Pd (0.4 wt.%) / $Al_2O_3$, (b) Pt (0.3 wt.%)/ $Al_2O_3$ and (c) Pt (0.1 wt.%)-Pd (0.2 wt.%)/ $Al_2O_3$.**

Temperatures above 180 $°C$ were again needed, and the points at which various levels of conversion were obtained are also provided in Table 2.1 **[2]**. Once again the mixed metal catalyst is distinctly more effective than either of the single metal catalysts, in terms of both the temperature needed for complete conversion and of the smaller range in which conversion rises from 0% to 100%. However in contrast with the situation with $TiO_2$ as support, the Pt catalyst is now distinctly more active than Pd catalyst. It is apparent that the Pt-Pd / $Al_2O_3$ catalyst is more active than Pt-Pd / $TiO_2$ which has the same metal concentrations; its light-off temperature is about 60 $°C$ lower and the conversion rises to completion more rapidly at about 350 $°C$ (due to its some what higher activation energy) **[2]**. It is also seen that the higher loadings of the two metals result in extremely active catalyst, giving good methane conversion at lower temperatures.

**Table 2.1 Catalytic oxidation of methane over supported Pt and Pd catalyst**

| Support | Metal | $T_{10}$ (°C) | $T_{50}$ (°C) | $T_{90}$ (°C) | $E$ (kJ mol$^{-1}$) | ln$A$ (mol s$^{-1}$ mol$^{-1}$) |
|---|---|---|---|---|---|---|
| $TiO_2$ | Pd | 315 | 375 | 450 | 58 | 3.98 |
| $TiO_2$ | Pt | 342 | 395 | 530 | 61 | 4.88 |
| $TiO_2$ | Pt–Pd (I) | 287 | 326 | 377 | 97 | 13.40 |
| $TiO_2$ | Pt–Pd (II) | 214 | 236 | 255 | 151 | 27.23 |
| $Al_2O_3$ | Pd | 305 | 362 | 435 | 83 | 9.50 |
| $Al_2O_3$ | Pt | 280 | 323 | 371 | 90 | 11.97 |
| $Al_2O_3$ | Pt–Pd | 228 | 261 | 294 | 109 | 18.96 |

(i) Pt-Pd (I) 0.1 wt.% Pt and 0.2 wt.%Pd

(ii) Pt-Pd (II) 0.2 wt.% Pt and 0.3 wt.%Pd

The general consensus is that Pd/ $Al_2O_3$ is a superior catalyst and has higher activity towards methane combustion. However, Pd when supported the experimental result showed that mixed Pt/Pd supported on $Al_2O_3$ and $TiO_2$, have exhibited greater efficiency for the oxidation of methane. Pt is less active than Pd when deposited on the surface of $TiO_2$, but Pd when deposited on $\gamma$ - $Al_2O_3$ is more active when compared to either metal individually.

The LB engines cannot able to provide good conversion efficiency, which is due to the fact that the temperature of the engine exhaust is not sufficient for oxidizing methane, and hence the research is much focused on increasing the temperatures of the engine exhaust, which would effectively achieve good conversion. One method of increasing the engine exhaust temperature of LB engines is by using reverse flow catalytic converter.

### 2.4.3 Methane Oxidation Using Reverse Flow Catalytic Converter

Reverse Flow Reactor (RFR) concept was originally patented by Cottrell in 1983 and this concept was used to enhance the temperature within the reactor by allowing the feed to flow in forward and reverse direction along the length of the reactor. M. Zheng and his co-workers applied this concept to a natural gas / diesel dual fuel engine to test the performance of reverse flow converter **[16]** and **[20]**. Such a dual fuel system is one, which is powered by natural gas and ignited by diesel fuel. The experimental set up for RFR is shown in Figure 2.7 **[16]**. The experimental set up consists of a catalytic converter with a number of thermocouples inserted in order to measure the temperatures at various positions along the length of the reactor. The thermocouples $T_{in,1}$ or $T_{in,2}$ measure the temperature at the inlet and the outlet of the reactor depending on the direction of the exhaust gas flow. Thermocouples $T_3$ and $T_4$ correspond to the temperatures at the middle of the reactor.

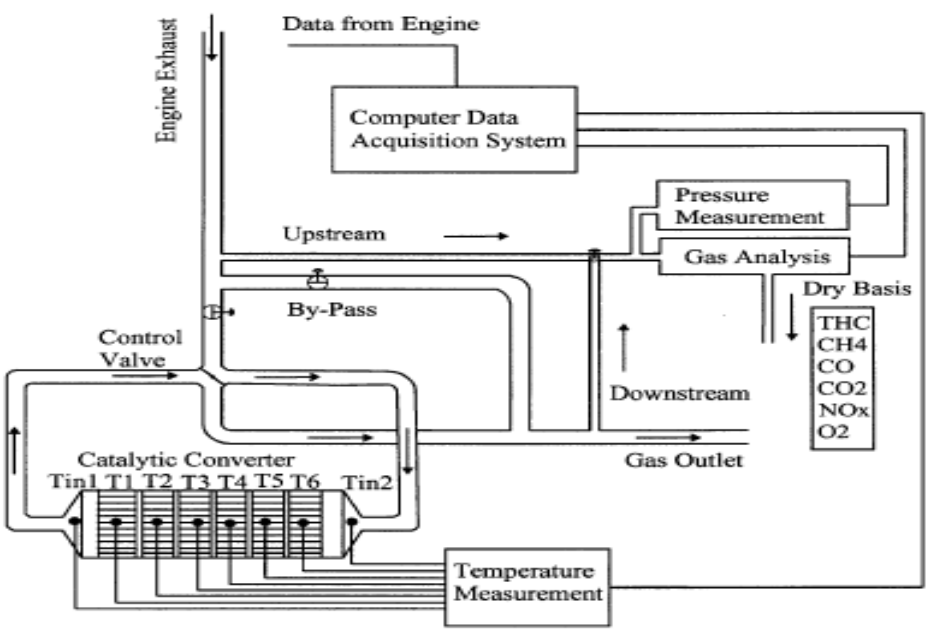


**Figure 2.7 Experimental set up of reverse flow reactor**

The control valve is used to switch the direction of exhaust gas flow in forward and reverse direction along the reactor. Gas analyzer is used to measure the composition of the exhaust gases before and after the converter. The data were initially recorded on a dry basis and were converted into a wet basis using Heywood relationship, $Y_i = (1 - Y_{H_2o})Y_i^*$, where $Y_i$ is the mole fraction of species 'i' in wet basis and $Y_i^*$ is the mole fraction of species 'i' in dry basis. The Pd-based oxidation catalyst was used which provided high methane conversion efficiency during flow reversal compared to the one obtained during unidirectional flow. In order to measure the performance of reverse flow catalyst experiment, three reverse flow tests were made under different engine mode (load, speed) conditions. The engine mode operation, the exhaust compositions and the engine exhaust temperatures for all the three cases are given in Table 2.2 **[16]**. Symmetric cycles were used for all the three cases with a switch time of 30s for cases 1 and 2 and 15s for case 3.

**Table 2.2 Exhaust gas properties for three cases**

| **Test Case** | **Engine mode** | | **Exhaust composition, HCs on a $C_1$ basis** | | | | | | | **Engine exhaust temp. ($°C$)** | **Mass flow rate (g/s)** |
|---|---|---|---|---|---|---|---|---|---|---|---|
| Case | Speed (rpm) | Torque (Nm) | HC | CO | NO | $O_2$ | $CO_2$ | $N_2$ | $H_2O$ | | |
| 1 | 1500 | 150 | 2139 | 1233 | 770 | 9.1 | 5.9 | 73.1 | 11.4 | 454 | 43.4 |
| 2 | 1500 | 150 | 2759 | 1264 | 737 | 9.0 | 5.9 | 73.3 | 11.3 | 449 | 42.7 |
| 3 | 1500 | 80 | 4724 | 1816 | 249 | 13.3 | 3.5 | 75.7 | 6.8 | 262 | 45.8 |

The reactor temperatures corresponding to the middle of the reactor for all the three cases, during the reverse flow operations are provided in Figure 2.8 **[16]**. It is seen in Figure 2.8 that the reactor temperatures increase with the time under flow cycling for each case. It is seen that case 2 has higher rate of increase of reactor temperature (temperature corresponding to the middle of the reactor) when compared to case 3 and case 1 and case 3 has the maximum reactor temperature. The conversion efficiency of hydrocarbon and carbon monoxide for reverse flow operation is provided in Figure 2.9 **[16]**. It is seen that the HC and CO conversion rate for cases 2 and 3 are gradual but because of a higher temperature, case 3 has the HC conversion of about 85% and CO above 90%. So, this increase in reactor temperature under flow reversal condition clearly demonstrates the presence of heat trap effect.

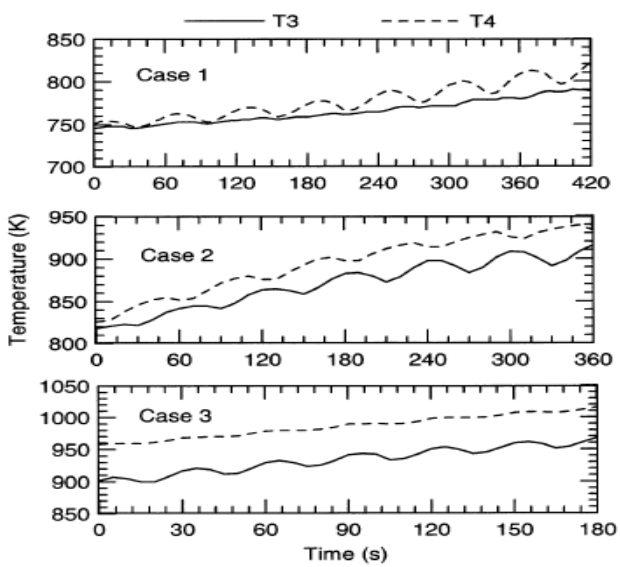


**Figure 2.8 Development of the middle reactor temperature $T_3$ and $T_4$ with reverse flow cycling**

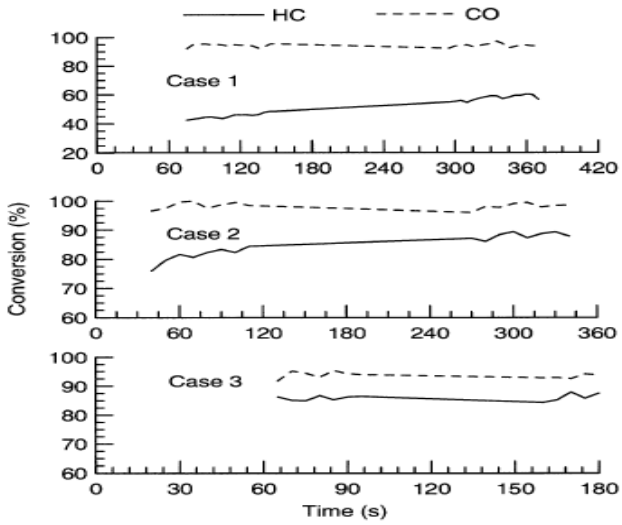


**Figure 2.9 HC and CO conversion with reverse flow cycling**

The performance of unidirectional and reverse flow operation was compared to analyze the effectiveness of reverse flow operation. Two courses of experiments were made. In the first set, the catalytic converter was initially operated in unidirectional flow mode and the temperature profile was noted, which is shown as a centerline in Figure 2.10 **[16]**. Then the engine-operating mode was changed to light load condition and that time the converter was operated in the reverse flow manner. The temperature was initially raised to 698 K and after steady state condition the maximum reactor temperature was at 850 ºK. This temperature profile is shown as the uppermost line in Figure 2.10. In the second set of experiment, the initial condition of the engine was same but after the change of engine mode, the converter was continued to operate in unidirectional mode and the temperature profile for this test was noted, which is shown as the bottom most line in Figure 2.10. The methane conversion for the first case was about 77% and the methane conversion for the second case was only 20%. This experiment effectively demonstrates that reverse flow operation is much effective compared to unidirectional mode.

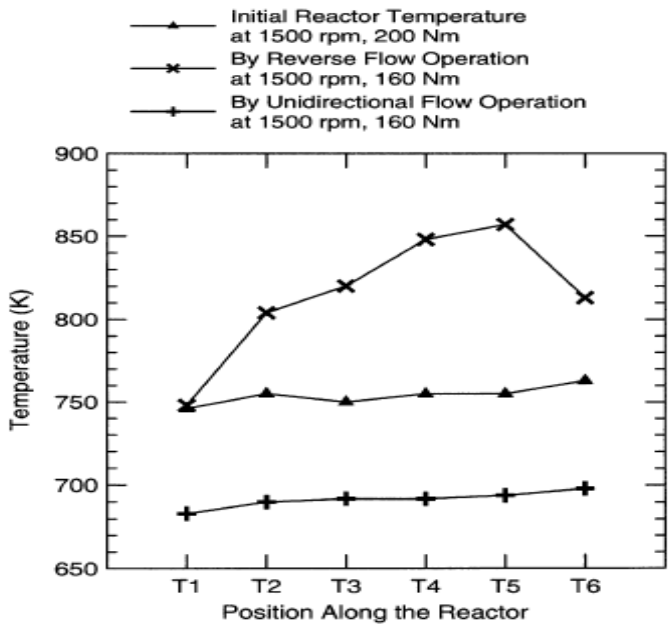


**Figure 2.10 Comparison between the unidirectional operation and the reverse flow operation**

### 2.4.4 Experiments Using Bench Flow Reactor

In this section, the results obtained in the Bench Flow Reactor (BFR) experiment are provided to show that the PFR demonstrates good methane conversion by enhancing the temperature within the reactor. As the current research would implement the work done in BFR into the real engine system it would effectively use the techniques followed in BFR.

Experimental results of BFR show that the $CH_4$ conversion is considerably improved in the flow reversal process when compared to the unidirectional flow. Figures 2.11 and 2.12 **[23]** illustrate methane conversion and the temperature profile across the catalyst for a typical experimental run at a constant reactor furnace temperature of 450$^{o}$C, a gas hourly space velocity (GHSV) of 40,000 hr$^{-1}$, and a switching time (ST) of 10 seconds. It is seen that the methane conversion increases by 47% during flow reversal when compared to unidirectional flow.

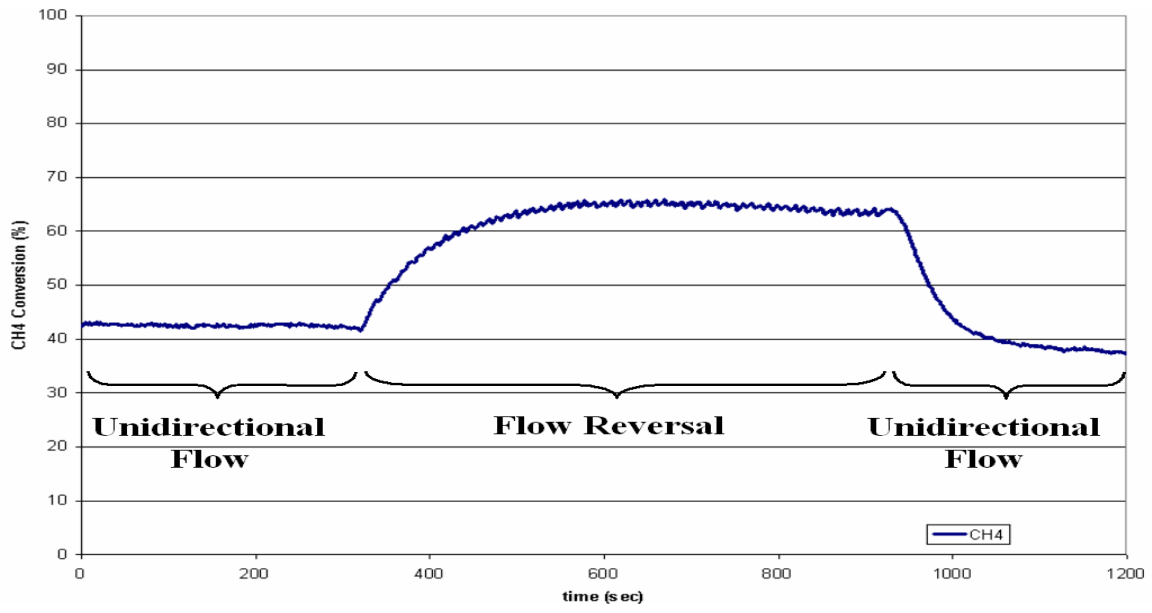


**Figure 2.11 Methane conversions at a reactor furnace temperature of 450°C, GHSV of 40,000 hr$^{-1}$, and a ST of 10s.**

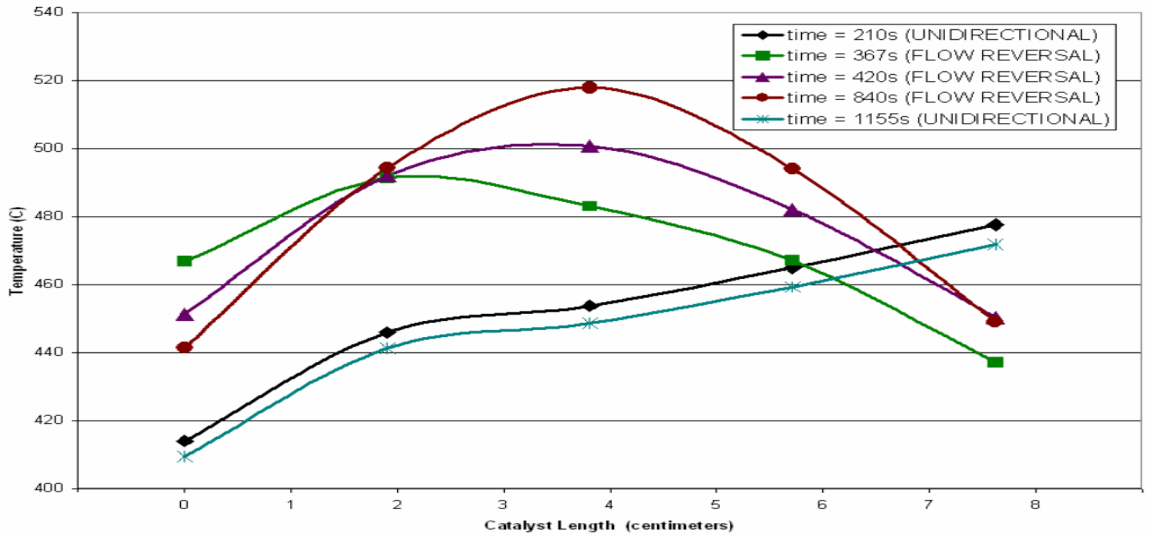


**Figure 2.12 Temperature profiles across the catalyst length at various times at a reactor furnace temperature of 450°C, GHSV of 40,000 hr$^{-1}$, and a ST of 10s.**

Experimental results also show that the effect of switching time contributes a major factor in achieving good methane conversion **[23].** The effects of methane conversion vary significantly with GHSV and temperature. Maximum methane conversion could be accomplished at lower frequency switching time while high frequency switching time provides minimum methane conversion. The minimum methane conversion at high frequency switching time is due to premature flow reversal, which results in a failure to trap large portion of heat across the catalyst. Figure 2.13 shows the effects of switching time on $CH_4$ conversion with GHSV as a parameter at a temperature of 400$^o$C. The idea of this switching time technique will be effectively used in the design of FWSDV **[23]**.

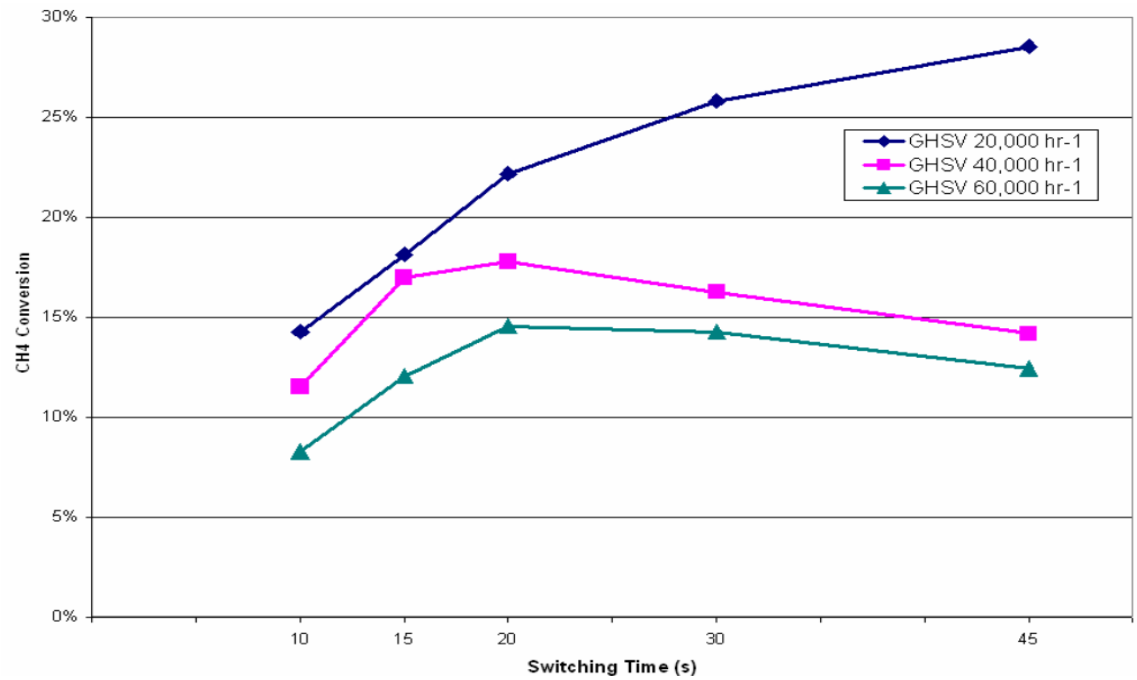


**Figure 2.13 Effects of switching time on $CH_4$ conversion with GHSV as a parameter at a temperature of 400$^o$C.**

### 2.4.5 Few Other Common Methods

Other common methods of methane oxidation include oxidation over Pt/$\gamma - Al_2O_3$ catalysts **[9],** oxidation over Pd catalyst **[14],** oxidation over Pt and Pd catalysts **[23]** etc.

Grisel et.al. have suggested the strong improvement of $CH_4$ oxidation over Pt/$\gamma - Al_2O_3$ catalysts, but it requires the small amount of addition of propane in the gas feed **[11].** As propane combustion occurs at lower temperatures relative to methane combustion, propane combustion heat may be transferred to activate the $CH_4$ dissociative adsorption over the catalyst surface, increasing methane oxidation rate at lower temperatures.

Based on the experiments, Patrick et.al. have suggested that the Pd catalyst supported on $\gamma - Al_2O_3$ exhibits the best catalytic activity in the oxidation of methane traces under lean-burn conditions. But the presence of water (even 10 vol. %) or $H_2$S in the feed causes a strong decrease of the catalytic activity of the fresh and aged Pd catalysts and the fresh Pt catalyst

Jordan et.al. have proposed that the Natural Gas Vehicles (NGV) equipped with palladium oxidation catalysts meet total hydrocarbon regulations using steady state tests and they also meet NMHC and particulate standards for the US heavy duty transient test. The presence of $SO_x$, even 1 ppm in the exhaust of a lean burn natural gas engine strongly inhibits the oxidation of $CH_4$ over a Pd containing catalyst. **[14].** But, Pd on sulfating supports, that is $\gamma - Al_2O_3$, deactivate more slowly and can tolerate more $SO_x$ because the $SO_x$ is also absorbed onto the carrier and $CH_4$ oxidation is also dramatically increased after $SO_x$ poisoning for all Pd catalysts.

Previous research efforts showed the potential for methane emission abatement by enhancing the temperature of the exhaust gases and various methods were suggested for accomplishing it. Most methods could not provide good methane conversion because the exhaust temperature was not sufficient to provide complete oxidation. Methane oxidation by Reverse Flow Catalyst (RFC) mechanism provides good methane conversion, but the complexity involved in designing RFC system, intricacy of using various control valves and numerous actuators, and the leakage of gases due to dead volume created in the passage way make the system much complicated and hence requires redesign.

## 2.5 Problem Statement and Research Objective

The objective of this research is to develop a PFR system consisting of an oxidation catalyst with the flow control device. This involves designing and fabricating a Four-Way Single Diversion Valve (FWSDV), investigating its capability to act as a flow control device, designing catalyst canisters, and associated exhaust system plumbing. The project also develops the Actuator / Rotation Control Mechanism (RCM) for the valve rotation. Some of the technical issues such as the effect of switching time, Gas Hourly Space Velocity (GHSV), and the exhaust gas temperature have also been addressed. Also, based on the results obtained in this project, suggestions regarding Supplemental Fuel Injection (SFI) are given.

# CHAPTER 3

# CONCEPTUAL DESIGN AND CALCULATIONS

It has been decided, based on the literature review and various experimental results that improved methane conversion could be achieved through Periodic Flow Reversal (PFR) mechanism using oxidation catalysts. This chapter discusses the conceptual design of PFR mechanism, its working principle, the conceptual design of FWSDV and its associated calculations.

## 3.1 Conceptual Design of Reverse Flow Catalytic Converter

The concept of the catalyst with reciprocating flow was discussed and verified both theoretically and experimentally **[16].** The working principle of RFC system is quite simple. The exhaust gas flow stream is periodically switched to obtain both forward and reverse flow along the catalyst. The idea of providing this system is to increase the temperature within the catalyst. The operation could be achieved by using four control valves that control the direction of the exhaust gas stream as shown schematically in the Figure 3.1 **[16].** In Figure 3.1 (a), the control valves 1 and 4 are opened and the control valves 2 and 3 are closed, hence the exhaust gases flow in the forward direction along the length of the catalyst, which is indicated by a set of arrows in Figure 3.1 (a). In Figure 3.1 (b), the control valves 1 and 4 are closed and the control valves 2 and 3 are opened. Hence, the exhaust gases flow in the reverse direction, which is indicated by the set of arrows. Total time of the cycle equals to the sum of the times of the forward and reverse mode and this is called the cycle time.

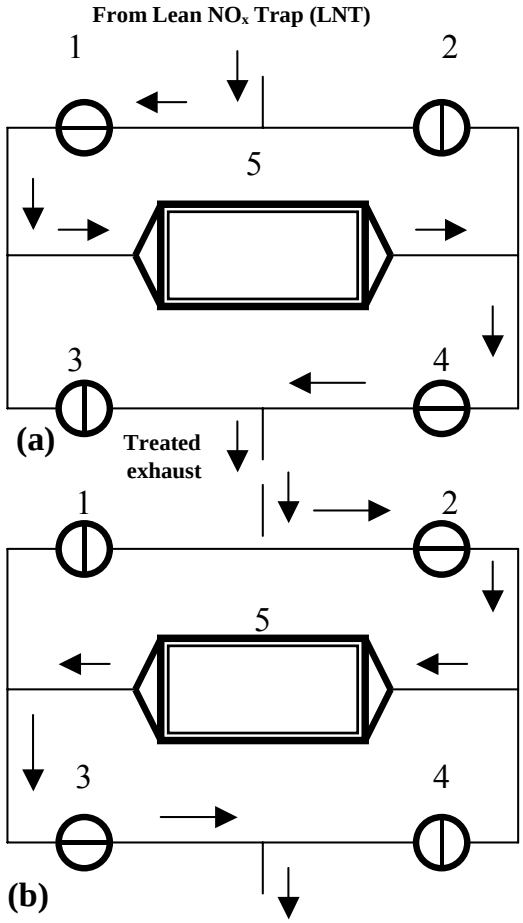


**Figure 3.1 The reverse flow catalytic converter concept**

**1,2,3,4 – Control Valve;**

**5 – Catalyst Converter**

Figure 3.2 compares the effect of unidirectional flow and reverse flow along the reactor **[16]**. Figure 3.2 clearly shows the heat trap effect within the catalyst **[18]**. During the unidirectional flow, the temperature rises slowly as the reaction commences and then, started increasing more sharply due to the exothermic reaction takes place inside the catalyst. The temperature rise, $\Delta T$, across an oxidation catalyst due to unidirectional flow is shown in Figure 3.2. During the reverse mode, the high temperature at the exit of the catalyst is used to heat up the incoming exhaust gas stream. The natural gas, primarily methane, diffuses in the oxidation catalyst and increasing the reaction rate inside the catalyst, there by the temperature is raised to the higher level. After a sufficient amount of flow reversal, a considerable amount of heat is trapped inside the oxidation catalyst, which is clearly shown by the temperature rise, $\Delta T$, with flow reversal in Figure 3.2

A number of schematics can be proposed to implement the reverse flow catalyst system. One arrangement for reverse flow is to use four shut-off valves **[24]** as shown in the Figure 3.1, but this gives complexity in the design of both the valve and the actuators. Also the cost involved in getting a single valve is very high. Additionally, a higher level of leakage of exhaust gases is also expected for "four – valves" design. As the exhaust gas stream is switched back and forth quite often, there would be a finite amount of the exhaust gas that may bypass the catalyst reactor due to the dead volume associated with the Reverse Flow Reactor (RFR). The dead volume is expressed as a volume in the flow system, where a dead-end passageway or cavity retains a portion of the exhaust gas mixture.

The improved method combining both the concepts is a "four – way single valve" system, as shown in the Figure 3.3 **[19]**. The advantages of this conceptual schematic are: relatively simple design, opportunity to minimize the leakage in comparison with four shut-off valves, reducing the complexity of having different controls, comparatively small torque required for the valve's rotor rotation and finally, reducing the over all cost. The cost of single shut off valve is $40,000 and hence the total cost for four valves is $160,000 **[4].** It has been decided to design this novel valve and fabricate it in the machine shop of the University of Tennessee.

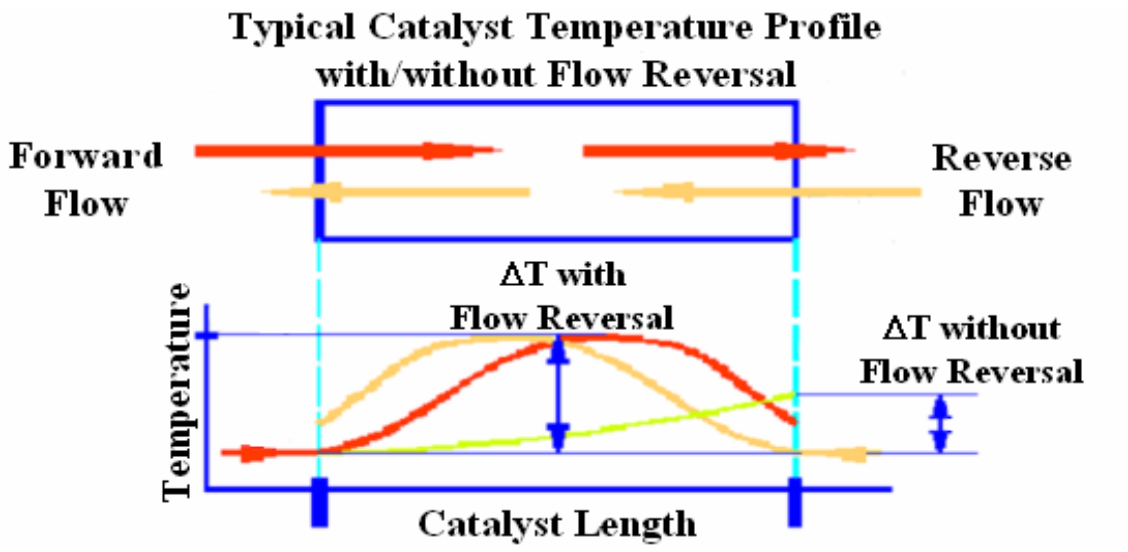


**Figure 3.2. Temperature profile across the length of the catalyst**

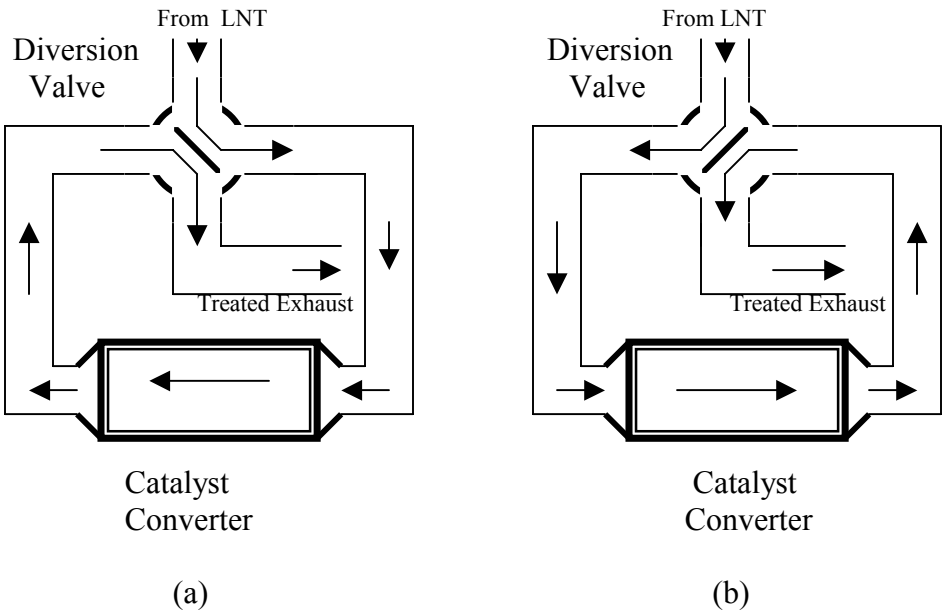


**Figure 3.3 Four – way single valve system: (a) - forward mode; (b) reverse mode**

The periodic reverse flow catalyst mechanism, showed in the Figure 3.3 consists of two main systems: catalytic converter (CC), Four – Way Single Diversion Valve (FWSDV) and exhaust pipes system (EPS).

Having found the several benefits of using a novel valve, which produces optimal system design compared to the shut off valve systems, it has been decided to develop and design the FWSDV for PFR. It is always a wise idea to develop the conceptual design first and do some mathematical calculations to make sure the original design and fabrication are conforming to the engineering principles.

### 3.2 Four – Way Single Diversion Valve Conceptual Schematic and Operation

As shown earlier, the FWSDV is an attractive and appropriate device for Reverse Flow Catalyst (RFC) design. The conceptual schematic of FWSDV realizes reverse flow with two cylinders, inner cylinder (inner ram / rotor) and outer cylinder (stator), which will be shown later in this section.

The stator has four openings, arranged at right angle: exhaust gas inlet from the LNT; two-exhaust gas outlets/inlets to/from Palladium catalyst converter and treated exhaust outlet. The rotor has four regular openings, arranged at right angle and four perforated openings, arranged at alternating 90 degree. The set of perforated openings provides smooth transition period from forward to backward flow modes, minimizes the peak backward pressure during the switch of modes, and, at the same time, prevents leakage of gases between neighboring openings of the stator. The gap between the rotor and stator's surface should be minimized to provide smooth rotation of inner cylinder inside the outer one and to prevent the leakage of exhaust gases between their two walls. The partition / diverter plate arranged in the inner cylinder divides the same into two equal volumes and separates forward and reverse flow of the exhaust gases. The inner ram, rotating inside the outer cylinder, redirects exhaust gases cyclically and provides the forward and reverse flow of exhaust gases through the catalyst. Two options of the valve

operation are proposed viz. (i) Unidirectional rotation and (ii) Multi directional rotation. The consequences of the operation of the unidirectional rotation and its corresponding flow rate/rotation diagrams are shown in the Figures 3.4 and 3.5.

### 3.2.1 Unidirectional Rotation (Figure 3.4 and Figure 3.5)

Looking at Figures 3.4 and 3.5, the total cycle of Reverse Flow Catalyst (RFC) mechanism takes four submodes. Points a, b, c and d are the starting points of each submode). Each submode takes 45° of the rotor rotation and each mode takes 180° of the rotor rotation. Consider the initial position of the rotor in Figure 3.4 (a). Let the volume of the chambers is divided into chamber "X" and Chamber "Y" as shown and the position of the chamber "X" and the chamber "Y" changes when the rotor rotates. Let us fix that before the submode '**a'** we had the **steady – state forward exhaust gas flow**, as shown in Figures 3.4 (a) and 3.5 (horizontal solid curve of the exhaust gases flow rate before point '**a'**). As can be seen from Figures 3.4 (a) and 3.5, starting with point '**a'** the submode '**a'** begins. During this submode the LNT exhaust gases flow through the stator's opening into the chamber "X" of the rotor's volume through the regular opening of the rotor, which is gradually replaced by the perforated one, and exit through another regular opening of the rotor that is gradually replaced by another perforated one. This period is named as a transition in Figure 3.5 because of the rotor rotation. At the same time 100% forward flow of the exhaust gases is maintained. Starting with point '**b'** (submode '**b'**) the LNT exhaust gases flow into both chambers of rotor (chamber "X" and chamber "Y"), which is not shown in the figure, through the perforated and regular rotor's openings correspondingly and flow out (via chamber "X" and chamber "Y") through the corresponding openings both in forward and reverse directions. It means that during this short period of time the flow bypasses the catalyst. At point '**c',** the initial direction of the exhaust gases flow is completely switched from the forward to the reverse one (as shown in Figures 3.4 and 3.5, (Submode c)).

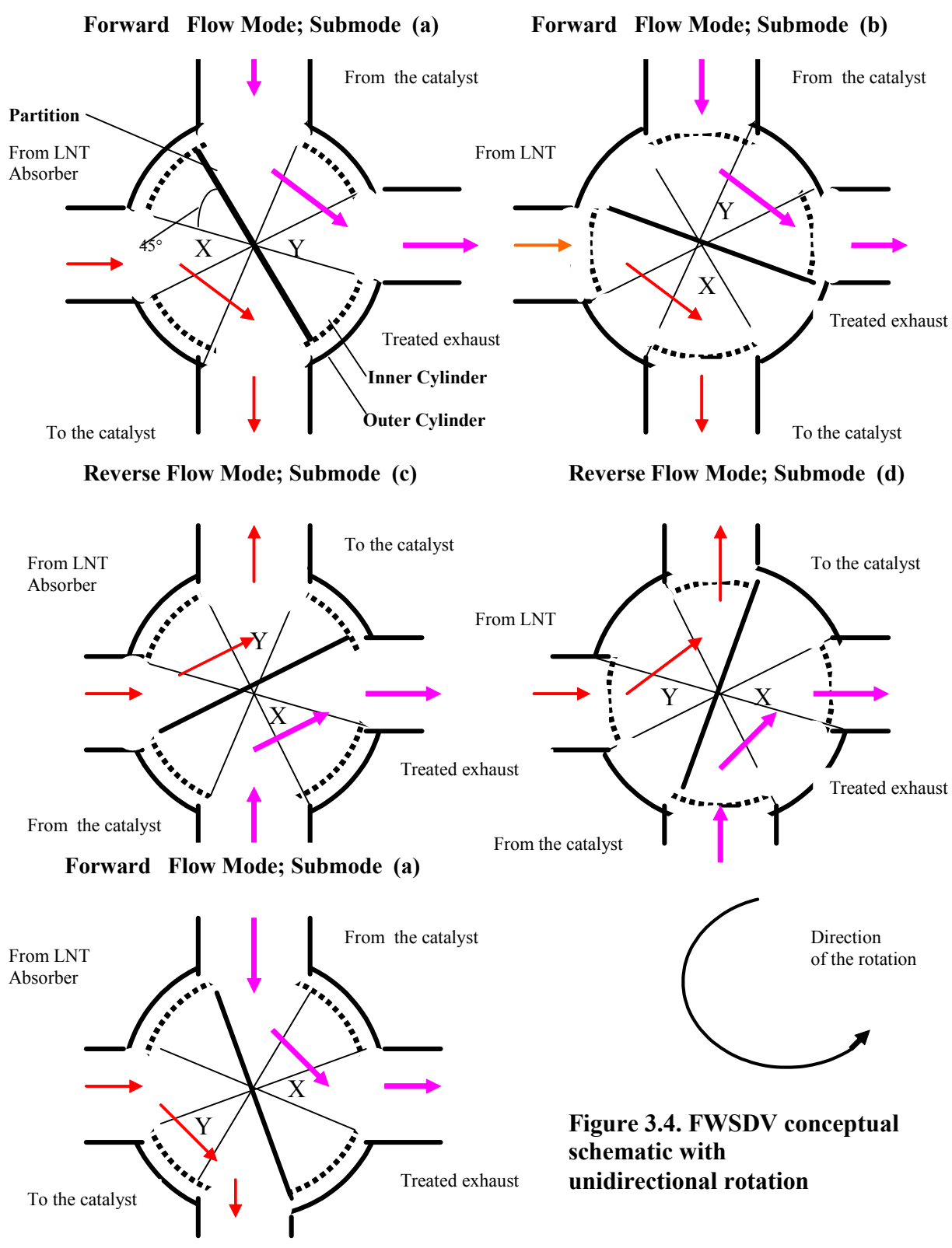


**Figure 3.4. FWSDV conceptual schematic with unidirectional rotation**

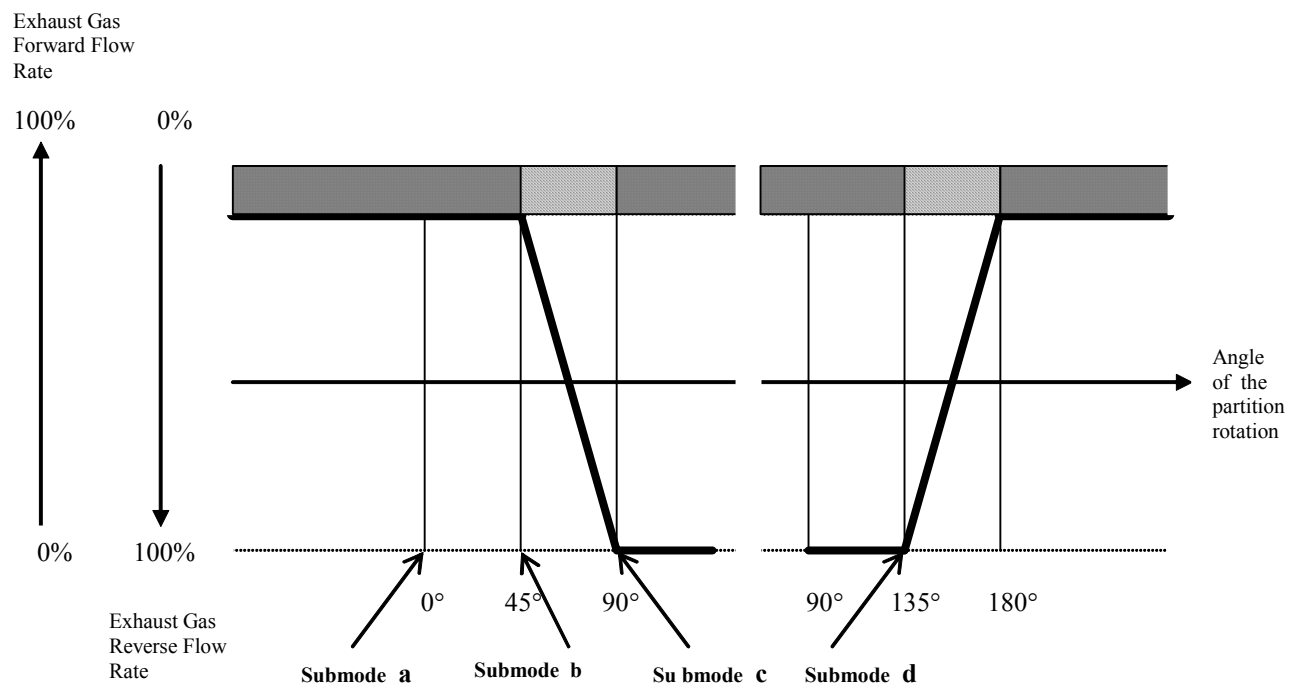


**Figure 3.5 Flow rate/rotation diagram for FWSDV with unidirectional rotation**

So, the period of **steady – state reverse exhaust gas flow** begins. The duration of this regime depends on the requirements for the effective $CH_4$ oxidation in the RFC mechanism. After the end of the **steady – state** reverse exhaust gas flow regime, the new **transition period** begins.

Starting with point '**c'** the rotor resumes its rotation in the same direction. The LNT exhaust gases come through the regular opening of the rotor, which is gradually replaced by the perforated one, entering into the chamber "Y" and come out through the regular opening that is gradually replaced by another perforated one. The treated exhaust gases come into the chamber "X" through the regular opening of rotor, which is gradually replaced by the perforated one and go out to the treated exhaust outlet through another regular opening that is gradually replaced by another perforated one. At the same time 100% reverse flow of the exhaust gases is maintained. Starting with point'd' **(**submode 'd') the LNT exhaust gases come into both chambers (Chambers "X" and "Y") of the rotor through the perforated and regular rotor's openings correspondingly and come out from these chambers through the corresponding openings both in forward and reverse directions. It means that during this short period of time the exhaust gas flow bypasses the catalyst.

Higher speed of rotation of the rotor minimizes the leakage and the switching time should be given in such a way to provide good methane conversion. Experiments of flow reversal using BFR shows that at a reactor temperature of 400 ˚C, GHSV of 20,000 hr-1, a maximum methane conversion is obtained at lower frequency switching times (30 and 45 seconds), which has already been discussed in section 2.4.4 and was shown figure 2.13 **[23].** But high frequency switching times (10-20 seconds) gives minimum methane conversion, which is due to premature flow reversal. The premature flow reversal temperature profile is shown in Figure 3.6 **[23].** It was also noted that when the switching duration is maintained correctly, maximum temperature profile would be obtained across the length of the catalyst. Figure 3.7 shows the switching time of 30 seconds with GHSV of 20,000 hr-1 and reactor temperature of 400 C **[23]**.

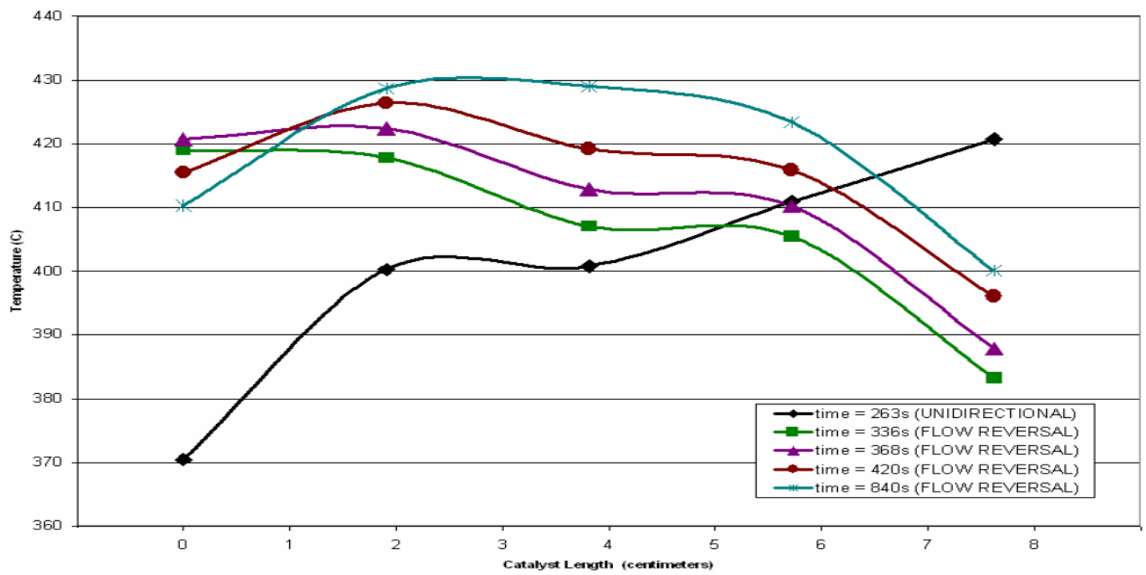


**Figure 3.6 Temperature profile across the catalyst at a reactor furnace temperature of 400°C, a GHSV of 20,000 $hr^{-1}$, and a ST of 10s at various experimental run times.**

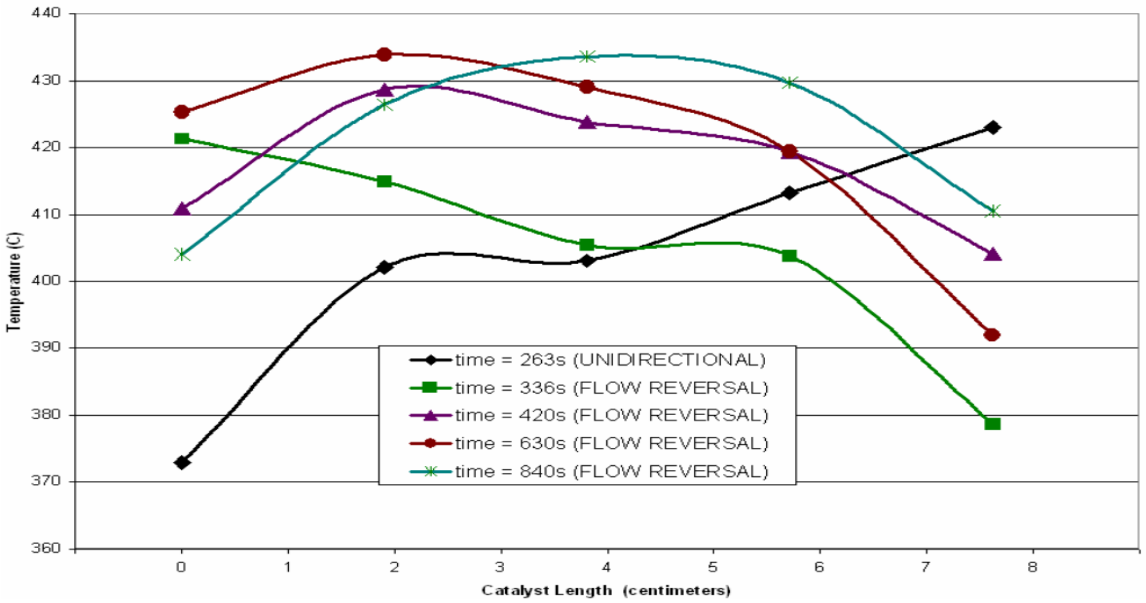


**Figure 3.7 Temperature profiles across the catalyst at various times during an experimental run at a reactor furnace temperature of 400°C,GHSV of 20,000 $hr^{1}$, and a ST of 30s.**

At the end of the submode‘d’ the reverse direction of the exhaust gases flow is completely switched to the forward one and the **steady – state forward exhaust gas flow regime** begins. Again the duration of this regime depends on the requirements for the effective $CH_4$ oxidation in the PRF catalyst mechanism. After the end of this regime rotor resumes its rotation in the same direction and submode ‘**a’** begins.

### 3.2.2 Multidirectional Rotation (Figures 3.8and 3.9)

The consequences of the operation of the multidirectional rotation and its corresponding flow rate/rotation diagrams are shown through Figures 3.8-3.9. This option of the FWSDV operation differs from the previous one from the beginning of the submode ‘**c’**. Starting from point ‘**c’** the rotor resumes its rotation in the opposite direction that changes a bit the rest part of the Flow rate/rotation diagram.
The main difference between Option 1 and Option 2 is:

For Option 1 the duration of the steady **– state forward and reverse exhaust gas flow regimes** is the same (if the velocity of the rotor’s rotation is not changed during reverse flow catalyst mechanism operation).

For Option 2 the duration of the steady **– state reverse exhaust gas flow regime** is less than duration of the **forward one** by 45°. It seems not to be very critical since the switching time of the flow modes (duration time of the forward and reverse flow modes) is much less than the duration of the **steady – state forward or reverse exhaust gas flow regimes**. Another reason to investigate Option 2 is a more simple design of the valve’s drive that uses the reciprocating principle in comparison with rotational one.

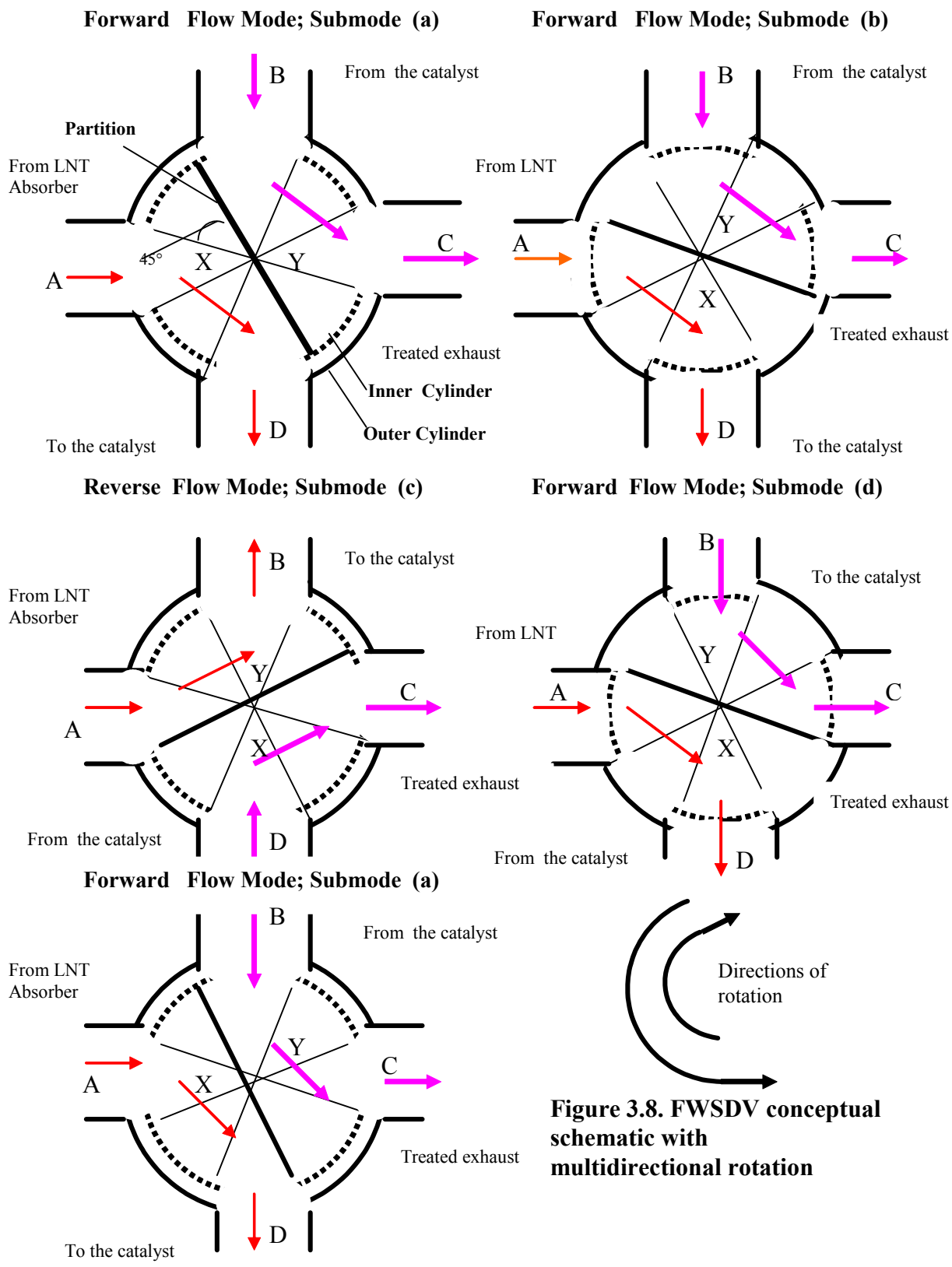


**Figure 3.8. FWSDV conceptual schematic with multidirectional rotation**

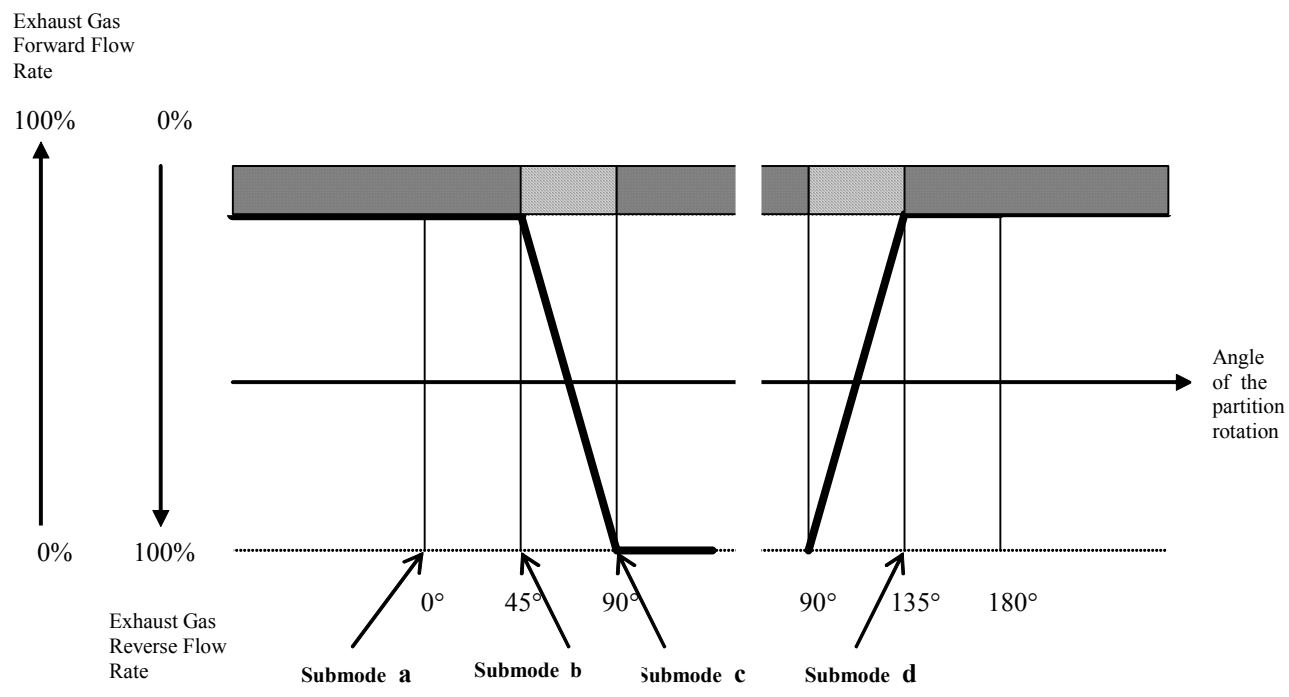


**Figure 3.9 Flow rate/rotation diagram for FWSDV with multidirectional rotation**

## 3.3 Calculations

The conceptual design of the FWSDV and the PFR system aids in developing the actual system. It is always wise from an engineering point of view to develop mathematical calculations in order to make sure that the real design conforms to all the requirements. It was discussed earlier that the Palladium based oxidation catalyst with alumina wash coat provides a good performance for methane oxidation and also it is suggested in the earlier chapter that two such catalysts are required for the complete oxidation of methane. The engine out exhaust gas flow rate, the exhaust temperature, both at the peak power and at the peak torque are the known parameters. This project uses the standard Pd oxidation catalyst brick of diameter 9.5 inches and the length 6 inches. For the given volume of the catalyst brick, the volumetric flow rate of the exhaust gas and the maximum catalyst space velocity, the number of catalysts required is found out as follows:

### 3.3.1 Calculations for Catalyst Dimensions

Calculations are made to support the dimensions of the catalyst as well as the number of catalysts required to attain PFR. Reverse Flow Catalyst Mechanism should be sized for the testing with 8.3-liter C Gas Plus (CG-280) natural gas engine that has the properties as given in Table 3.1.

The standard oxidation palladium catalyst brick was chosen for the design with the standard dimension of length $L_c$ = 6 inches and diameter $D_c$ = 9.5 inches. The maximum space velocity for the given catalyst is SV = 50,000 $hr^{-1}$. Based on the maximum space velocity, the minimum residence time / the standard residence time is calculated as $T_{rs}$ = 1 / 50,000 = 0.00002 hr.

Now, it is required to find the original residence time for two catalysts for both peak power and peak torque condition.

**Table 3.1 Exhaust gas properties of C 8.3 Gas Plus Engine**

| Parameters | Symbols | Units | Peak Power | Peak Torque |
|---|---|---|---|---|
| Exhaust gas flow rate | $V_e$ | Liter/sec | 817 | 539 |
| Exhaust gas temperature | $T_e$ | $^0C$ | 643 | 587 |
| Exhaust pipe diameter | $D_e$ | Inches | 4 | 4 |

### 3.3.2 Residence Time for the Peak Power Condition

The exhaust gas flow rate under peak power condition is 817 liter /sec and the volume of single catalyst brick is 0.006966 cubic meters. Now, the original space velocity corresponds to the exhaust temperature under peak power condition is $SV_{916.15} = 817 \times 10^{-3} \ / \ 0.006966 = 422{,}222.22 \ \ hr^{-1}$. Recalculation of the original space velocity for the standard temperature of $25\,°C$ / 298.15 K gives:

$$SV_{298.15} = SV_{916.15} / (\rho_{298.15} / \rho_{916.15}) \tag{3.1}$$

The equation of state for an ideal gas is given by

$$P\,V = n\,R\,T \tag{3.2}$$

where P is the pressure of the gas in Newton per square meter, V is the volume of the gas in cubic meters, n is the number of moles, R is the Universal gas constant in Joules per moles per Kelvin and T is the temperature in Kelvin. Dividing equation 4.1 by mass would give

$$P\,v = \frac{nRT}{M} \Rightarrow P = \rho\ R\ T \tag{3.3}$$

where v is the specific volume which is the ratio of Volume and mass and $\rho$ is the density of gas. From equation (3.3),

$$P_{916.15} = \rho_{916.15}.R.T_{916.15} \text{ and } P_{298.15} = \rho_{298.15}.R.T_{298.15} \tag{3.4}$$

As pressure of the exhaust gas is constant, equation (3.4) becomes,

$$\rho_{916.15}(916.15) = \rho_{298.15}(298.15) \tag{3.5}$$

$$\Rightarrow \rho_{298.15} / \rho_{916.15} = 916.15 / 298.15 \tag{3.6}$$

Plug in equation (3.6) into equation 3.1 gives

$$SV_{298.15} = SV_{916.15} /(916.15\ / 298.15) = 137{,}407.144\, hr^{-1} \tag{3.7}$$

The original residence time corresponding to the standard temperature is 1 / 137,407.144 $hr^{-1}$ = 0.000007277 hr = 0.026197 sec, which is less than the standard residence time for the catalyst brick (0.00002 hr = 0.072 sec).

In the case of the arrangement of two catalysts in line, the original space velocity equals to $SV_{298.15(2)} = SV_{298.15}/2 = 68{,}703.572\, hr^{-1}$ and the original residence time is $T_{or}$ = 1 /68,703.572 = 0.000014555 hr = 0.052398 sec, which is still less than the standard residence time for the catalyst bricks arranged in line, which is 0.00002 hr = 0.072 sec, but it is very close to the standard residence time. This would provide more residence time, based on the above calculation, for the exhaust gases to react with the catalysts, increase the chemical reaction, which would elevate the temperature of the exhaust gases.

### 3.3.3 Residence Time for the Peak Torque Condition

The space velocity corresponds to the peak torque condition is,

$$SV_{peaktorque} = \frac{volumetricflowrate}{volumeofcatalyst}$$

$$SV_{peaktorque} = \frac{539 \times 10^{-3}}{0.006966} = 278{,}552.97\ hr^{-1} \tag{3.8}$$

Recalculation of original space velocity for the standard temperature of 25 °*C* / 298.15 K gives:

$$SV_{298.15} = SV_{860.15}/(860.15\ /\ 298.15) = 96{,}543.1884\, hr^{-1} \tag{3.9}$$

The original residence time could be calculated as 1/96,543.1884 = 0.000010358 hr (0.037288 sec), which is again less than standard residence time for the catalyst brick.
In the case of arrangement of two catalysts in line, the original space velocity equals to

$$SV_{298.15(2)} = SV_{298.15}/2 = 48{,}271.5942\ hr^{-1} \tag{3.10}$$

and the original residence time is $T_{or}$ = 1 / 48,271.5942 = 0.000020716 hr = 0.07457 sec, which is more than the standard residence time for the catalysts bricks arranged in line (0.00002 hr = 0.072 sec).

The conclusion is that the two catalysts of 9.5 inches diameter and 6 inches length would provide the appropriate methane oxidation both for peak power and peak torque conditions.

## 3.4 Dimensions for the Rotor's and Stator's Openings

The FWSDV is designed in such away that it has to have four openings through which the exhaust gases flow in order to make flow reversal reaction. Taking into account that the diameter of the engine exhaust pipe downstream of turbo charger is 4 inches, following to the valve's schematic, shown in the Figures 3.4 and 3.8 one can expect that the diameter of the FWSDV could reach up to 11-12 inches. In order to decrease the size or to be more precise, to reduce the diameter of the FWSDV, two approaches were considered.

1. Decreasing the area of the openings into two times
2. Switching the circular shape of the openings to the elliptical ones

The exhaust pipe has the cross section area equal to 12.56 $in^2$ or 81,032 $cm^2$. The velocity of the exhaust gases could be estimated for the peak power regime that corresponds to the maximum flow rate of the exhaust gases, which is $v_{exh} = \frac{vol.flowrate}{areaofpipe} = \frac{0.817}{0.0081} = 100.8$ m/s.

Following the first approach, the cross section area of the valve's manifolds should be decreased into two times, which would be roughly 40.5 $cm^2$. So, correspondingly the diameter of the exhaust manifold would be 7.2 cm.

The second approach is to switch the circular shape into the elliptical ones. So, the dimensions of major axis and minor axis of the elliptical openings having the cross section of 40.5 $cm^2$ are calculated to be 10.8 cm and 4.8 cm respectively. As the cross section area is decreased by two times, the velocity through the exhaust pipe increases correspondingly by two times, which would make the velocity as 201.6 m/s. The FWSDV rotor has four perforated openings as shown in Figure 3.4. As will be shown later each perforated opening consists of 43 circular holes with diameter of 0.8 cm. So the velocity of exhaust gases through the perforated openings is calculated to be:

$$v_{op} = 4 \times \frac{817 \times 10^{-3}}{\pi (0.0081)^2 \times 43} = 368.717 \text{ m/s.}$$

The thermodynamic calculations of the fuel-lean combustion of natural gas with air with an equivalence ratio of 1.7 was performed in order to estimate the sound velocity of the exhaust gases and compare with the calculated velocity of the gases that pass through the perforated opening. The temperature, molecular mass and the specific heat ratio of the combustion products provided by **Dr. Naoumov** are provided in Figure 3.10.

The following results of the thermodynamic calculations were used for the estimation of the sound velocity:

Temperature of combustion products: T=1642 K;

The Universal Gas Constant is R = 8.314 J / mol-K

Molecular mass of combustion products: $\mu$=28.2

Specific heat ratio: $\gamma$=1.272

Taking into account the relaxation of the combustion products temperature up to 643 $^0$C ($\approx$ 916.25 K), the sound velocity could be estimated from:

$a = (\gamma \times R \times T/\mu)^{1/2}$ = **595.62 m/s**,

So, the velocity of the exhaust gases in the perforated opening will not exceed the velocity of sound.

As a result of this analysis following dimensions for the stator's and rotor's regular and perforated openings were established:

Ellipse's axes: 108 mm × 48 mm;

The diameter of the holes in the perforated opening: 8mm;

The quantity of holes: 43.

These dimensions became the base for the estimation of the rough outer diameter of the valve that assumes roughly 167 mm

Appendix „A"

Software for the calculation of thermodynamic parameters of combustion products.

```
 ZADANNII NABOR PRIZNAKOV:
 TD
 ZADANNII NABOR PRIZNAKOV:
 EK
*******************************
          GOMOGENNIE PRODUKTI SGORANIA
0„AB<EH^E = 0.3000E+07(H/M2)
 ZADAN NABOR KOMPONENTOV:
 AR              ;O              ;H              ;N              ;E
;C               ;
 H1O2            ;O1H1           ;H2             ;O2             ;H2O1
;C1O1            ;
 C1O2            ;C1H4           ;C2H2           ;C2H4           ;C2H6
;C1H3            ;
 C1H2            ;C1H1           ;C2H1           ;C2H3           ;C2H5
;H2C1O1          ;
 H1C1O1          ;H1C2O1         ;N2H2           ;N2H1           ;N1H3
;N1H2            ;
 N1H1            ;H1N1O1         ;H1C1N1         ;C1N1           ;N1C1O1
;N1O1            ;
 N1O2            ;N2O1           ;C1H1O1PE1      ;H3O1PE1        ;N1O1PE1
;C3H8            ;
 C3H7            ;C3H6           ;N2             ;O2E1           ;O1H1E1
;
 *  *  *  *  *  *  *  *  *  *  *  *  *  *  *  *  *  *  *  *  *  *  *  *  *  *  *  *
*  *  *  *  *  *  *  *  *  *  *
        TERMODINAMICHESKI RASCHET
        ---------------------------------
 KOEF-T IZBITKA OKISLITELA(PERVAIA ZONA)= 0.1700E+01
 ENTALPIA OKISLITELA= 0.10460E+01KDG/KG
 USLOVNAIA FORMULA OKISLITELA:
 O        0.14480E+02
 N        0.53910E+02
 AR       0.32040E+00
 ENTALPIA GORIUCHEGO=-0.46547E+04KDG/KG
 USLOVNAIA FORMULA GORIUCHEGO:
 C        0.10000E+01
 H        0.40000E+01
 ENTALPIA TOPLIVA=-0.15282E+03KDG/KG, MOLECUL.VES TOPLIVA= 0.48545E+03KG/KMOL
 USLOVNAIA FORMULA TOPLIVA:
 AR         0.15046E+00
 O          0.68000E+01
 H          0.40000E+01
 N          0.25317E+02
 C          0.10000E+01
 PARAMETRI RASCHETA:
 RAVNOVESNII SOSTAV PRODUCTOV SGORANIA V MOLNIH DOLIAH
 PORIADOK KOMPONENTOV:
 AR              O               H               N               E
 C               H1O2            O1H1            H2              O2
 H2O1            C1O1            C1O2            C1H4            C2H2
 C2H4            C2H6            C1H3            C1H2            C1H1
 C2H1            C2H3            C2H5            H2C1O1          H1C1O1
 H1C2O1          N2H2            N2H1            N1H3            N1H2
 N1H1            H1N1O1          H1C1N1          C1N1            N1C1O1
 N1O1            N1O2            N2O1            C1H1O1PE1       H3O1PE1
 N1O1PE1         C3H8            C3H7            C3H6            N2
```

$\times 10^1$

equivalence ratio

$0.1700 \times 10$

Chemical comp. of air

Chemical comp. of gas

Chemical composition of air + gas for $\alpha = 1.7$.

**Figure 3.10 Thermodynamic data for the combustion mixture**

```
O2E1                O1H1E1
DAVLENIE(N/M2),TEMPERATURA(K),MOLECUL.VES(KG/KMOL),
RAVNOVESNAIA SKOROST ZVUKA(M/S),
UDELN.ZAMOROZ.TEPLOEMKOST PRI P=CONST(KDG/KG K),
UDELN. RAVNOVESN. TEPLOEMKOST PRI P=CONST(KDG/KG K),
OTNOSHENIE CP/CV, PROIZVEDENIE IZOBAR.KOEF-TA RASHIRENIA
NA TEMPERATURU, PROIZVEDENIE IZOTERM.KOEF-TA SZATIA NA P;
KOEF-T PRANDTL, ZAMOROZ.TEPLOPROVODNOST(WT/M*K),
RAVNOVESN. TEPLOPROVODNOST(WT/M K),
KOEF-T DINAMICHESKOI VIAZKOSTI(N*S/M2)
KAMERA SGORANIA
0COCTAB:
0.87433E-02 0.12263E-05 0.13700E-07 0.26262E-12 0.85701E-16
0.16822E-28 0.63424E-06 0.89956E-04 0.79636E-06 0.80579E-01
0.11617E+00 0.12786E-05 0.58107E-01 0.44423E-26 0.10000E-29
0.10000E-29 0.10000E-29 0.37855E-26 0.29503E-25 0.24995E-29
0.10000E-29 0.10000E-29 0.10000E-29 0.22793E-16 0.46718E-13
0.62123E-24 0.58010E-19 0.17712E-08 0.78611E-12 0.89281E-13
0.13327E-12 0.23618E-08 0.62548E-18 0.80950E-20 0.35558E-17
0.14637E-02 0.18961E-04 0.43000E-06 0.16579E-24 0.15329E-16
0.34472E-15 0.10000E-29 0.10000E-29 0.10000E-29 0.73482E+00
0.12831E-15 0.14604E-15
0.3000000D+07
0.16420E+04; 0.28209E+02; 0.78464E+03; 0.13556E+01; 0.13786E+01;
0.12721E+01; 0.10003E+01; 0.10000E+01;
0.69497E+00; 0.12822E+00; 0.13040E+00; 0.65736E-04;
* * * * * * * * * * * * * * * * * * * * * * * * * * * * * *
END TERM
KIT(2)=          0
NB=          47
END MAINTL
```

**Figure 3.10 Continued**

### 3.5 Permissible Leakage Bypassing the Catalysts

The oxidation catalyst is developed to create an exothermic reaction thereby reducing methane emission from engine exhaust. The FWSDV was used to switch the flow through oxidation catalyst thereby enhancing reaction rate. The exhaust gases while flowing through FWSDV, may bypass the catalyst and hence it is very crucial to find out the leakage rate of exhaust gases that could be allowed to bypass the catalyst. The exhaust composition (HC and CO) downstream of the LNT ( $NO_x$ absorber) is required in order to determine the leakage HC and CO that could be allowed to bypass the oxidation catalyst. Before the actual calculation is performed, the allowable emissions for HC and CO were found from the emission standard set for Non-road Diesel / Natural gas engines. The allowable emission for HC and CO in gms/hp-hr for natural gas engines is taken from Tier 4 emission standards. The Tier 4 says that the emission reductions can be achieved through the use of control technologies – including advanced exhaust gas after treatment and the allowable limits are given as follows:

Tier 4 Standards

The Tier 4 emission standards – to be phased-in from 2008-2015-are listed in Table 3.2 **[5]** for engines below 560 kW / 750 hp. These standards introduce substantial reductions of $NO_x$ (for engines above 56 kW) and PM (above 19 kW), as well as more stringent HC limits. CO emission limits remain unchanged from the Tier 2-3 stage.

For the current project, we are interested in the emission standards of HC and CO,

a. HC → 0.14 gms/hp-hr.
b. CO → 2.6 gms / hp-hr (from the table above)

**Table 3.2 Tier 4 Emission Standards for Engines up to 560 kW**

| Tier 4 Emission Standards – Engines up to 560 kW, g/kWh (g/bhp-hr) | | | | | | |
|---|---|---|---|---|---|---|
| Engine Power | Year | CO | NMHC | NMHC + $NO_x$ | $NO_x$ | PM |
| KW <8 (hp<11) | 2008 | 8.0 (6.0) | - | 7.5 (5.6) | - | 0.4[a] (0.3) |
| 8 ≤ kW < 19 (11 ≤ hp<25) | 2008 | 6.6 (4.9) | - | 7.5 (5.6) | - | 0.4 (0.3) |
| 19 ≤ kW<37 (25 ≤ hp<50) | 2008 | 5.5 (4.1) | - | 7.5 (5.6) | - | 0.03(0.22) |
| | 2013 | 5.5 (4.1) | - | 4.7 (3.5) | - | 0.03(0.022) |
| 37 ≤ kW<56 (50 ≤ hp<75) | 2008 | 5.0 (3.7) | - | 4.7 (3.5) | - | 0.3(0.22) |
| | 2013 | 5.0 (3.7) | - | 4.7 (3.5) | - | 0.03(0.022) |
| 56 ≤ kW<130 (75 ≤ hp<175) | 2012 2014[c] | 5.0 (3.7) | 0.19 (0.14) | - | 0.4 (0.30) | 0.02 (0.015) |
| 130 ≤ kW ≤ 560 (175 ≤ hp ≤ 750) | 2011 2014[d] | 3.5 (2.6) | 0.19 (0.14) | - | 0.4 (0.30) | 0.02 (0.015) |

a- hand-star table, air-cooled, DI engines may be certified to Tier 2 standards thru 2009 and to an optional PM standard of 0.6 g/kWh starting in 2010

b- 0.4 g/kWh (Tier 2) if manufacturer complies with the 0.03 g/kWh standard from 2012

c- PM/CO: full compliance from 2012; NOx/HC: Option 1 (if banked Tier 2 credits used)—50% engines must comply in 2012-2013; Option 2 (if no Tier 2 credits claimed)—25% engines must comply in 2012-2014, with full compliance from 2014.12.31

d- PM/CO: full compliance from 2011; NOx/HC: 50% engines must comply in 2011-2013

Data sets correspond to the engine speed of 1800 rpm are obtained and the leakage calculations are made for various engine speeds (10%, 25%, 50%, 75% and 100%). Leakage rate, both volumetric and mass flow rate, for 100% engine load is provided for sample. The engine is allowed to run at 1800 rpm and the exhaust composition downstream of LNT (Lean $NO_x$ Trap) is taken. As we are interested in finding out the leakage rate for Hydrocarbon (HC) and Carbon monoxide (CO), their corresponding compositions downstream of LNT are found, which are HC = 1117 ppm and CO = 546 ppm. Allowable emissions for Hydrocarbon (HC) and Carbon monoxide (CO) by Federal Regulation are 0.14 gms/hp-hr and 2.6 gms/hp-hr respectively. As the engine runs at 252 hp, the amount of Hydrocarbon (HC) and Carbon monoxide (CO) allowed by Federal Regulation in terms of grams per minute is calculated as HC = 0.588 $\frac{gms}{\min.}$ and

CO = 10.92 $\frac{gms}{\min.}$ respectively. Now, it is required to find out the amount of HC and CO that are allowed to bypass the catalyst for the same engine load and speed. The calculation involves various steps including determining the volumetric flow rate, temperature, partial pressure, density and mass flow rate of the exhaust compositions.

**Step 1: Determining the Exhaust flow rate of the gas from the engine**

Knowing the diameter and the length of catalyst, the total volume for 2 catalysts is found to be 0.49197 cubic feet. The space velocity corresponding to 1800 rpm and 100% engine load is 68,409 $hr^{-1}$. Now, the Exhaust flow rate = space velocity X Volume of catalyst, which is 68,409 X 0.49197 = 560.9196 cubic feet per minute.

**Exhaust flow rate = 15.88 cubic meter per minute (1 feet = 0.3048 m).**

**Step 2: Partial pressure of HC and CO**

The pressure of the exhaust composition down stream of the LNT is 2 $psi_{(g)}$.. So the partial pressure of Hydrocarbon (HC) and Carbon monoxide (CO) is calculated as follows:

$pp_{(HC)}$ = 16.7psia x 1117 x $10^{-6}$ = 0.01865psia = **128.587** $N/m^2$

$pp_{(CO)}$ = 16.7psia x 546 x $10^{-6}$ = 0.00912psia = **62.880** $N/m^2$

**Partial pressure of HC = 128.587** $N/m^2$

**Partial pressure of CO = 62.880** $N/m^2$

**Step 3: Density of HC and CO**

The density of HC is $\rho_{HC} = \dfrac{Pp(HC)}{R_{HC} \times T}$ and the density of CO is $\rho_{CO} = \dfrac{Pp(CO)}{R_{CO} \times T}$.

$R_{HC}$ = 8.314472 (J/mol-K) / 16 (gms/mol) = 0.5197 J/gms-K
$R_{CO}$ = 8.314472 (J/mol-K) / 28 (gms/mol) = 0.297 J/gms-K

The temperature of HC and CO downstream of LNT is 873 K and the gas constants for HC and CO are 0.6395 J/gms- K and 0.297 J/gms- K respectively.

Now,

a. Density of HC is $\rho_{HC} = \dfrac{128.587}{0.5197 \times 873}$ = **0.2834 grams per cubic meter**.

b. Density of CO is $\rho_{CO} = \dfrac{62.880}{0.297 \times 873}$ = **0.2425 grams per cubic meter**.

**Step 4: Mass flow rate for HC and CO**

a. Mass flow rate of HC is $\dot{m}_{HC}$ = $\rho_{HC}$ x Exhaust flow rate from the engine

= 0.2834 x 15.88

= **4.50 grams per minute**

b. Mass flow rate of CO is $\dot{m}_{CO} = \rho_{CO}$ x Exhaust flow rate from the engine

= 0.2425 x 15.88

= **3.85 grams per minute**

**Step 5: Leakage rate**

It is required that the allowable mass flow rate of the exhaust gas composition should be greater than or equal to the mass flow rate of the gas coming out of the system, which is given by

$$\dot{m}^*_{\text{limit}} \geq \dot{m}^*_{\text{through the catalyst}} + \dot{m}^*_{\text{past the catalyst}}$$

$$\geq (1 - \text{Conversion efficiency})\ \dot{m}^*_{engine} + \dot{m}^*_{(leakage)}$$

a. Leakage rate for HC:

$$\dot{m}^*_{(leakageHC)} \leq \dot{m}^*_{\text{limit}} - (1 - \text{conversion efficiency})\ \dot{m}^*_{engine}$$

$$\leq 0.588 - (1 - 0.90) \text{ x } 4.50$$

$\leq$ **0.138 grams per minute**

b. Leakage rate for CO:

$$\dot{m}^*_{(leakageCO)} \leq \dot{m}^*_{law} - (1 - \text{conversion efficiency})\ \dot{m}^*_{engine}$$

$$\leq 10.92 - (1 - 0.90) \text{ x } 3.85$$

$\leq$ **10.535 grams per minute**

Thus, it is calculated that the maximum leakage that is allowed to by pass the catalyst for Hydrocarbon **(HC) is 0.138 grams** per minute and that of Carbon monoxide **(CO) is 10.535 grams per minute.** Therefore, HC is the controlling factor from the engine exhaust.

### 3.6 Maximum Momentum Acted Against Valve's Partition

As the exhaust gases from the LNT flowing through the control valve impact directly the partition plate of FWSDV it is necessary to find the maximum momentum that the valve's partition plate could withstand based on the pressure of the exhaust gases. The normal operation of the valve will be in such away that the exhaust gas stream impacts on both the sides of the partition plate with the same pressure and hence there is no possibility of deformation / any failure. The calculation of maximum momentum for the valve's partition is made to ensure that the given system will work without failure even in any extreme critical situation. If we assume that the partition plate is experiencing the impact equally, then this problem could be considered as a beam supporting a uniform distributed load as shown in Figure 3.11. Now, the maximum moment '$M_b$' in a simple beam supporting a uniform load occurs at the centre and is $M_b = \frac{WL^2}{8}$, where 'W' is the load per unit length in 'N/m', and 'L' is the span in 'm' **[13]**.

For the current problem, the area of the partition plate = 6.457" x 6.105" = 39.4199 $in^2$

**A = 0.0254** $(m^2)$

The pressure of the gas coming out from the engine exhaust is 2psi(g) = 16.7 psi(a)

**P = 115,142.447** $(N/m^2)$

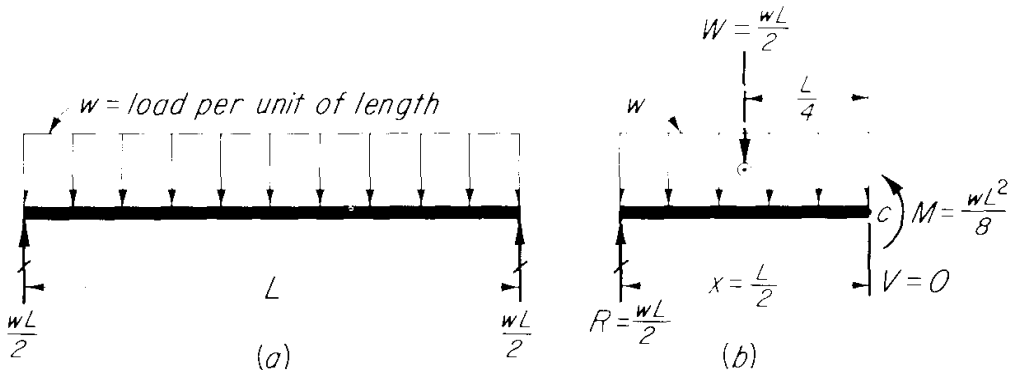


**Figure 3.11 Uniform distributed load of simply supported beam**

The static force acting on the partition is $F_{static} = PA$

$= 115{,}142.447 \times 0.0254$

$\mathbf{F_{static} = 2924.618\ (N)}$

The dynamic force acting on the partition plate is $F_{dynamic} = \dfrac{\rho v_{max}^2 A}{2}$

The density of exhaust gas at 875 K is, $\rho_{875(K)} = 0.393825\ kg/m^3$

We know the max. velocity corresponds to peak power is, $v_{max} = 100.8$ m/s

⇨ $\mathbf{F_{dynamic} = 50.82\ (N)}$

So, the total force acting on the partition plate is $\mathbf{F_{total} = F = F_{static} + F_{dynamic}}$

$\Rightarrow F = 2924.618 + 50.82 = 2975.438\ (N)$

$\mathbf{F = 2975.438\ (N).}$

Now, the actual load (W) acting against the partition is W = F/length = 25,219.209 (N/m)

$\mathbf{W = 25{,}219.209\ (N/m)}$

Maximum bending moment acting on the valve's partition is $M_b = \frac{WL^2}{8}$

$$M_b = \frac{25{,}219.209 \times (6.105)^2 (6.4516 \times 10^{-4})}{8} = 49.9138 \text{ (N-m)}$$

The yield strength of the 409 stainless steel is $\sigma_y = 207 \times 10^6 \, Pa$

The stress due to bending is $\sigma_b = \frac{M_b y}{I}$

Where y = t/2 and I = $\frac{1}{12} wt^3$.

Based on the dimension of the partition plate, t = 0.1181 inches and w = 6.105 inches y = 1.4998 x $10^{-3}$ (m)

I = 1.37327 $\times 10^{-8} \, (m^4)$

Therefore, $\sigma_b = 5.45 \times 10^6 \, (N/m^2)$, which is much lower than $\sigma_y = 207 \times 10^6 \, Pa$

Hence the current design will not lead to any failure even under any extreme critical situation.

# CHAPTER 4

# ACTUAL DESIGN OF PFR MECHANISM WITH THE FWSDV

Having developed with the conceptual design and mathematical calculations, the actual design of PFR mechanism is started. Before start designing the components, it is always wise to develop the schematic of the model to make sure of the components and their dimensions needed. This chapter introduces the schematic of PFR and later on discusses the actual design of FWSDV and the Rotation Control Mechanism (RCM).

## 4.1 Detailed Schematic and Specification of Periodic Flow Reversal Mechanism

The construction of the PFR system involves design and fabrication of many components. The main components in PFR mechanism are the control valve, which is used to switch the direction of exhaust gas, catalyst canisters, flanges, pipes and pipe connectors. The loop of PFR is constructed using set of pipes connecting the oxidation catalysts to FWSDV. Standard size of oxidation catalyst of size 9.5 inches in diameter and 6 inches in length is enclosed in a catalyst canister. The two catalyst canisters are used and they are connected using a set of flanges and once again the entire assembly is connected to the exhaust pipe using a pipe reducer in a conical shape. A set of L-connecters and steel pipes are needed in connecting the catalyst canisters to FWSDV to complete the PFR loop. Four sets of pipe connectors are used connecting the valve with the exhaust pipe. Thus the whole loop of PFR is constructed. Figure 4.1 shows the schematic of PFR loop.

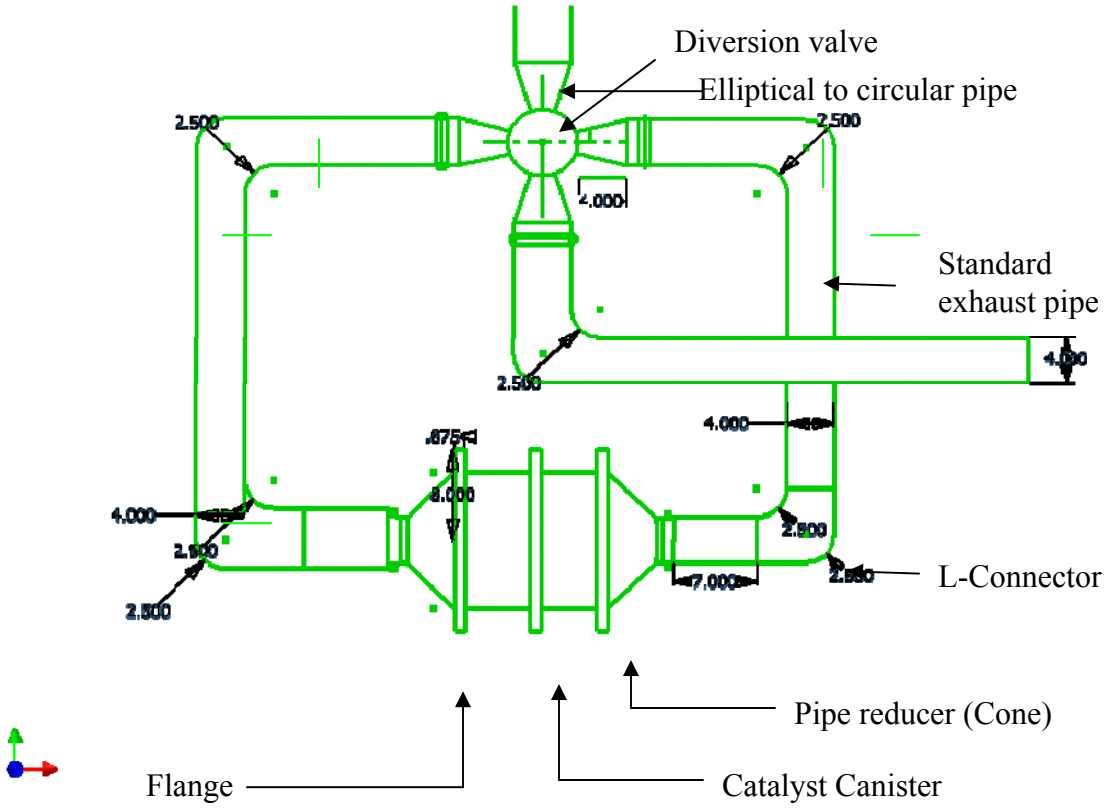


**Figure 4.1 Schematic of the loop**

### 4.1.1 Design of Catalyst Canisters

Catalyst canisters are the cylinders, which act like a housing for the catalyst. There are several oxidation catalysts available for various applications but studies and experiments show that the Palladium catalyst with alumina wash coat provides high methane conversion **[16].** The exhaust gases coming out from LNT pass through 4 inches diameter pipe and then through the catalysts for oxidizing methane. The standard size of 9.5 inches diameter and 6 inches length of Palladium catalyst is used. As the length of the single catalyst, 6 inches, is not sufficient for complete methane conversion, two catalysts of same sizes are used so that the length of the combined catalysts is 12 inches. This is done in order to increase the residence time, which in turn increases the conversion of methane (Calculations to support the above statements were provided in

the previous chapter). The two catalysts are wrapped with 'fiber wool' in order to avoid the exhaust gases flowing over the outer surface of the catalyst, where there is no wash coat available for the reaction to take place and also to provide mechanical and thermal insulation. The Pd catalyst consists of the number of channels through which the exhaust gases flow and, as the channels are equipped with an alumna wash coat the rate of reaction increases further to provide enhanced temperatures for methane conversion. The catalyst canister used to enclose the catalyst consists of two cylinders of standard dimensions, 10.02 inches inner diameter and 10.75 inches outer diameter. The length of the catalyst canister is fabricated to 6 inches to match with the length of the catalyst. For clarity, the catalyst canister is shown in Figure 4.2. Two canisters are used, which are connected by flanges. Flanges are fabricated according to the dimension of the catalyst canister. Two types of flanges are used, a male flange and a female flange, which, are designed in such away that they provide a minimum leakage by accommodating a steel gasket and the flanges are fabricated according to the required dimensions.

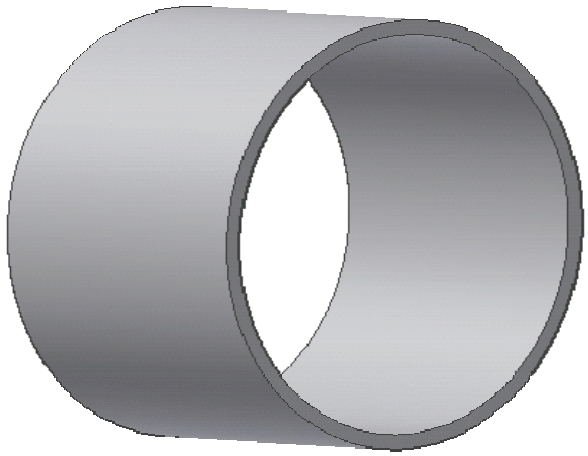

**Figure 4.2 Catalyst Canister**

Two pipe reducers, in the conical form, are used to connect the catalyst canister to the standard exhaust pipe. Four sets of standard Marman flanges are used to connect the pipe reducers to the exhaust pipe on both sides.

### 4.1.2 Design of Flanges and Pipe Reducers

Flanges are normally used to connect pipes together. Male flange and female flange connect two catalyst canisters and these two flanges are joined using set of standard bolts and nuts. Each flange is provided with twelve circular holes of standard bolt dimension. The flanges are also provided with separate seating arrangement for gasket. The gasket avoids the leakage and it also provides the firm grip when tightened with bolts.

Apart from gasket, a copper washer is also provided corresponding to the bolt circle diameter for even stress distribution. The diameter of the canister is 10 inches and the diameter of the exhaust pipe is 4 inches, so a pipe reducer in conical form is employed and a set of Marman flanges are used to connect the pipe reducer with the exhaust pipe. The pipe reducer, which is a cone, is fabricated using stainless steel sheet in order to withstand high temperature of the exhaust gases flowing through it. The ends of the pipe reducers are fabricated as flat edges for the ease of connecting and welding with the flange. Hence the loop made for the design of PFR consists of two cylinders, which act as catalyst canisters, a set of flanges fabricated to connect the cylinders with the pipe reducers and a set of Marman flanges to connect the cone with the exhaust pipe. Figures 4.3 through 4.6 show the male flange, female flange, pipe reducer and the sectional view of the catalyst system assembly.

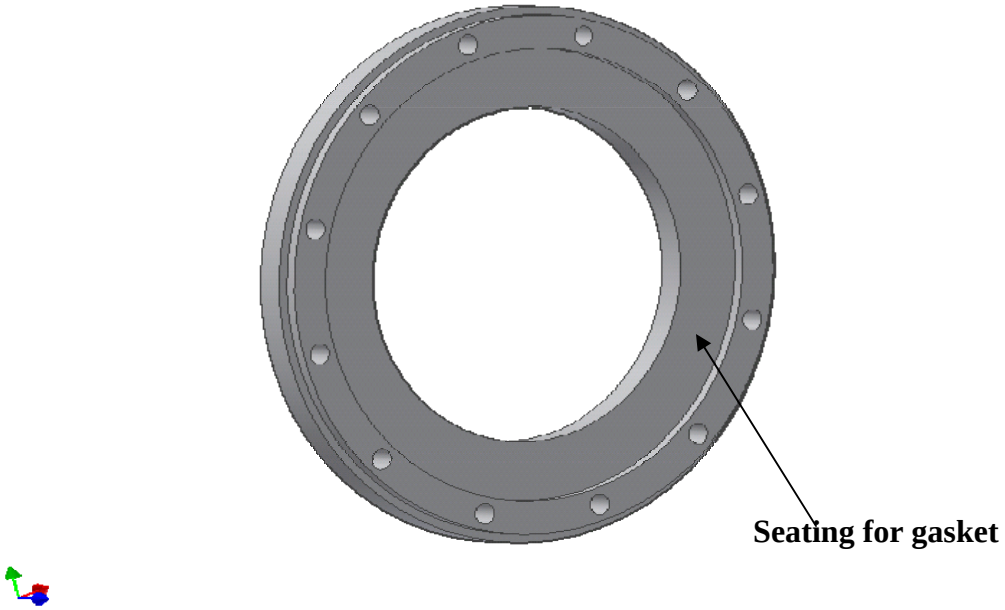


**Figure 4.3 Male flange**

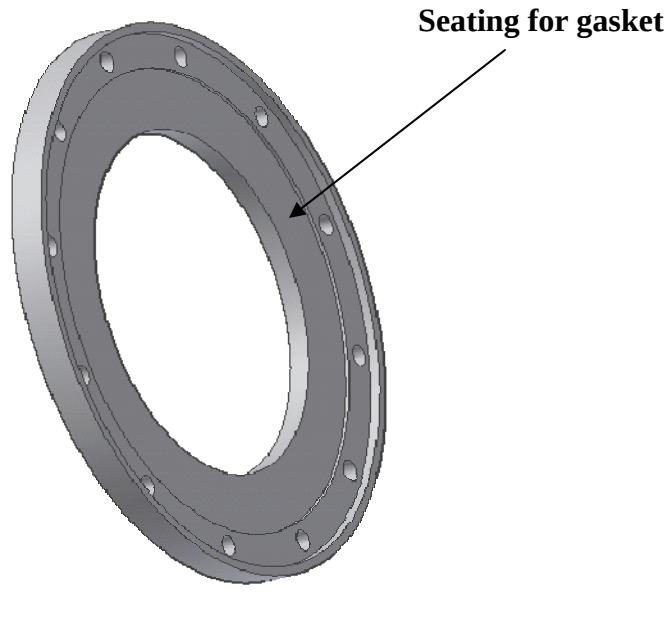


**Figure 4.4 Female flange**

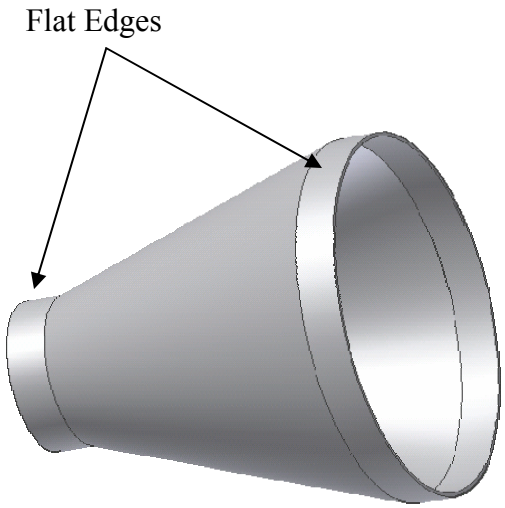


**Figure 4.5 Pipe reducer (Cone)**

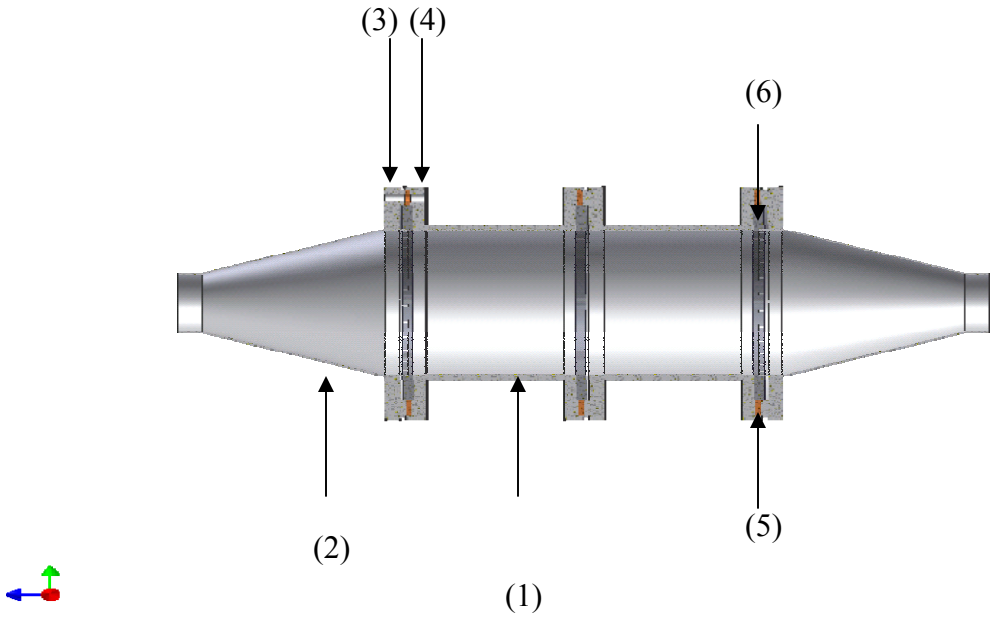


**Figure 4.6 Sectional view of assembly**

(1) Catalyst can
(2) Pipe reducer (cone)
(3) Male flange
(4) Female flange
(5) Copper washer
(6) Stainless steel gasket

## 4.2 Design of Four Way Single Diversion Valve

The FWSDV consists of two cylinders, (an outer cylinder and an inner cylinder), an inner cap, an outer cap, a stainless steel flange and a partition plate / diversion plate. The outer cylinder is the stator, which is stationary, and the inner cylinder is the rotor, which rotates inside the stator. The diverter plate divides the volume of the inner ram into two chambers. The inner cap is used to cover the inner cylinder and the outer cap is used to cover the whole assembly of the valve. A stainless steel flange is used to connect the outer cap with the outer cylinder and hence the entire assembly is covered. A copper gasket is employed between the outer cap and the stainless steel flange to minimize leakage and to provide firm grip when tightened. A stainless steel gasket is also employed to provide appropriate gap, which will be discussed later in this section. For clarity, the four-way single diversion valve is shown in Figure 4.7.

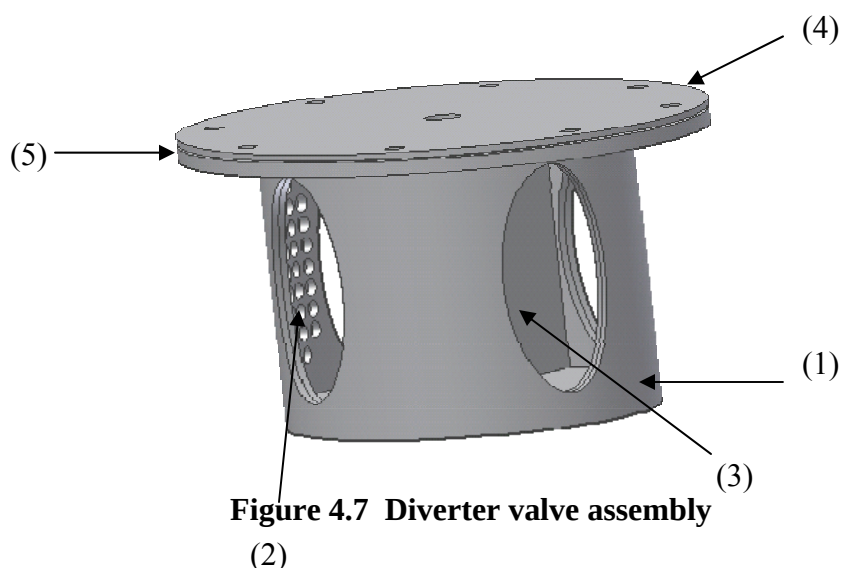


**Figure 4.7 Diverter valve assembly**

(1) Outer cylinder
(2) Inner Cylinder
(3) Partition plate
(4) Outer cap
(5) Stainless steel flange

### 4.2.1 Description of the Outer Cylinder

For the ease of fabrication, the outer cylinder is designed as two parts, the base plate and the hollow cylinder. “Rotational Clearance” tolerance is provided between these two parts to fit together and setscrews are used around their circumference in order to hold them together rigidly. The dimensions are chosen based on the calculations performed and also the standard size of the stainless steel pipe available in the market. The OD of outer cylinder is Φ 6.585” and its ID is.345”. Four elliptical holes are provided through 90-degree increments in order to facilitate both forward and reverse flow. The need for providing elliptical holes rather than circular ones and also their dimensions were already explained in Chapter 4. The base plate of the outer cylinder is provided with a number of channels called labyrinth seals to minimize leakage. A small circular depression has been made at the center of the base plate to a finite depth to accommodate the sleeve to avoid the direct wearing.

### 4.2.2 Description of Inner Cylinder

The inner cylinder is also designed as two parts like the outer one for the same reason and the same design criteria are followed for connecting the base plate with the hollow cylinder. The inner cylinder is also provided with four elliptical holes corresponding to the ones provided for the outer cylinder. In addition to the four solid elliptical holes, four alternating sets of circular holes in elliptical patterns are also provided in order to provide smooth transition and to avoid complete blockage of exhaust gases during its rotation. The elliptical holes were machined on a CNC milling machine and the small circular holes were machined on manual machines with a rotary table. A small circular protuberance is made at the center of the lower side of base plate, which goes inside the circular depression of the outer cylinder and the appropriate length / thickness of the circular protuberance determines a gap between the bases of the inner and outer cylinders.

The labyrinth sealing is also fabricated at the lower side of the base plate. For the ease of accommodating a partition plate in the inner cylinder, a longitudinal slot has been made at the desired depth at the upper base of the inner cylinder corresponding to the dimension of the partition plate. The inner cap closes the inner cylinder with the partition plate and a small lip of 2mm deep and a 45-degree chamfer is provided at the place for the ease of holding the inner cap at the correct position. Then the setscrews are screwed in around the circumference of the inner cylinder with the inner cap. The outer cap and flange are used to cover the entire assembly, and they are tightened together using standard bolts and nuts.

The outer cylinder and the inner cylinder are machined from the commercially available standard dimension of stainless steel pipe. As the main objective is to reduce leakage, the foremost importance is given to avoiding the seepage through the gap between the walls of the inner and outer cylinders. Although "Sliding fit" tolerance is provided for both the inner and outer cylinders, the seepage through their wall gap is taken into consideration in order to make sure that this design provides only a minimal leakage. One idea for not letting out these gases is to create a pathway for these gases to pass over. Hence, the base plates of both the inner and outer cylinders are provided with a number of channels, called a labyrinth sealing. The labyrinth sealing is designed in such a way that when both the inner and outer cylinders are assembled, a small gap of 0.5 mm will be left in the labyrinth configuration between the two bases. This will leave the passageway for the seepage. So, the seepage gases pass over the labyrinth sealing and thereby avoiding the possibility of a small percentage of leakage. A Graphite sleeve is used between the bases of the inner and outer cylinders to minimize the surface area contact between the inner and outer cylinders to eliminate the possible wearing during rotation. The advantage of using the graphite sleeve is that it does not get softened or dried at high temperatures. The outer cap and the inner cap also have labyrinth sealing like the one provided for the bases. The stainless steel gasket of desired thickness placed between the stainless steel flange and outer cap creates a gap between the inner and outer cap. Figures 4.8 through 4.10 show the outer cylinder, inner cylinder and the sectional view of valve assembly.

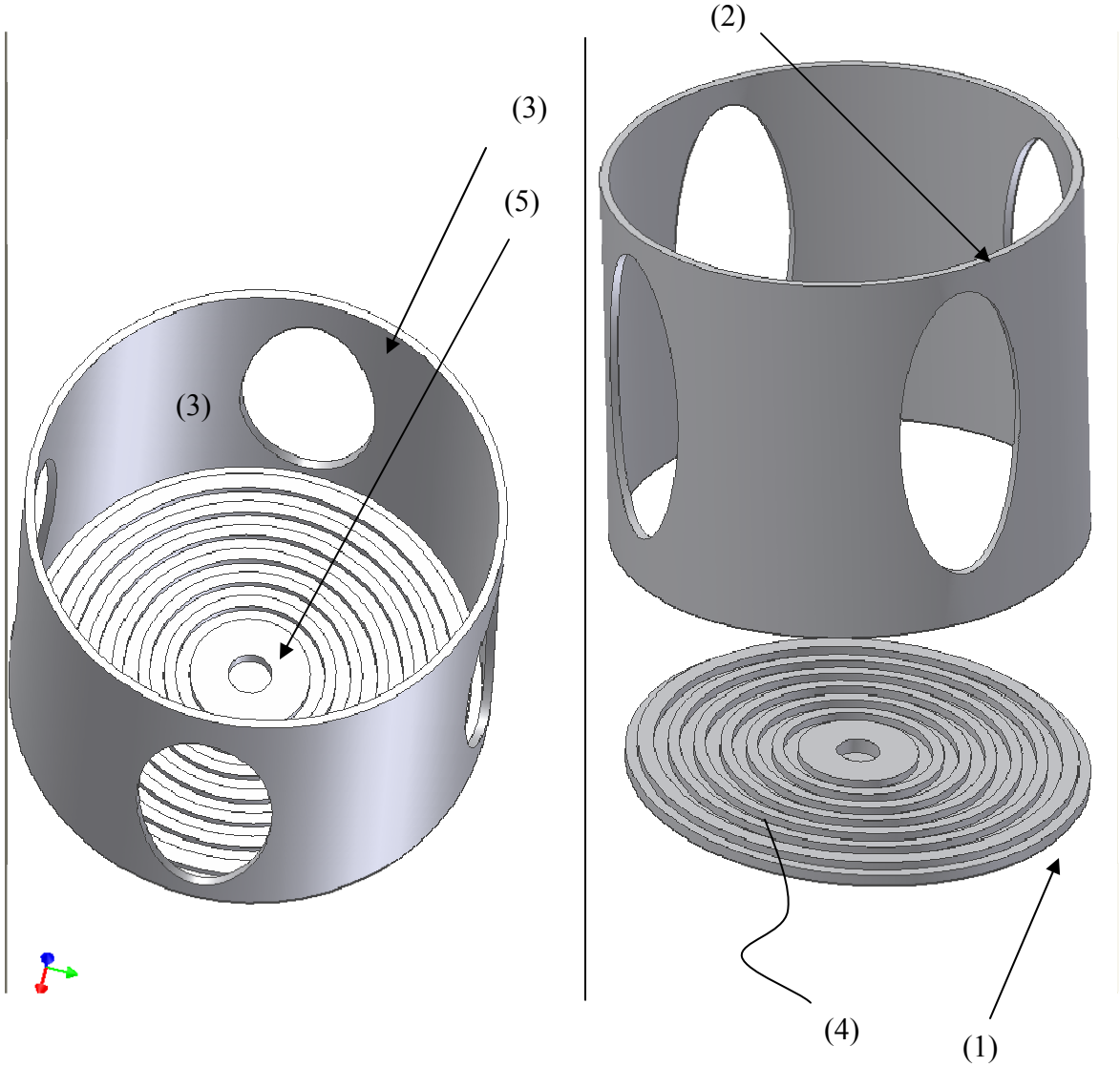


**Figure 4.8 Outer cylinder**

(1) Base plate
(2) Hollow cylinder
(3) Opening for an exhaust gas flow
(4) Labyrinth sealing
(5) Sleeve seating

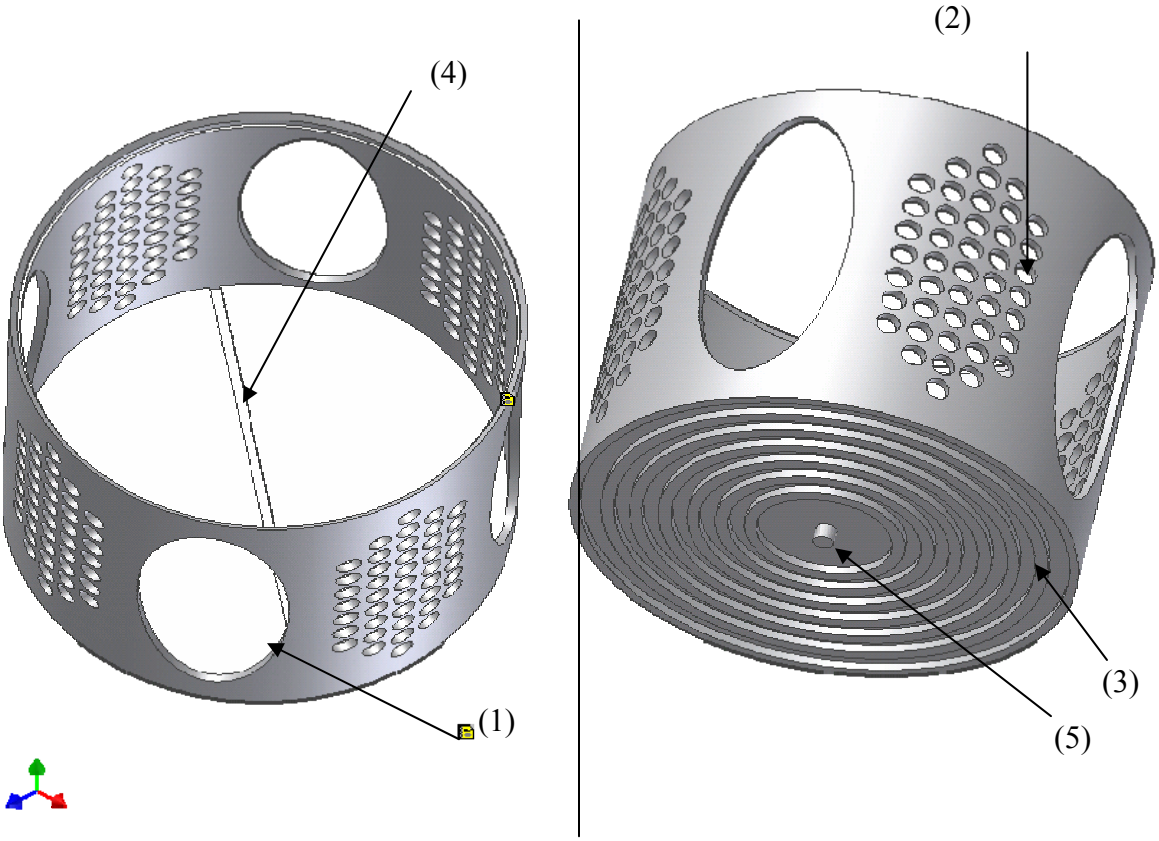


**Figure 4.9 Inner cylinder**

(1) Solid elliptical hole

(2) Circular holes in elliptical pattern

(3) Labyrinth sealing

(4) Groove for partition plate

(5) Projection to maintain gap

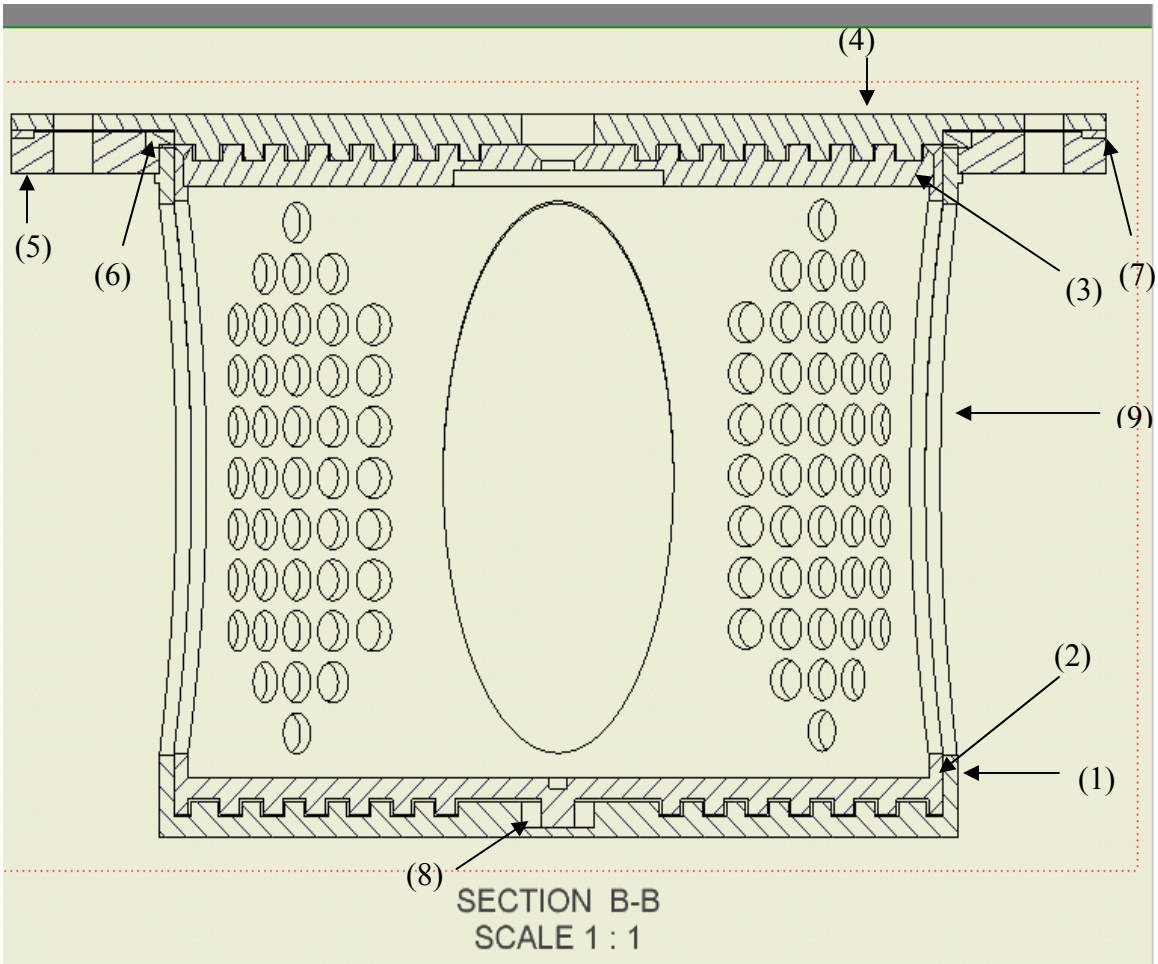


**Figure 4.10 Sectional view of the valve assembly**

(1) Outer cylinder
(2) Inner cylinder
(3) Inner cap
(4) Outer cap
(5) Steel flange
(6) Copper gasket
(7) Steel washer
(8) Graphite sleeve
(9) Elliptical opening

### 4.2.3 Description of the Inner Cap

The purpose of having the inner cap is to cover the inner ram and to hold the partition plate. So, the design is made in such a way that the OD of the inner cap corresponds to the lip diameter of the inner ram for the ease of holding. Apart from that, setscrews are used around the circumference of the inner ram and the inner cap to hold them rigidly. A longitudinal slot is made to the desired depth, which corresponds to the dimension of the partition plate like the one provided for the base plate of the inner ram. The slots of the inner cap and the base plate of the inner ram, hold the partition plate rigidly and securely. Again the channels are made at the upper base of the inner cap like the ones employed for the base plate. A small circular hole at the center of the inner cap lets the stainless steel shaft to pass through and holds the partition plate so that the rotation of the shaft also rotates the entire assembly of the inner ram, the partition plate and the inner cap. As the diameter of the shaft employed is small when compared to the diameter of the inner cap, it has been decided to transfer the entire load to the inner cap during rotation. Hence "Press Fit" tolerance is provided between the center hole and the stainless steel shaft. This "Press Fit" tolerance along with the slot provided in the stainless steel shaft to hold the partition plate rigidly rotates the assembly of the above-mentioned three parts without any breakage or failure.

### 4.2.4 Stainless Steel Shaft

The stainless steel shaft acts as an important component for rotating the valve. It acts as a driver for the actuator. A horizontal slot of desired thickness is provided in one end of the shaft, which corresponds to the thickness of the partition plate so that this slot will firmly hold the partition plate, and the other end of the shaft is connected to the steel arm through a rectangular block. The idea of providing this design is already explained in the previous subsection. A small step is provided in the shaft where the rectangular block would seat and then it is fitted tightly to the shaft using set screws. Figures 4.11 through 4.12 show the inner cap and the stainless steel shaft.

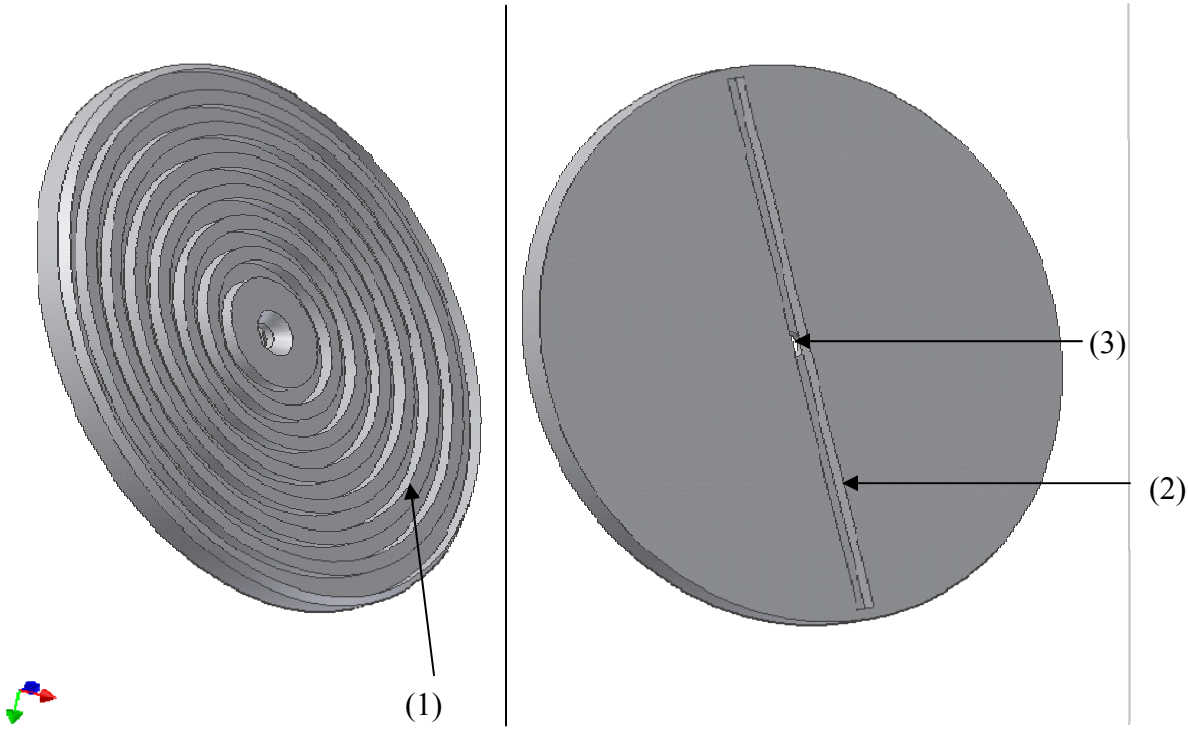


**Figure 4.11 Inner cap**

(1) Labyrinth sealing

(2) Slot for diverter plate (partition plate)

(3) Circular hole for the shaft

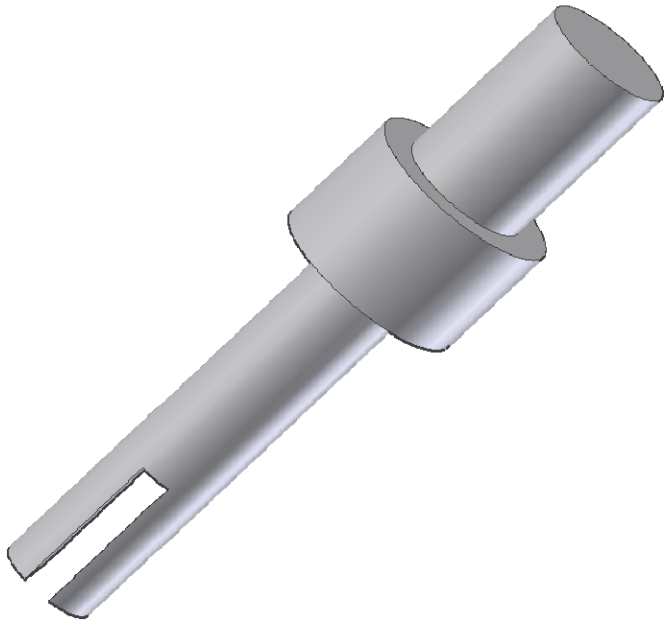

**Figure 4.12 Stainless steel shaft**

### 4.2.5 Rectangular Block

The rectangular block acts like a coupler, which connects the stainless steel shaft with the steel arm connected to the actuator (The design and the working principle of the actuator will be discussed later in this chapter). The rectangular block has got a threaded hole through which the steel arm will pass through. Two through holes, one for the stainless steel shaft and the other for the setscrews are made. A small circular notch is made on the steel shaft so that the setscrew could be used to fit the shaft to the block easily.

### 4.2.6 Description of the Outer Cap

The outer cap covers the top portion of the valve. The outer cap is connected to the flange using a set of bolts and nuts, and a labyrinth sealing is provided on the inner surface of the cap like the one used for the inner cap. The stainless steel gasket used between the outer cap and the steel flange effectively creates a gap between the outer cap and the inner cap, through which the seeping gas passes. A circular hole is made at the center of the cap where the graphite sleeve is fitted and the steel shaft passes through this hole to connect to the diversion plate.

### 4.2.7 Description of the Stainless Steel Flange

The stainless steel flange is welded with the outer cylinder, and it is connected to the outer cap with a set of bolts and nuts. A small step of desired depth leaves room for gasket seating. Copper gasket is used along the bolt circle, which provides sealing and gives a firm grip when tightened with bolt and nut. The flange has also got a seating arrangement for a steel washer. The steel washer is provided to leave a small gap between the inner and the outer cap and hence a depth of 1 mm is provided in the flange for the steel washer seating. The steel washer of 2mm thickness will seat in order to provide a gap for the rotation as well as to let the seeping gases to pass through. Figures 4.13 through 4.15 show the rectangular block, the outer cap and the stainless steel flange.

The entire assembly of the catalyst system with periodic flow reversal picture is shown in Figure 4.16. This system consists of two oxidation catalysts, which are enclosed in catalyst canisters, the FWSDV and exhaust plumping.

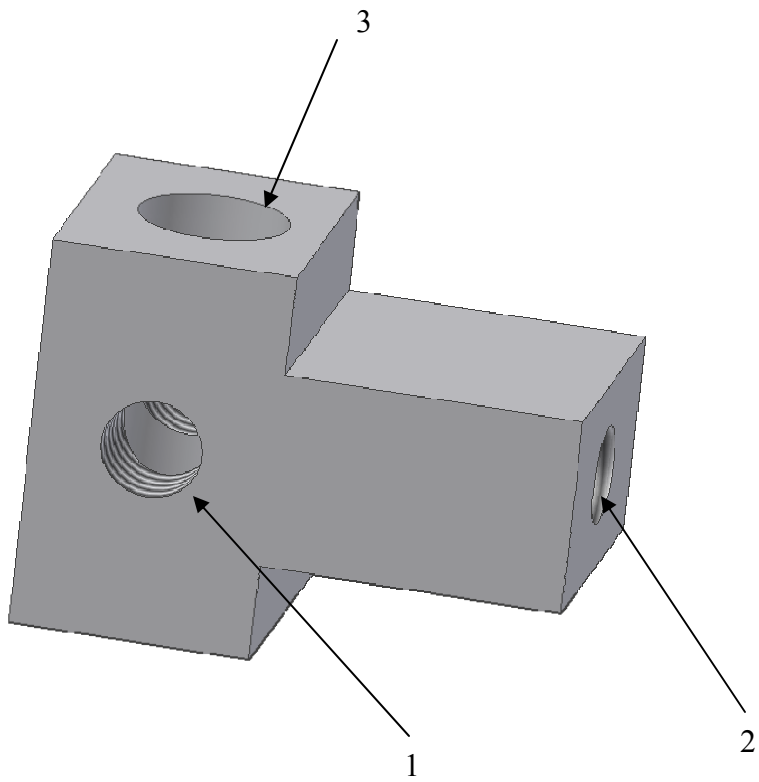


**Figure 4.13 Rectangular Block**

(1) Hole for the set screws (2) Hole connecting steel arm

(3) Hole through which Steel shaft passes

.

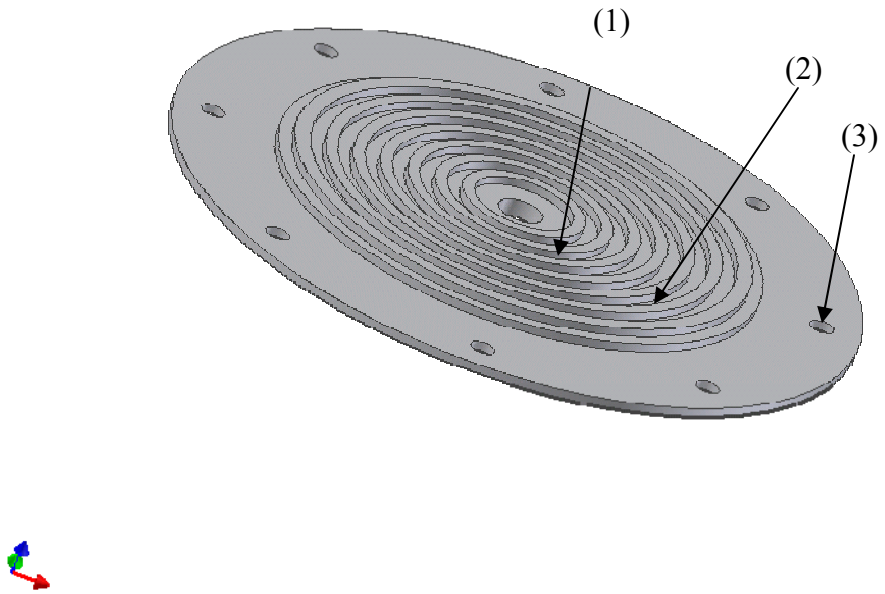


**Figure 4.14 Outer cap**

(1) Hole for the sleeve and shaft

(2) Labyrinth Sealing

(3) Bolt hole

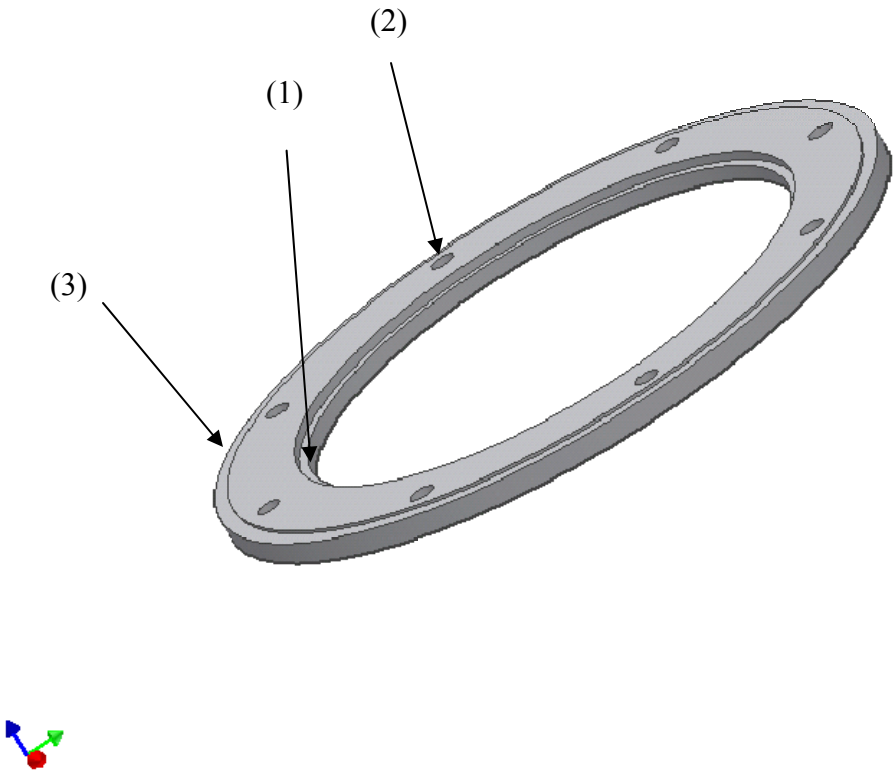


**Figure 4.15 Stainless steel Flange**

(1) Gasket seating

(2) Holes for bolt

(3) Steel washer seating

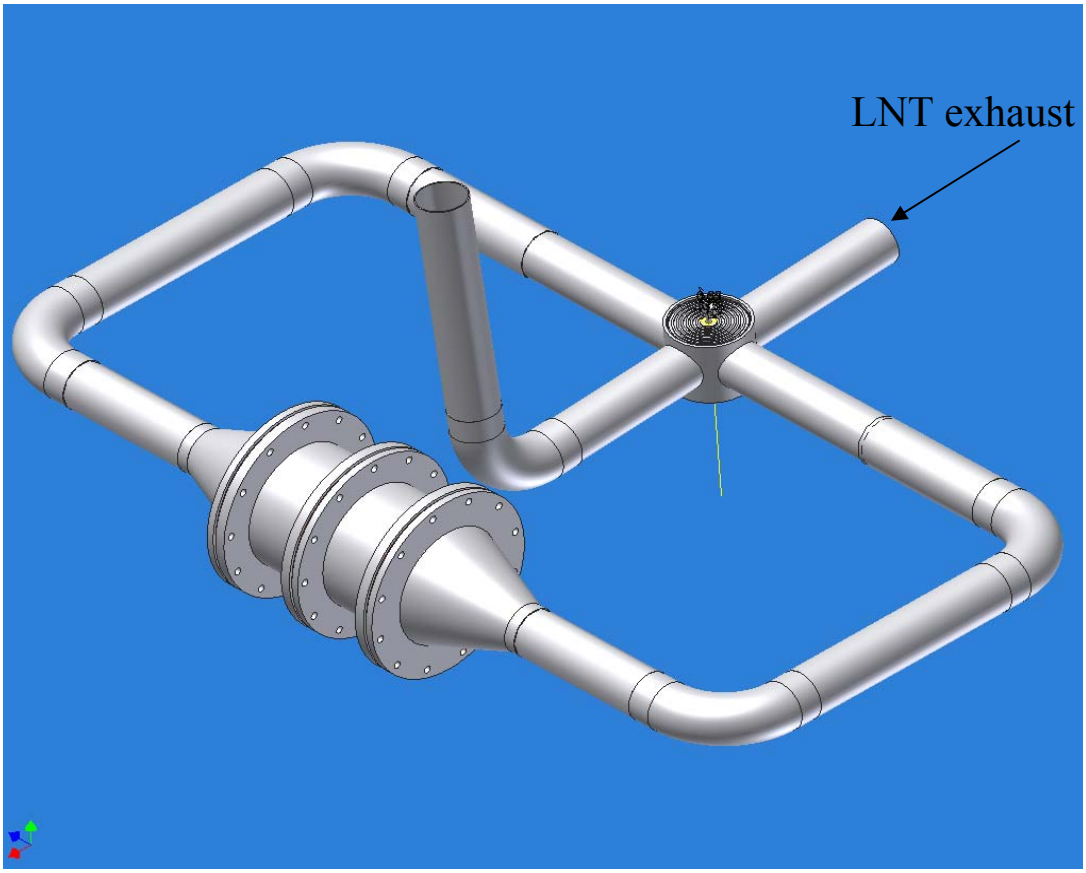


**Figure 4.16 Catalyst System with the FWSDV**

## 4.3 Actuator for the FWSDV

### 4.3.1 Description and Operation of Rotation Control Mechanism

The PFR mechanism is accomplished through the switching of exhaust gases using FWSDV. As we discussed earlier, an alternate rotation of the rotor assembly, an assembly of inner ram, partition plate and the inner cap of FWSDV, in either direction switches the exhaust gas flowing through the catalyst. The rotation of assembly is brought through an actuator mechanism called rotation control mechanism, which uses piston-cylinder arrangement. The unit "04-DUZ, Z Line Air Cylinder" of the required dimension is obtained from "Bimba manufacturers". The Z-Line air cylinder has rolled-in construction of the original line and it has got two-pieces of 303 stainless steel piston rod and piston-to-rod connection is threaded, sealed and riveted securely. The HEX-STUD rod end thread of heat-treated alloy steel is provided in order to facilitate easy removal in case of failure. The piston is connected to the shaft, which is "press fitted" with the inner cap and "tight fitted" with the partition plate of FWSDV. Figure 4.17 is shows the schematic diagram of the assembly and the estimated dimensions of the piston stroke based on the dimension of the valve. The base of "Z-Line" cylinder is hinged. Piston is connected to the steel arm through two tie rods, male tie rod and female tie rods. The linear movement of the piston rotates the rotor assembly. The rotor assembly makes an alternate 90-degree rotation for each stroke of the piston. The forward linear movement of the piston moves rotor assembly through 90 degree in the clockwise direction and the reverse linear movement of the piston rotates rotor assembly through 90 degree in anticlockwise direction. For the available bore size and the piston stroke, the position of the "Z-Line" cylinder with respect to the valve is estimated. The outer diameter of the outer cap is around 9 inches and hence the length of the steel arm is chosen little more than the radius of the top cap, i.e. 5 inches. This steel arm has to rotate 90 degree; hence the corresponding linear displacement of the piston will be 7 inches. The steel arm, which connects the piston to the stainless steel shaft of the valve, is 5 inches long and hence the piston stroke is estimated as 8 inches.

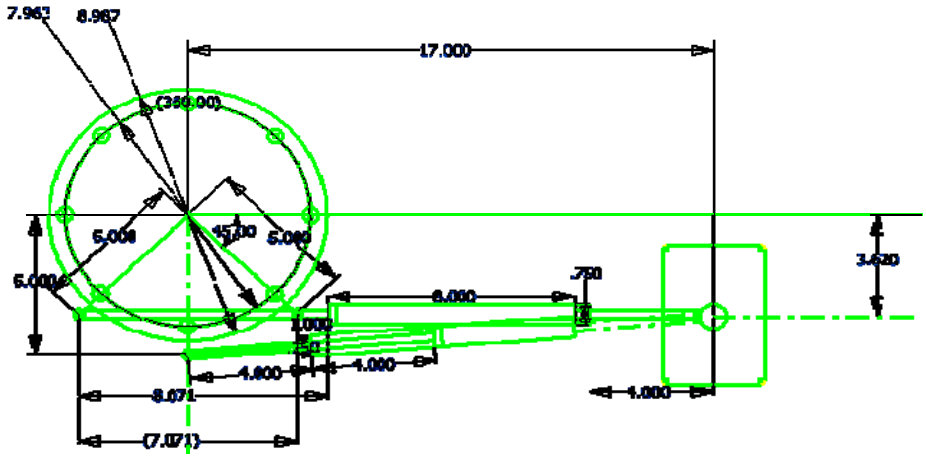


**Figure 4.17 Schematic diagram of the motion control mechanism**

The standard "Z-Line" cylinders are available for various bore sizes such as $3/4$", $1\,1/16$ and $1\,1/12$ inches and the piston stokes are available for various sizes that could be obtained according to the customer's requirement. The bore size of ¾" inches and the estimated stroke lengths of 8 inches were chosen based on the calculation. Accordingly, the position of the base of the Z-line cylinder with respect to the shaft is also estimated. The Z-line cylinder is fixed at one end and the piston rod is connected to the arm at the other end. Since the Z-line cylinder turns from the axial position during the displacement of piston, tie rods are used to connect the piston to the steel arm. The male tie rod is connected to the steel arm and the female tie rod is connected to the piston rod. The two tie rods are coupled so that the piston cylinder arrangement, which turns during the linear movement of the piston, rotates the steel arm through 90 degree. Hence the steel arm makes alternate rotation through 90 degree in both clock wise and anti-clock wise direction, which in turn rotates the inner cylinder of the valve through 90 degree alternatively.

The piston is operated by gas cylinder, which supplies gas / air with necessary pressure to drive the piston. The pressure of the gas driving the piston controls the speed of rotation of FWSDV. The gas cylinder is always operated at maximum pressure to provide the highest speed of rotation of FWSDV in order to provide minimal leakage. A set of shut off valves used for letting the air to drive the piston controls the switching time of the valve. The valves are operated through the terminal by using control software.

Figure 4.18 is provided, which clearly shows the complete schematic of the driving mechanism with tie rods, steel arm and the cylinder-piston arrangement. The working principle of the valve actuator is much clear from this figure.

The appendix is provided at the end of the chapters which shows all the design work made using CAD software.

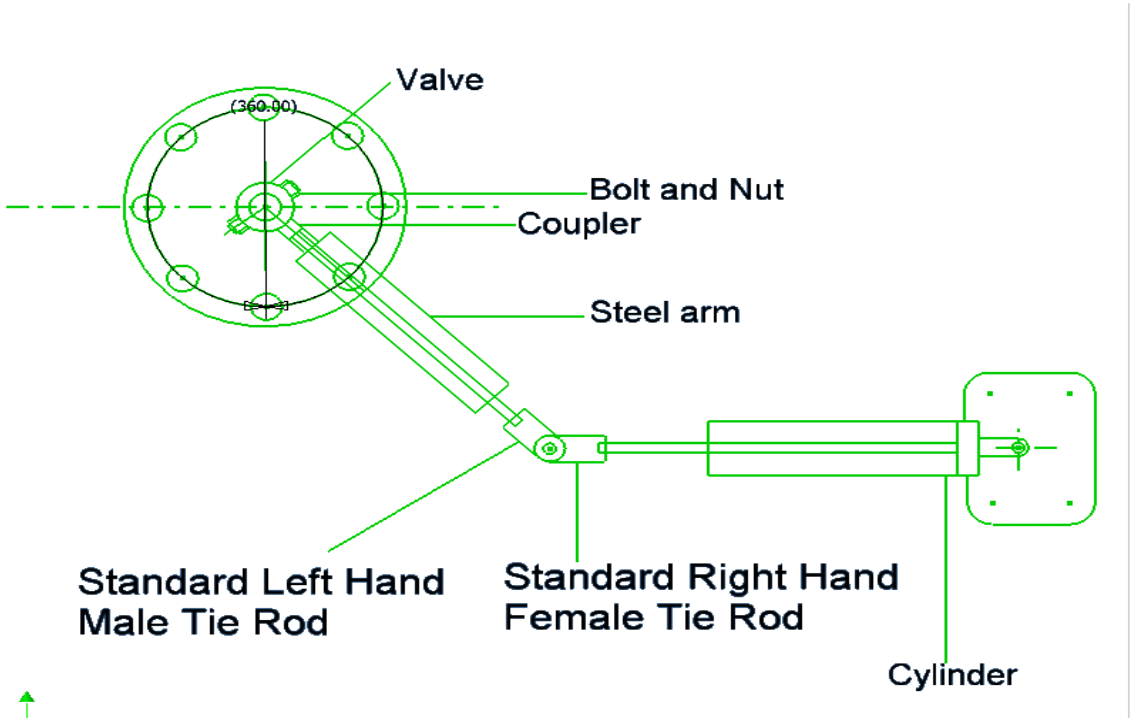


**Figure 4.18 Schematic of valve-actuator assembly**

# CHAPTER 5

# CONCLUSION AND RECOMMENDATIONS

## 5.1 Conclusion

In this research, the PFR system is designed successfully, which would effectively enhance the temperature within the catalyst to provide good methane conversion. Even though the experimental work has not yet been conducted, the necessary calculations for the catalyst dimensions, at both peak power and peak torque conditions provided a sufficient residence time for complete oxidation. The experimental work of RFC system using the Bench Flow Reactor (BFR), conducted by Dr. Nguyen and Mr. Scott Smith, for the same application, provided good methane conversion, which validates that the system developed in the current research would be effective in oxidation of methane. The design of the FWSDV overcomes many drawbacks of previous methods applied to RFC system. Not only does it reduce the complexity of having different controls in operating four shut off valves, but also it reduces the cost. The FWSDV minimizes leakage during switching and is also believed to act as a good switching device. Finally, catalyst canisters, flanges and other exhaust system plumbing are also successfully designed to complete the entire loop of the PFR catalyst system.

## 5.2 Recommendations for Further Research

Only the PFR system is conceptually designed in order to accomplish good methane conversion. But it is also to be noted that the methane conversion depends on various other factors such as the switching time, Gas Hourly Space Velocity (GHSV) and the exhaust temperature. Controlling these parameters in the experiments would provide good conversion efficiency. The effect of Supplemental Fuel Injection (SFI) would also contribute as a major role as supplementary fuel injected into the feed stream would raise the temperature of the exhaust stream in addition to the one achieved by RFC method and therefore it is possible to achieve even better conversion efficiency.

# BIBLIOGRAPHY

## BIBLIOGRAPHY


**1** Aaron Michael Williams, " Lean $NO_x$ Trap Catalysis For Lean Burn Natural Gas Engines", M. Sc. Thesis, Department of Mechanical Engineering, The University of Tennessee-Knoxville, 2004.

**2** Alan Janbey, Wayne Clark, Ehan Noordally, Sue Grimes, Saad Tahir, " Noble metal catalysts for methane removal", *Chemosphere 52 (2003) 1041-1046*.

**3** Burch. R and P. K. Loader, " Investigation of $Pt / Al_2O_3$ and $Pd / Al_2O_3$ for the combustion of methane at low concentrations". *Applied Catalysis B: Environmental, Volume 5, Issues 1-2, 31 December 1994, Pages 149-164.*

**4** CROSS Instrumentation, Precision Instrumentation For Process and Control Systems, "Flow Control Valve Quotation from CROSS Instrumentation", April 2004.

**5** Dieselnet maintained by Ecopoint Inc., " Heavy- Duty Diesel Truck and Bus Engines", 12 / 14 / 05, http://www.dieselnet.com/standards/eu/hd.html

**6** U.S. Department of Energy, " Alternative Fuel Data Center: Natural Gas and Benefits", 12 / 14 / 05, http://www.eere.energy.gov/afdc/altfuel/gas_benefits.html

**7** Euzen Patrick, Jean-HerveÂ Le Gal, Bernadette Rebours, GeÂrard Martin, "Deactivation of palladium catalyst in catalytic combustion of methane". Catalysis Today 47 (1999) 19-27.

**8** Frank-Kamenetski D.A., Diffusion and Heat Exchange in Chemical Kinetics, Princeton Universtity Press, Princeton, NJ, 1955.

**9** Grisel Corro, J.L.G. Fierro, Odilon Vazquez C., " Strong improvement on $CH_4$ oxidation over $Pt/\gamma - Al_2O_3$ catalysts", Catalysis Communications 6 (2005) 287-292.

**10** John B. Heywood, " Internal Combustion Engine Fundamentals", 1988, McGraw-Hill Inc.

**11** Inui T., Korean J.Chemical Engineering, 14 (1997) 44.

**12** International Rivers Network, " Neither Clean Nor Green: The Surprising Truth About Reservoirs and Climate Change", 12 / 14 / 05, http://www.12.org/programs/greenhouse/index.php?id=wrr16n2.truth.html

**13** Jensen Alfred and Harry H. Chenoweth, "Statics and Strength of Materials", 2nd Edition, Mc-Graw Hill Company.

**14** Jordan K. Lampert, M. Shahjahan Kazi, Robert J. Farrauto, "Palladium catalyst performance for methane emissions abatement from lean burn natural gas vehicles", Applied Catalysis B: Environmental 14 (1997) 211-223.

**15** W.E. Liss et al., GRI Report-92/0123 (1992)

**16** B. Liu, R.E. Hayes, M.D. Checkel, M. Zheng, E.Mirosh, "Reversing flow catalytic converter for a natural gas/diesel dual fuel engine", Chemical Engineering Science 56(2001) 2641-2658.

**17** Y.S. Matros, G.A. Bunimovich, Reverse-flow operation in fixed bed catalytic reactors, catal. Rev. 38 (1996) 1 – 68.

**18** Ming Zheng, David Irick, Jeffrey Hodgson, "Energy Efficient Thermal Management for Natural Gas Engine Aftertreatment via Active Flow Control", March 27, 2002.

**19** Ming Zheng, Graham T. Reader, "Energy efficiency analyses of active flow aftertreatment systems for lean burn internal combustion engines", Energy Conversion and Management 45 (2004) 2473-2493.

**20** Ming Zheng, Edward Mirosh, Wayne Klopp, Dale Ulan, Mark Pardell and Paul Newman, " Development of a Compact Reverse-Flow Catalytic Converter for Diesel Dual Fuel LEV", SAE 1999-01-3558.

**21** Naturalgas.org maintained by natural gas supply organization, "Electric Generation Using Natural Gas", 12 / 14 / 05, http://www.naturalgas.org/overview/uses_eletrical.asp

**22:** Patrick Gelin, Laetitia Urfels, Michel Primet, Emmanuel Tena, " Complete oxidation of methane at low temperature over Pt and Pd catalysts for the abatement of lean-burn natural gas fuelled vehicles emissions: influence of water and sulfur containing compounds", Catalysis Today 83 (2003) 45-57.

**23** Steven Scott Smith, " Reverse Flow Oxidation Catalyst With Supplemental Fuel Injection", M. Sc. Thesis, Department of Mechanical Engineering, The University of Tennessee-Knoxville, 2005.

**24** Strots, V.O., Bunimovich, G.A., Matros, Y.S., Zheng, M., & Mirosh, E.A. (1998), "Novel catalytic converter for natural gas powered diesel engines. SAE 980194.

**25** Willard W. Pulkrabek, “ Engineering Fundamentals of the Internal Combustion Engine”, 2nd Edition, Pearson, Prentice Hall.

**26** Yasunari Hanaki, Toru Sekiba, Mitsunori Ishii, Akihide Okada, Shizuo Ishizawa, “ Research on exhaust emission control characteristics of a natural gas vehicle-Characteristics of methane oxidation reaction of three-way catalysts”. Central Engineering Laboratories. Nissan Motor Co., Ltd., Natsusima-cho 1, Yokosuka-shi, Kanagawa, 237 Japan. *JSAE Review 17 (1996) 259-265.*

# APPENDIX

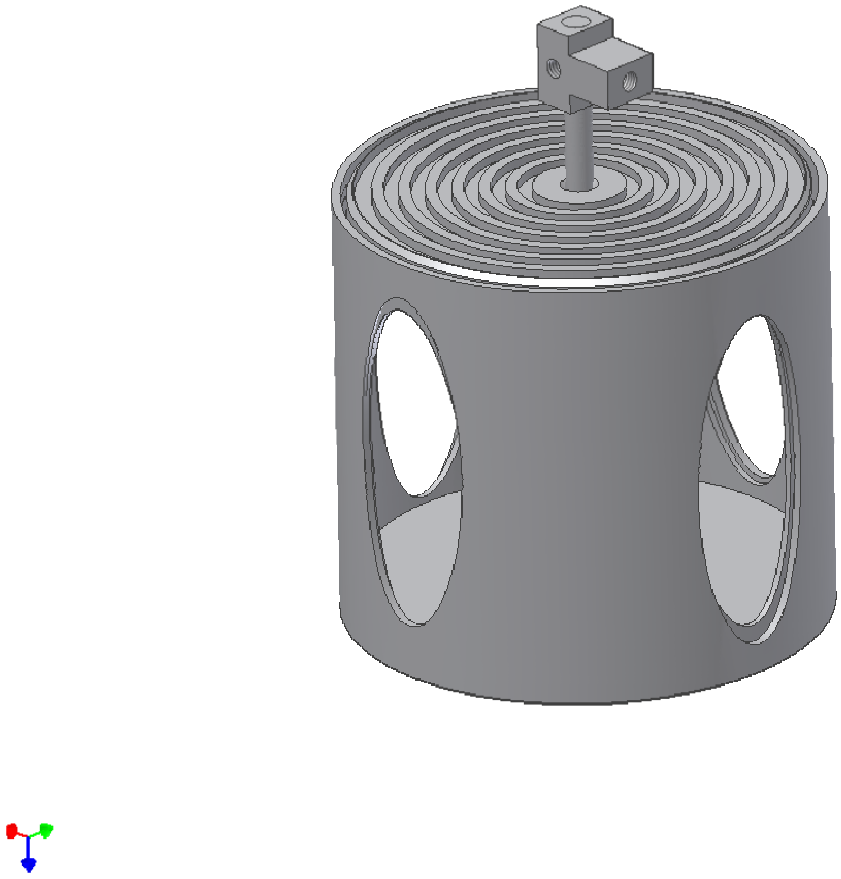

**Figure A-1 Valve Assembly**

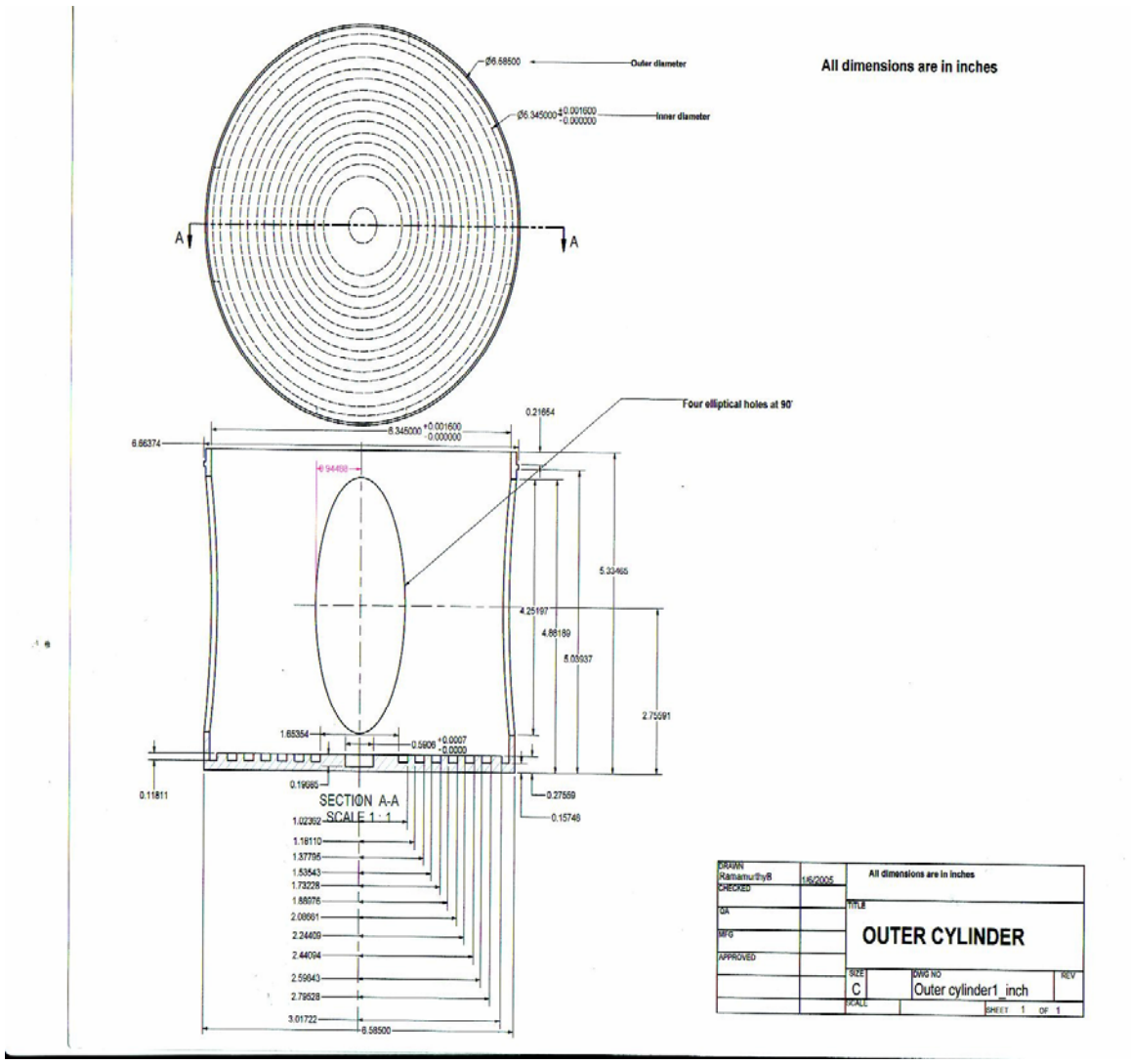


**Figure A-2 Sectional View of Outer Cylinder**

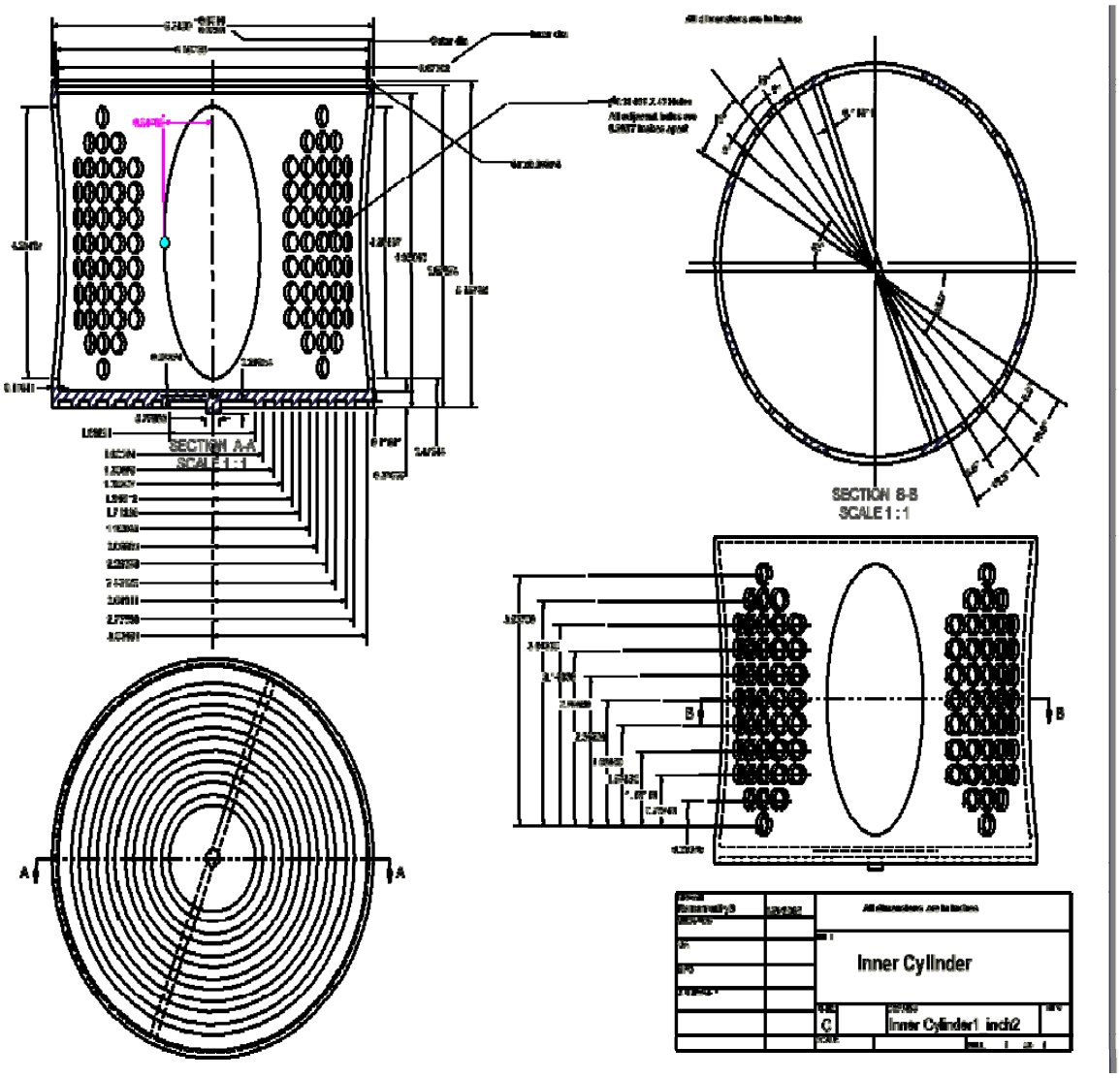


**Figure A-3 Sectional View of Inner Cylinder**

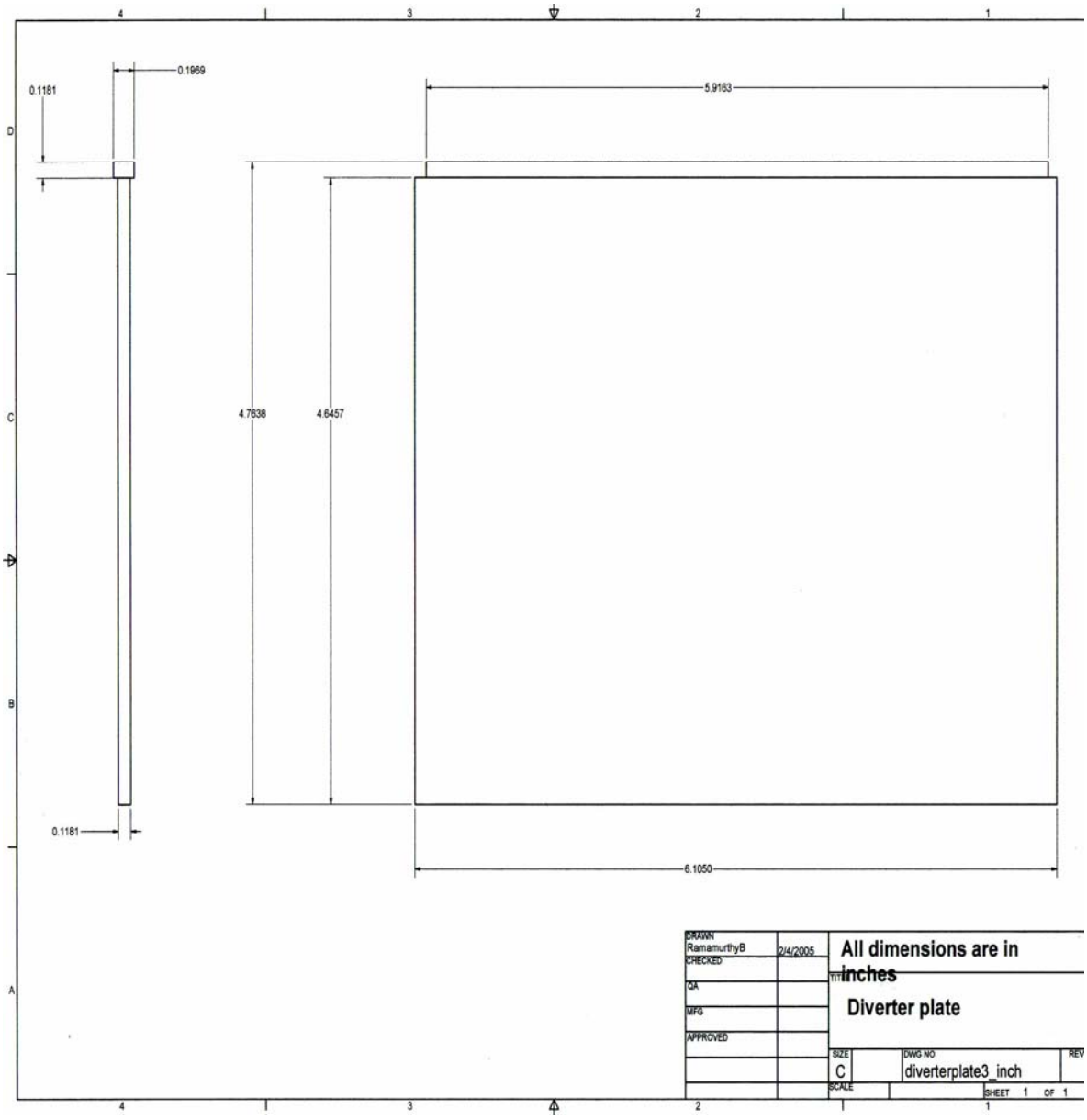


**Figure A-4 Diverter Plate**

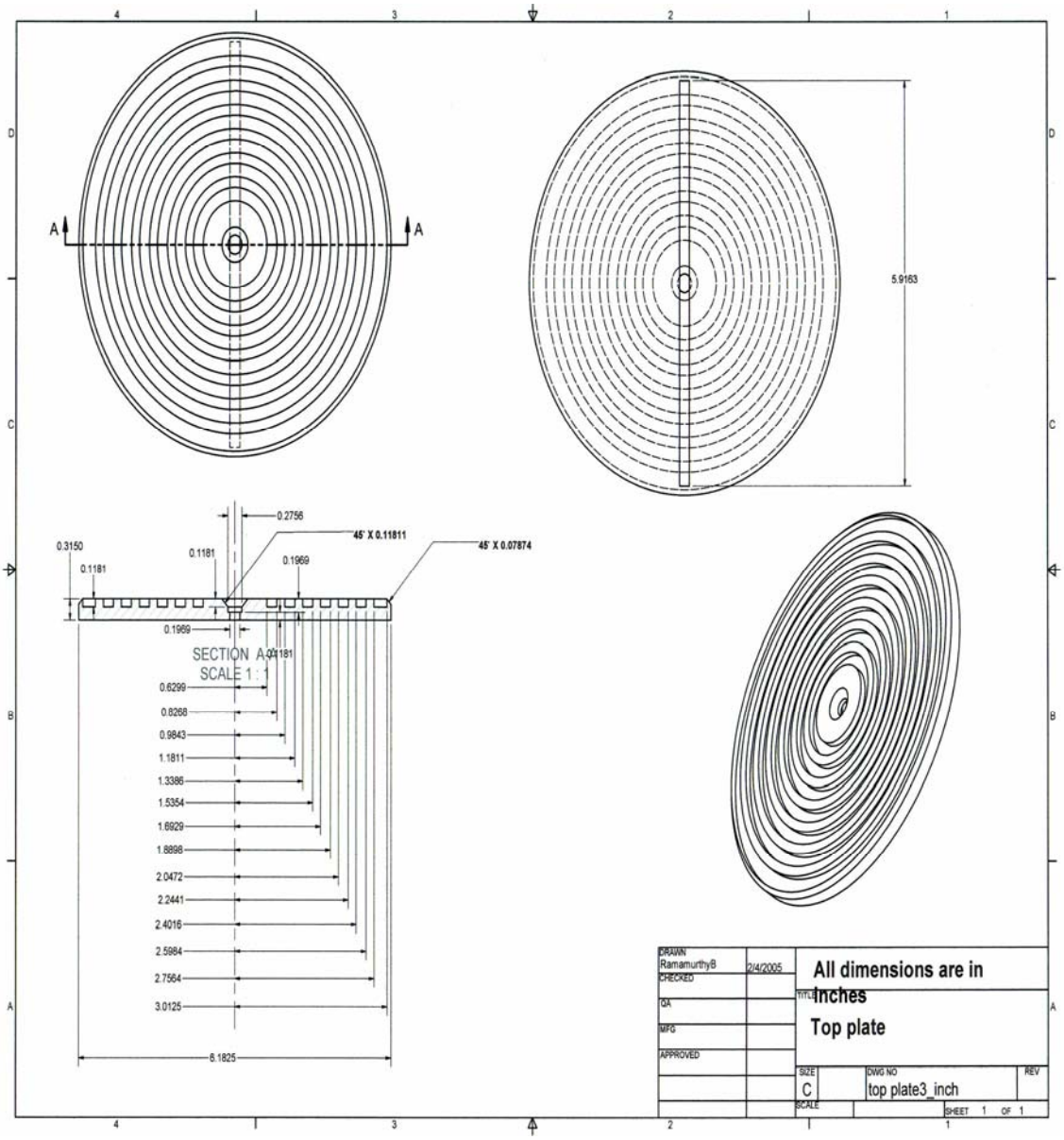


**Figure A-5 Sectional View of Inner Cap**

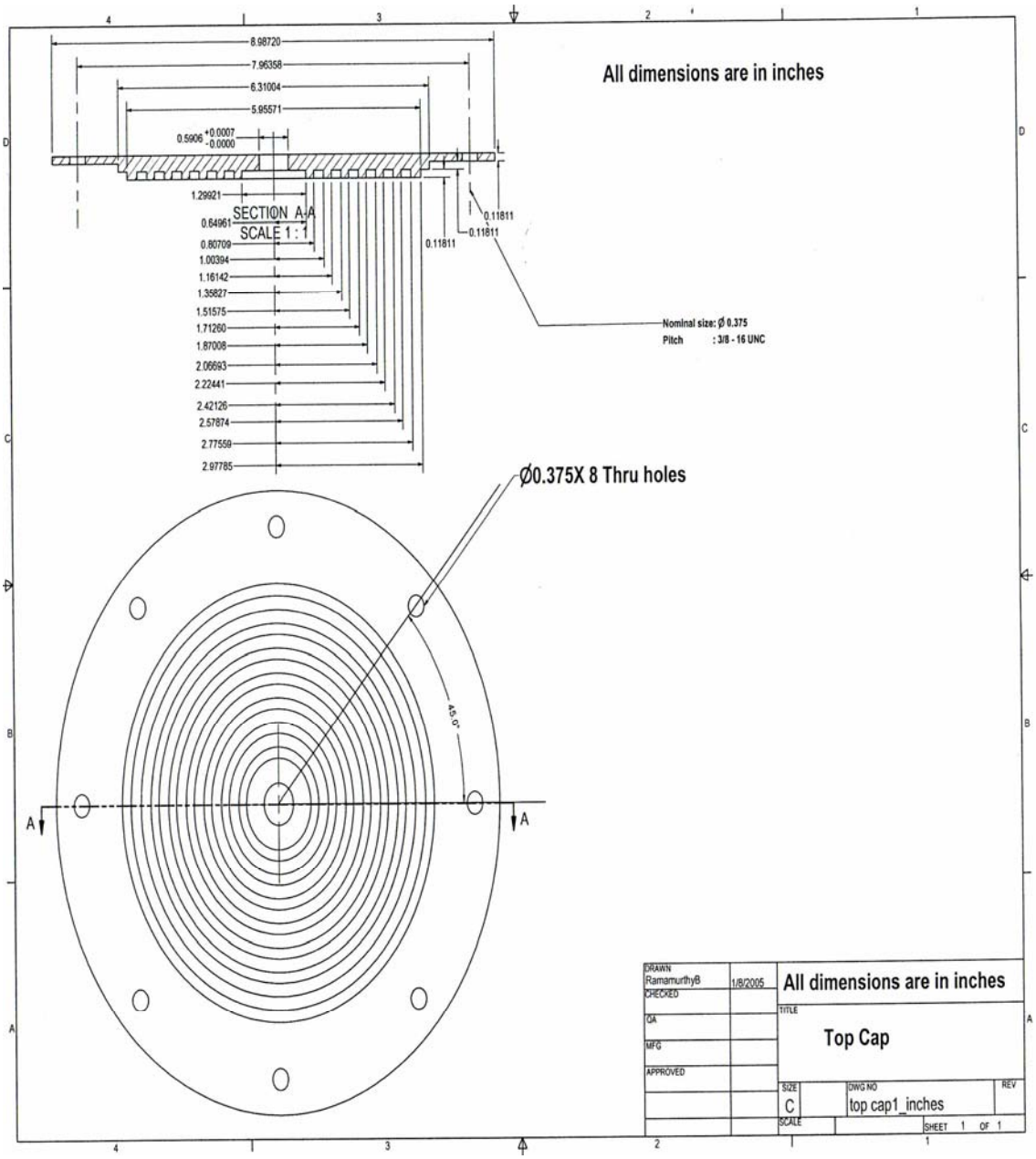


**Figure A-6 Sectional View of Outer Cap**

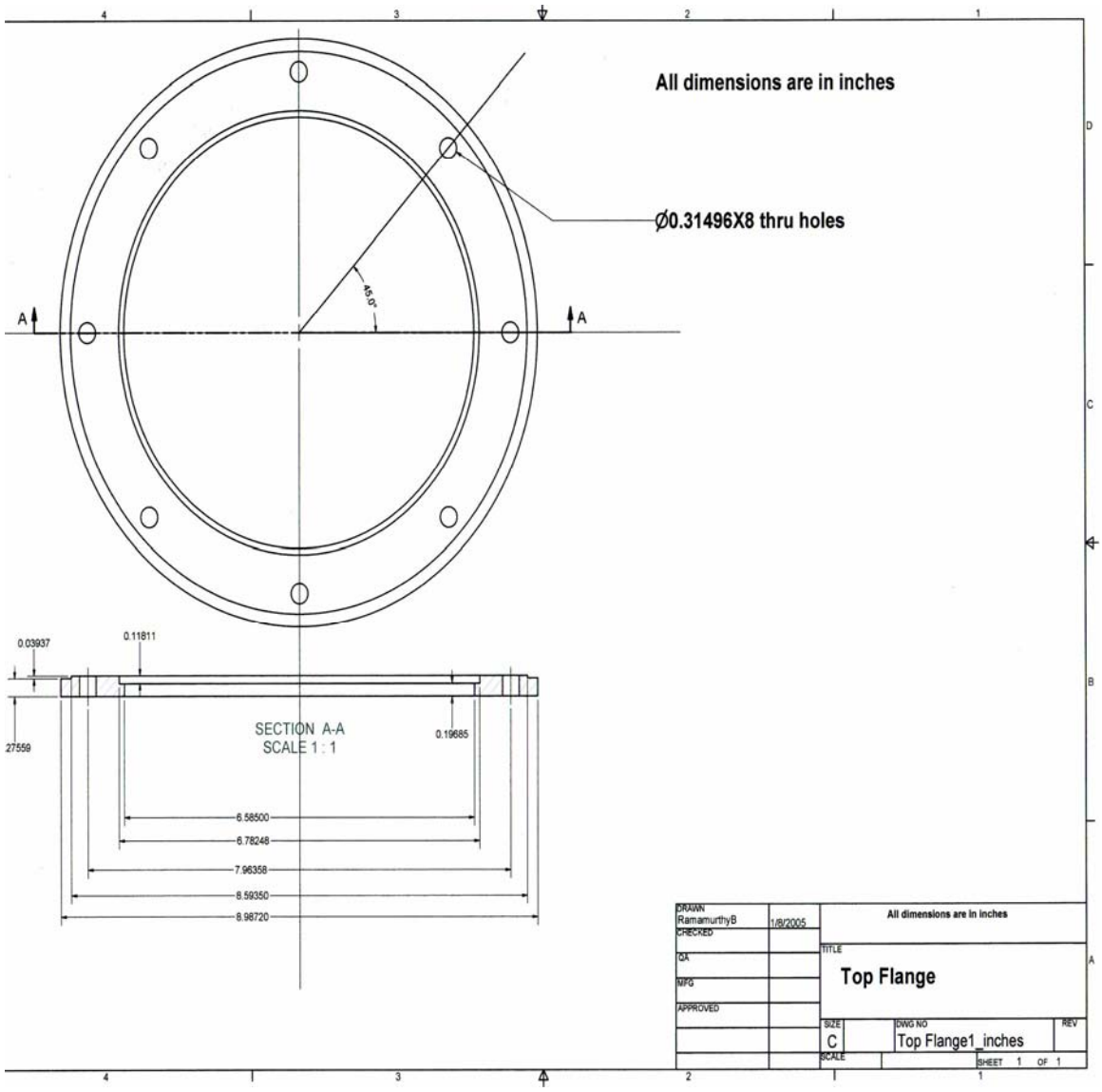


**Figure A-7 Sectional View of Stainless Steel Flange**

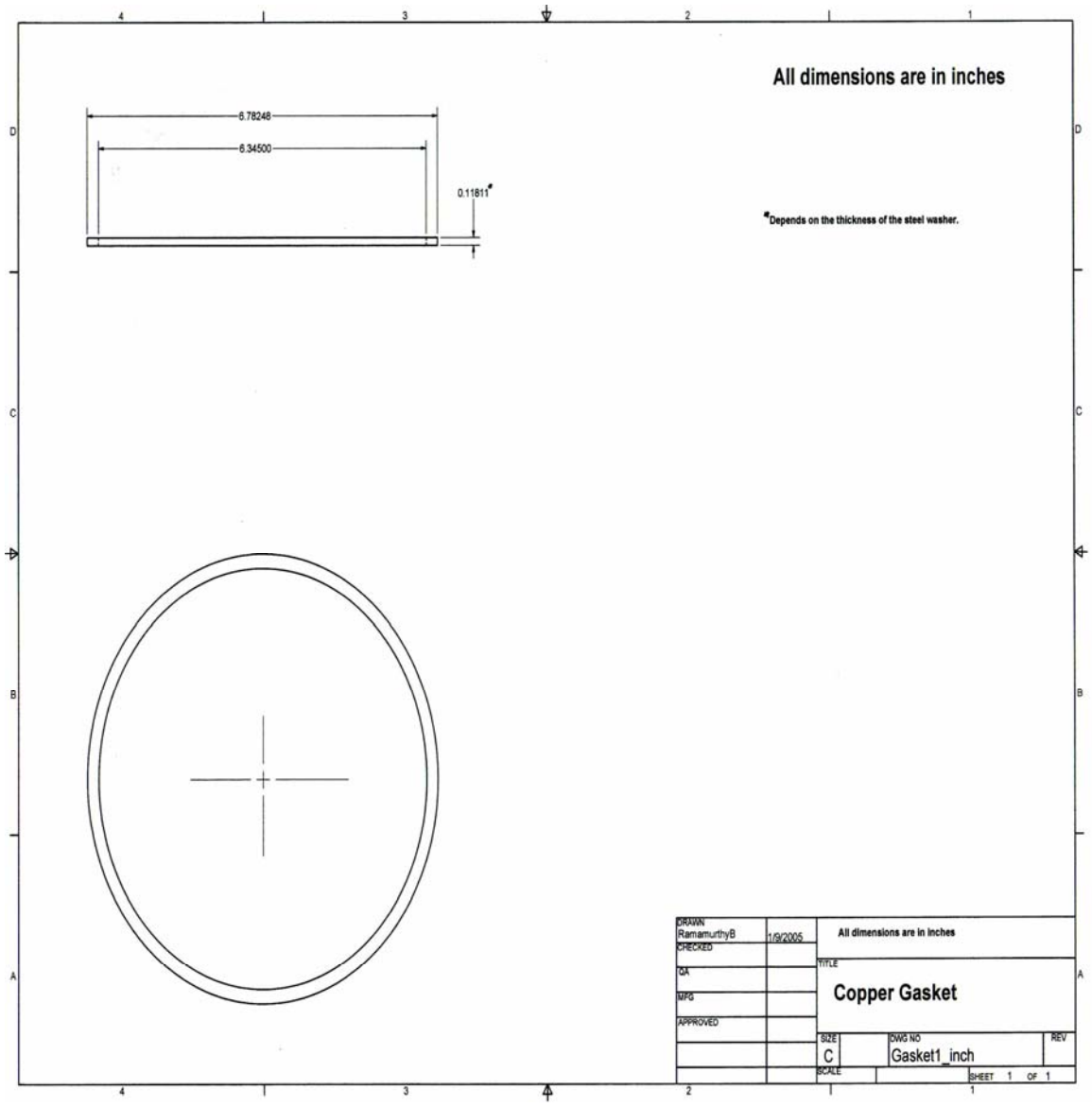


**Figure A-8 Copper Gasket**

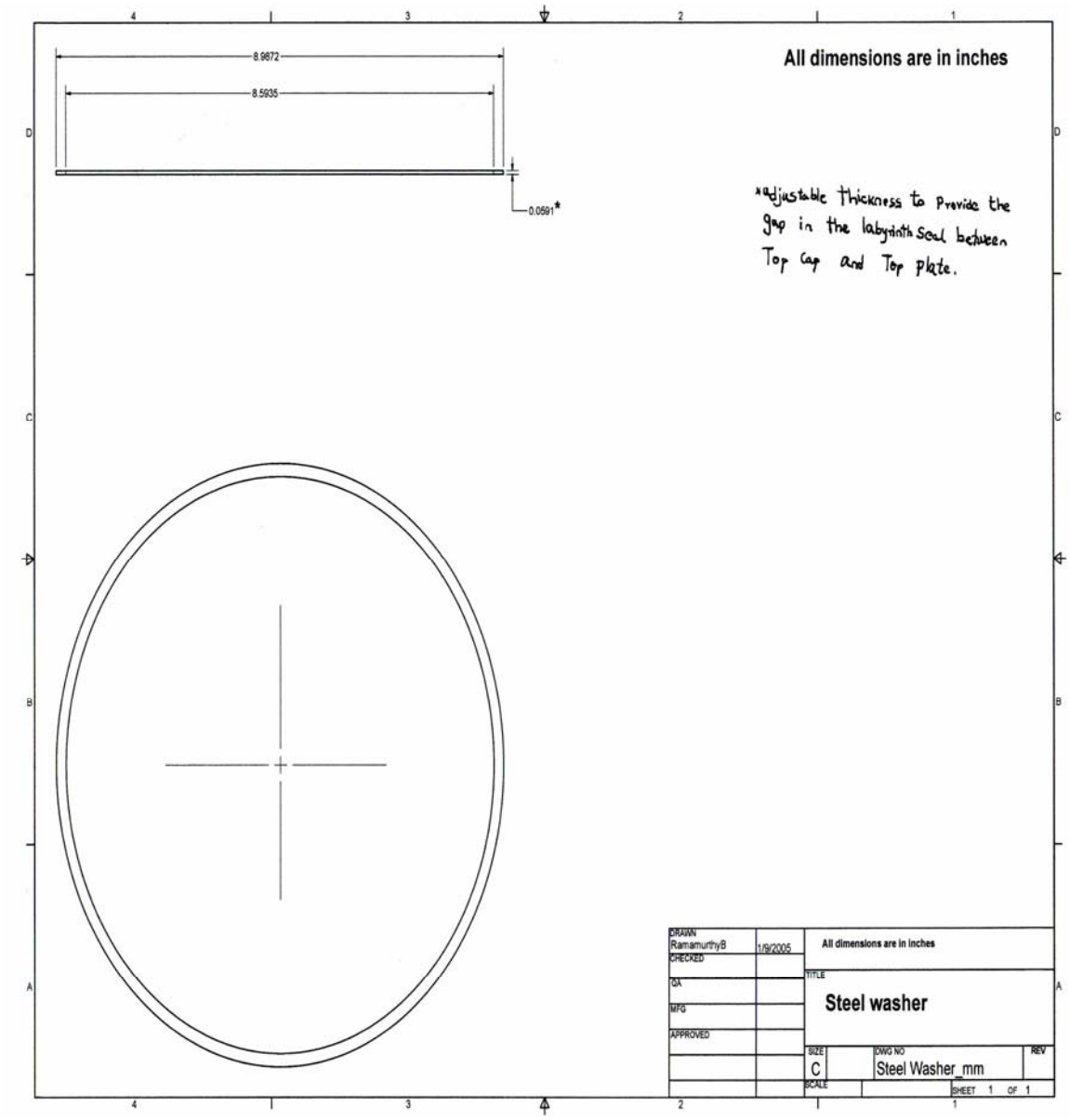


**Figure A-9 Stainless Steel Washer**

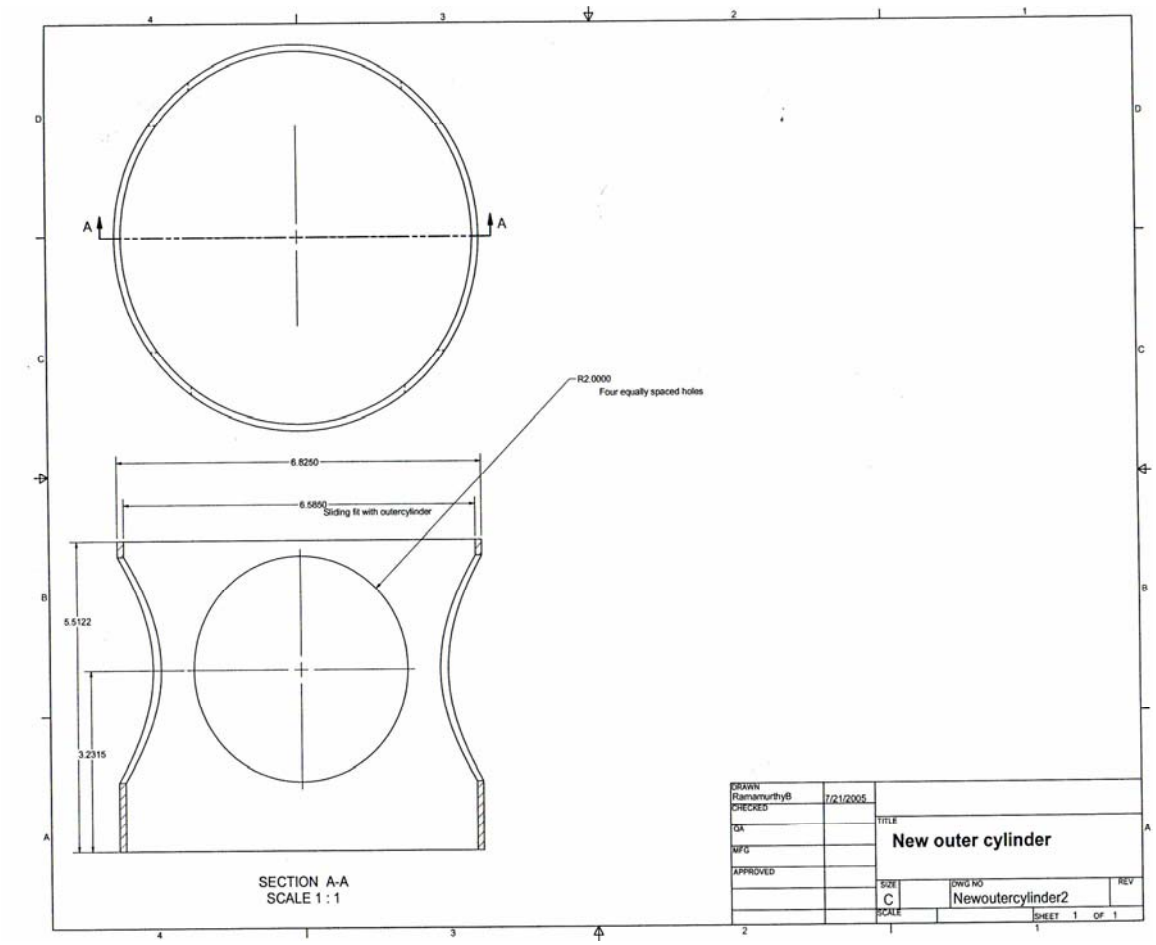


**Figure A-10 Sectional View of Valve Housing**

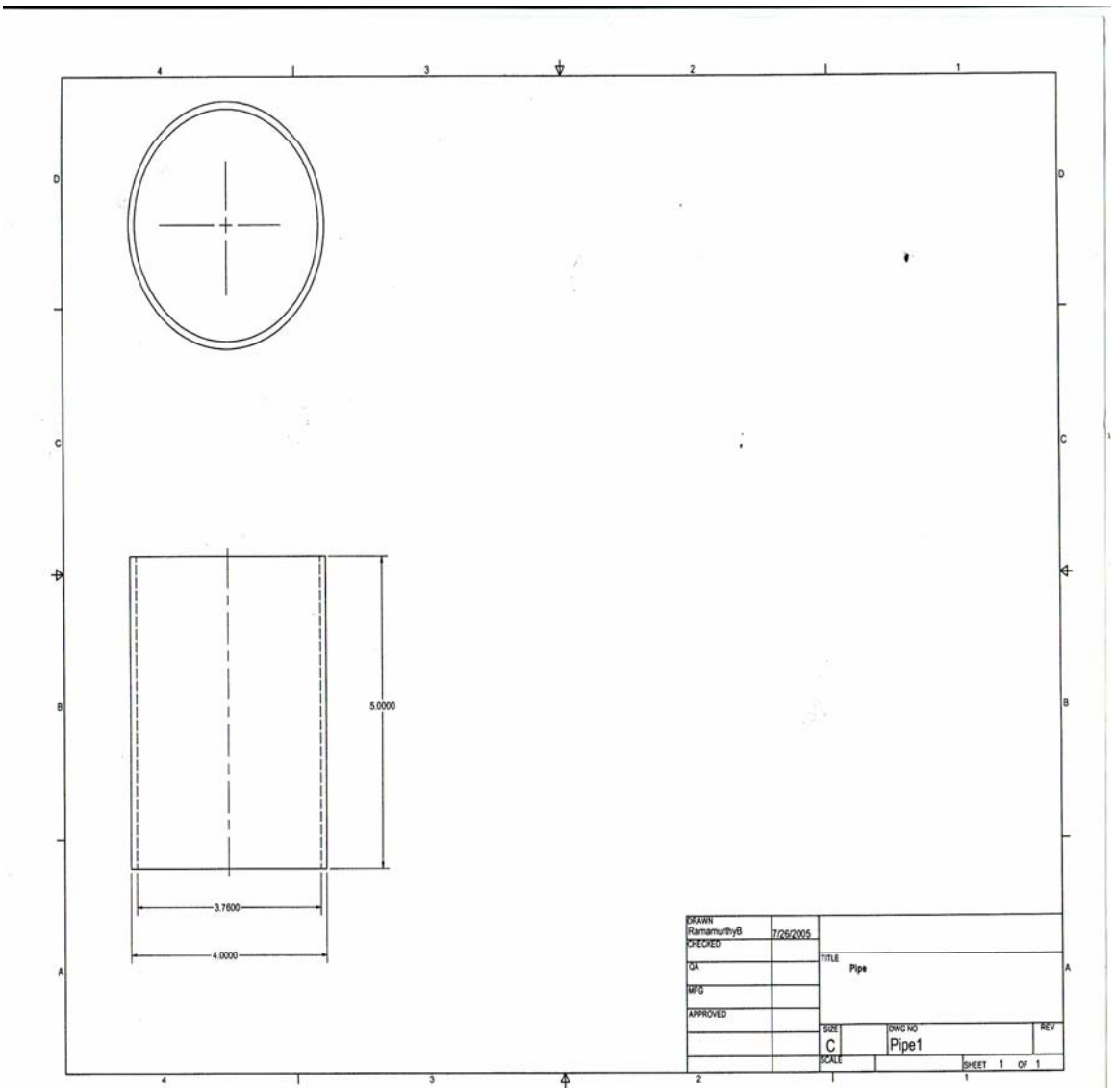


**Figure A-11 Exhaust Pipe**

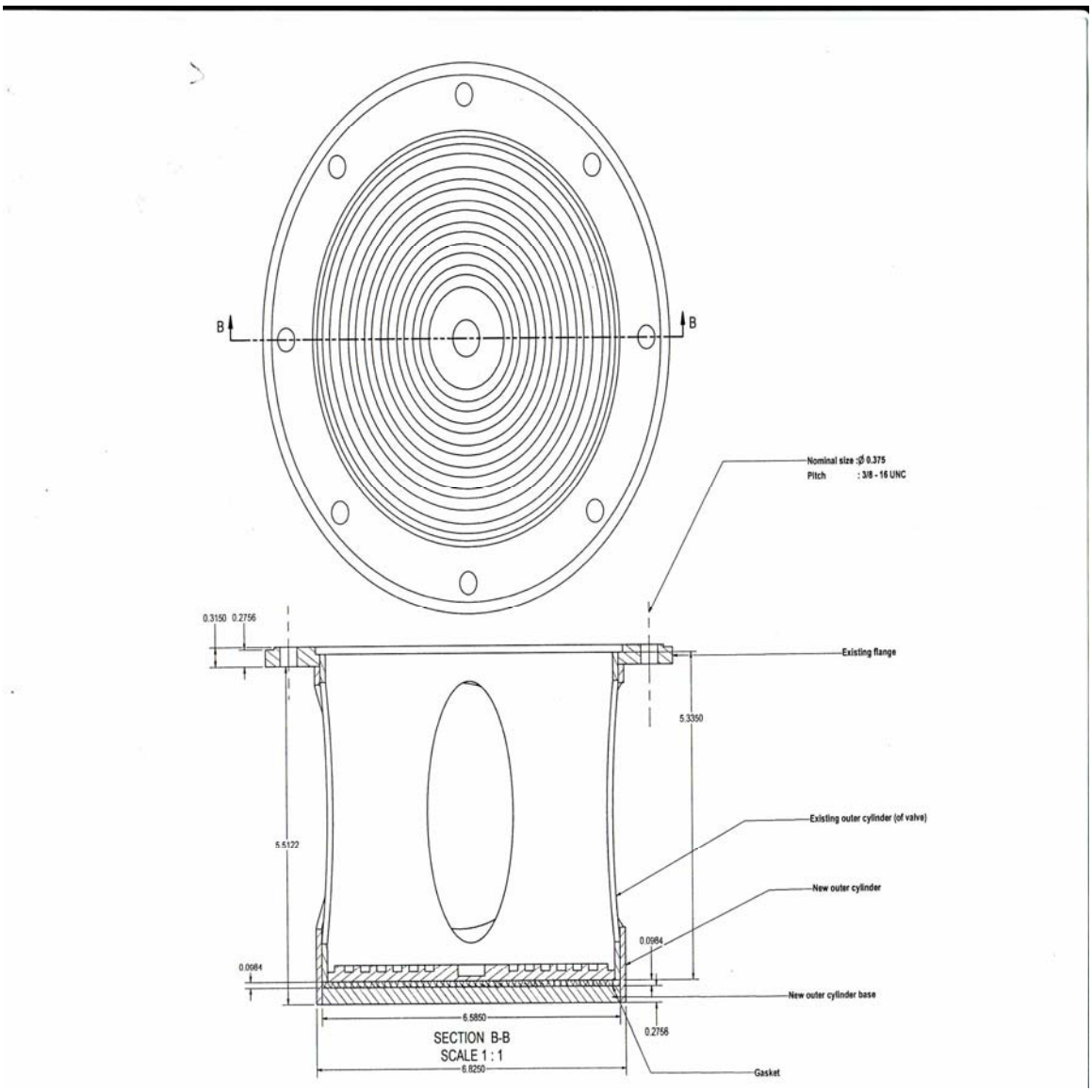


**Figure A-12 Sectional View of the Assembly with Valve Housing**

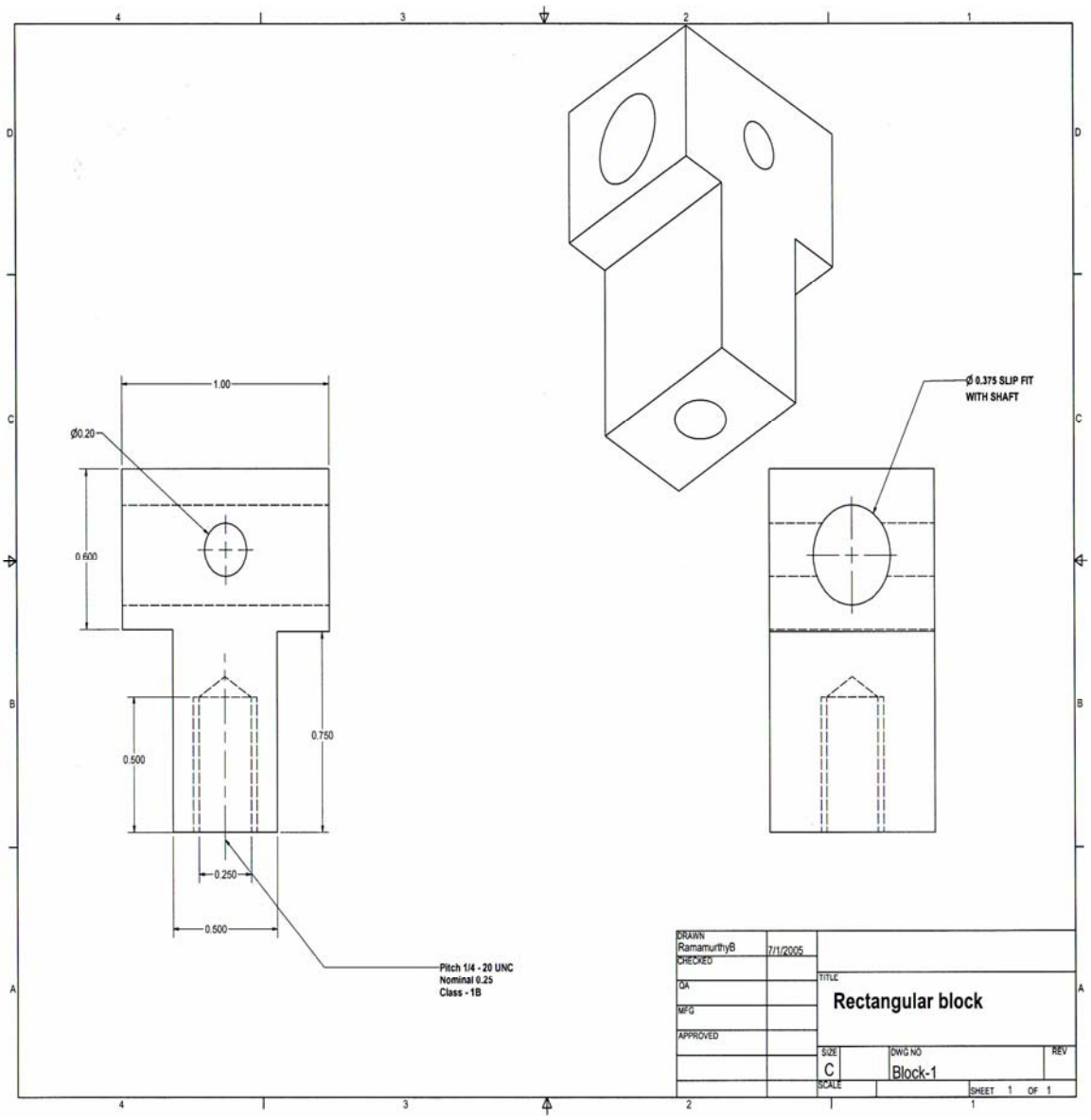


**Figure A-13 Rectangular Block in 2D and 3D**

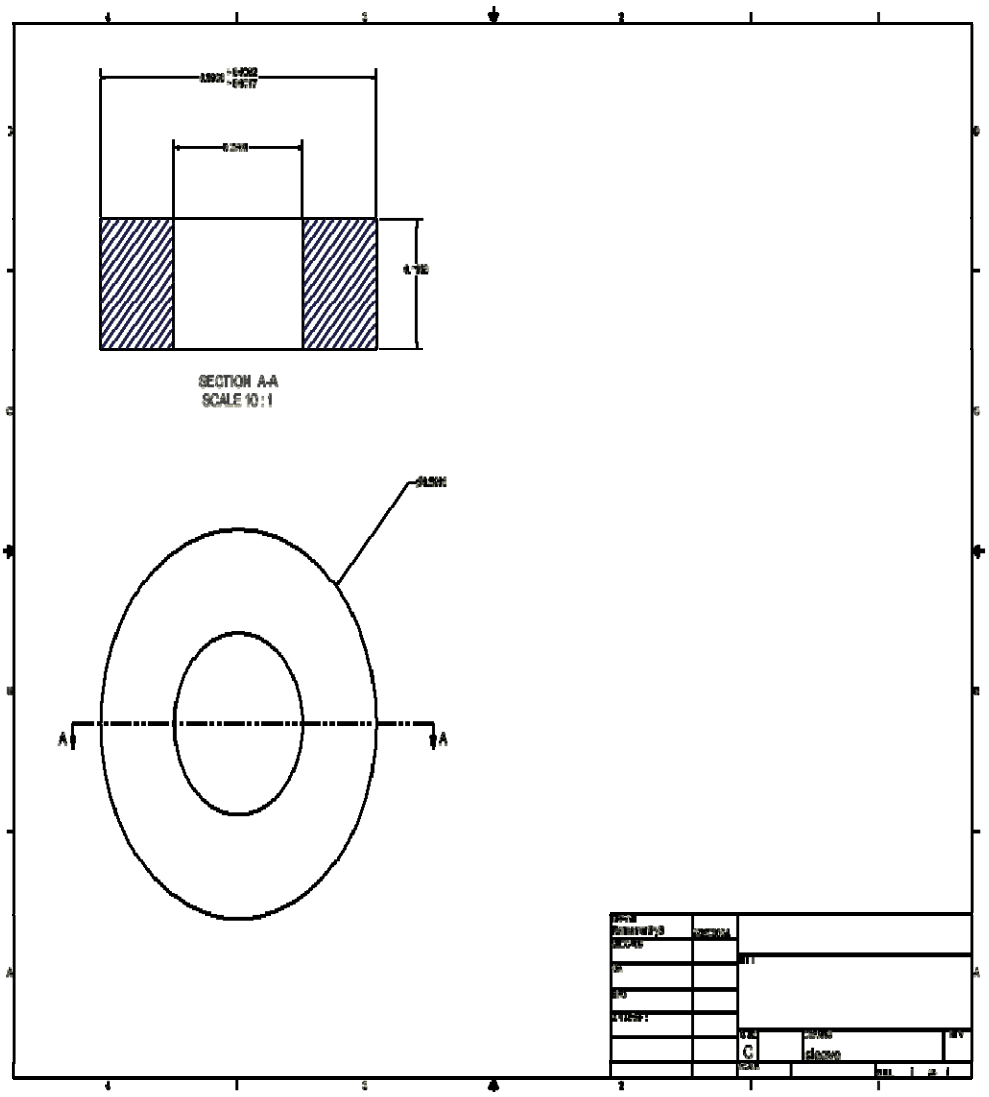


**Figure A-14 Sleeve**

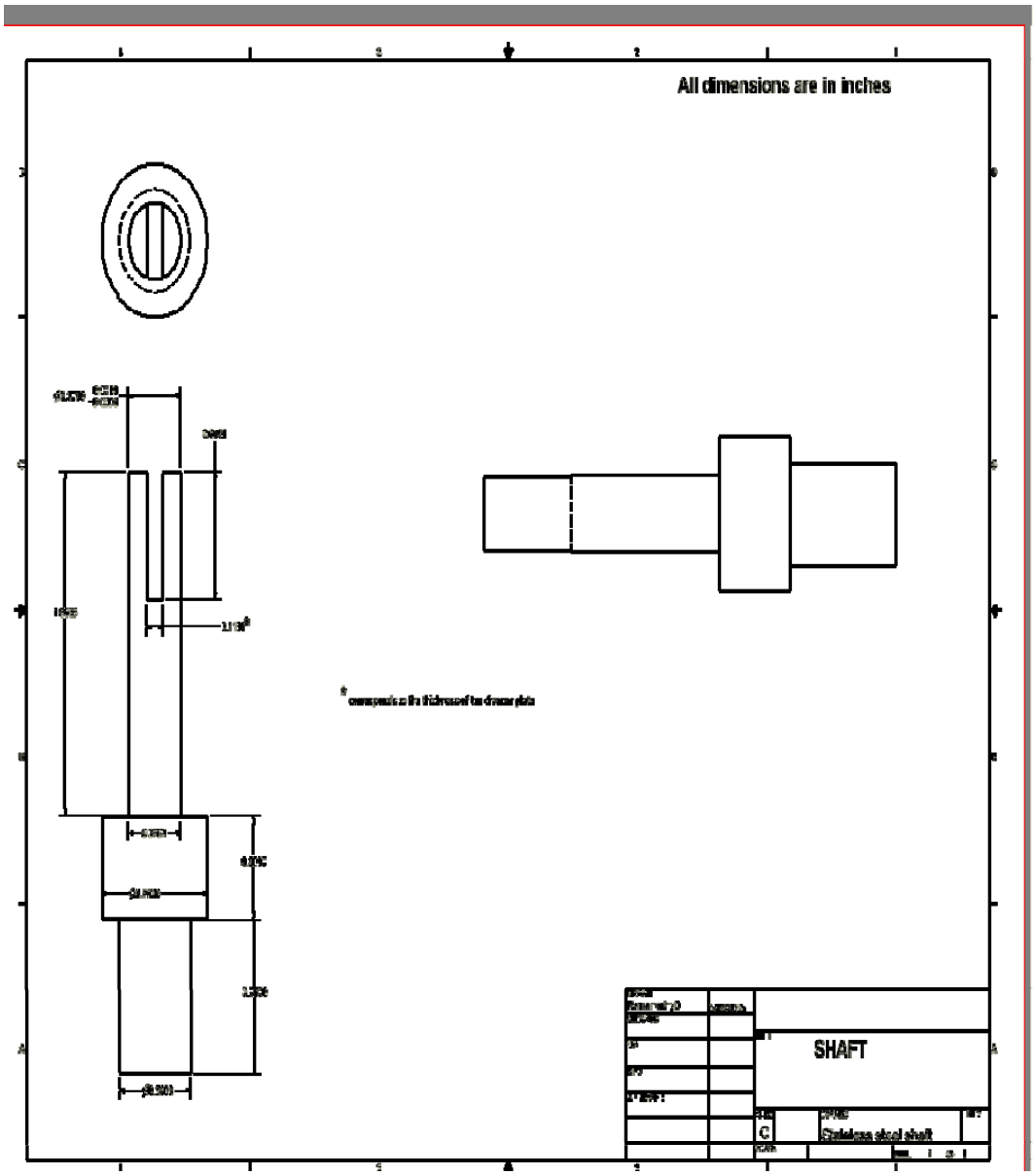


**Figure A-15 Stainless Steel Shaft in 2D**

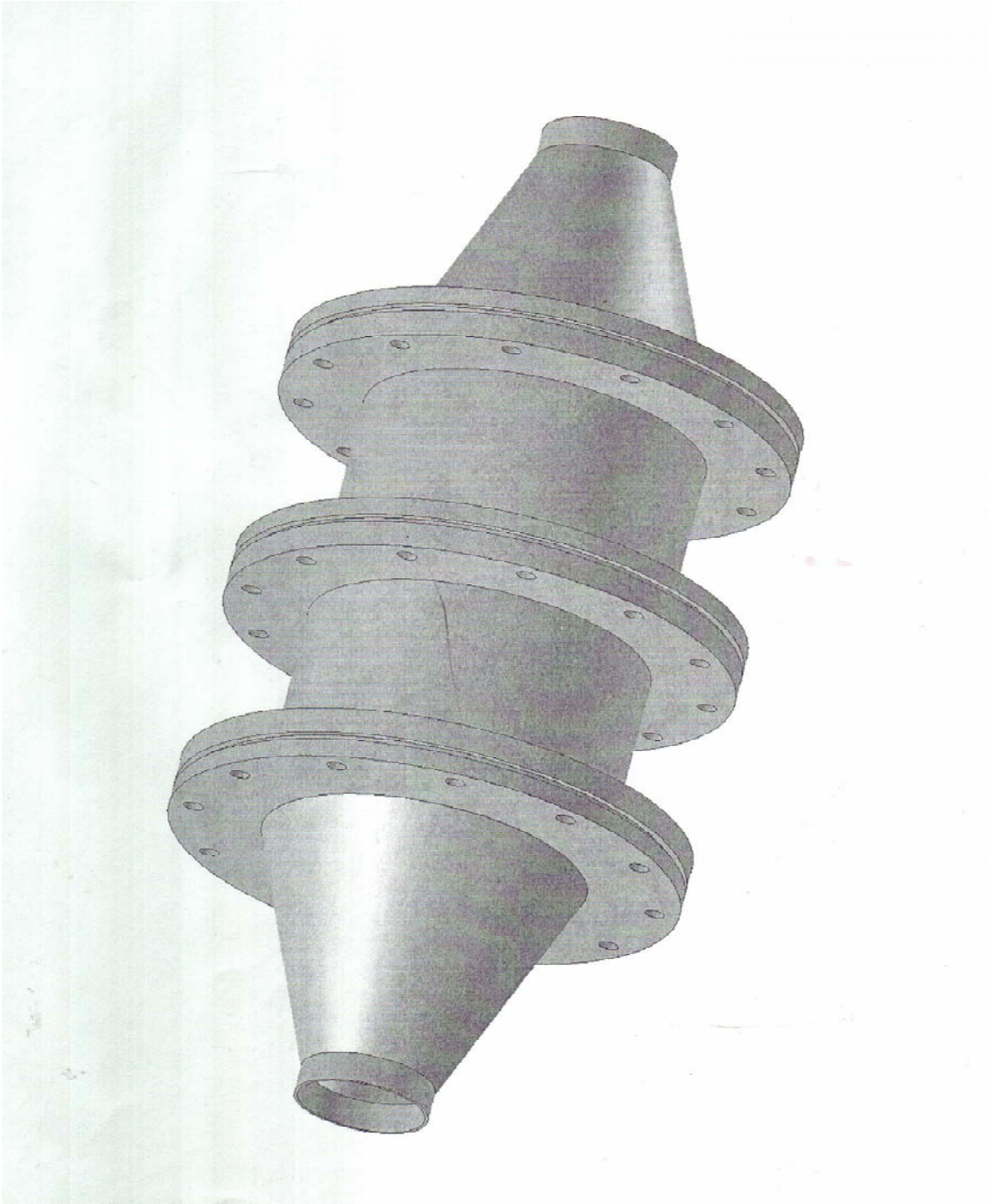

**Figure A -16 Catalyst System Assembly**

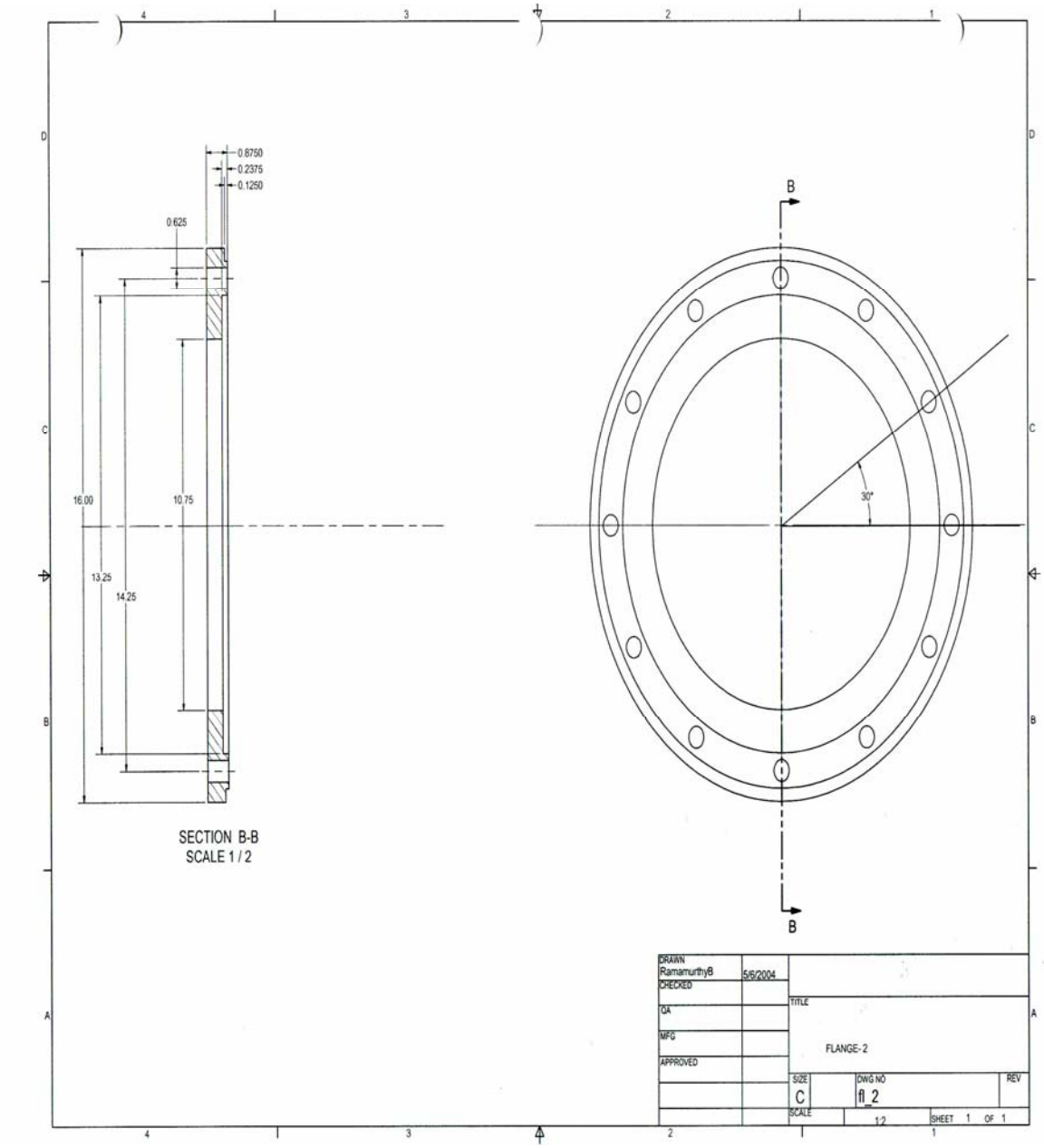


**Figure A-17 Sectional View of Male Flange**

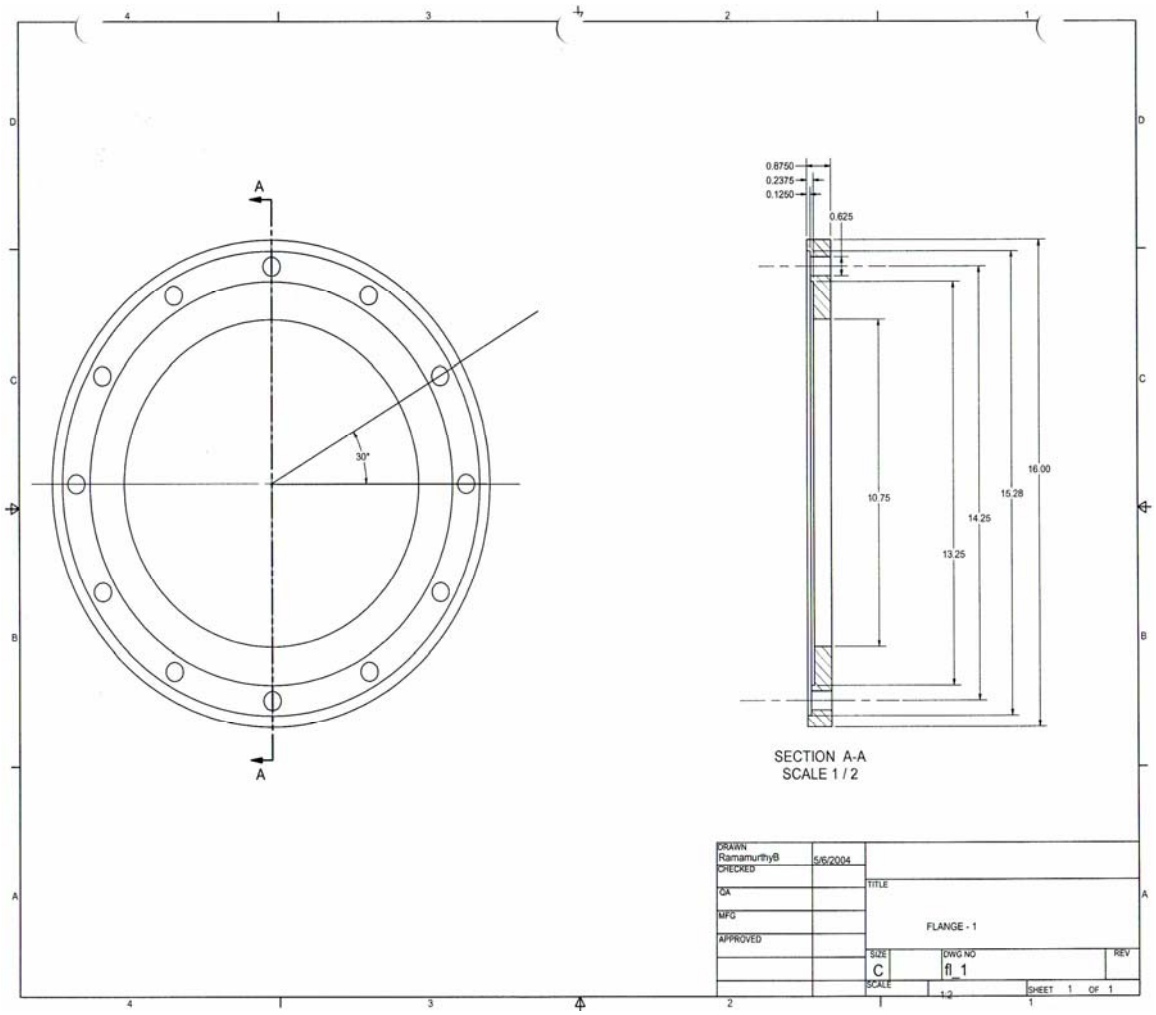


**Figure A-18 Sectional View of Female Flange**

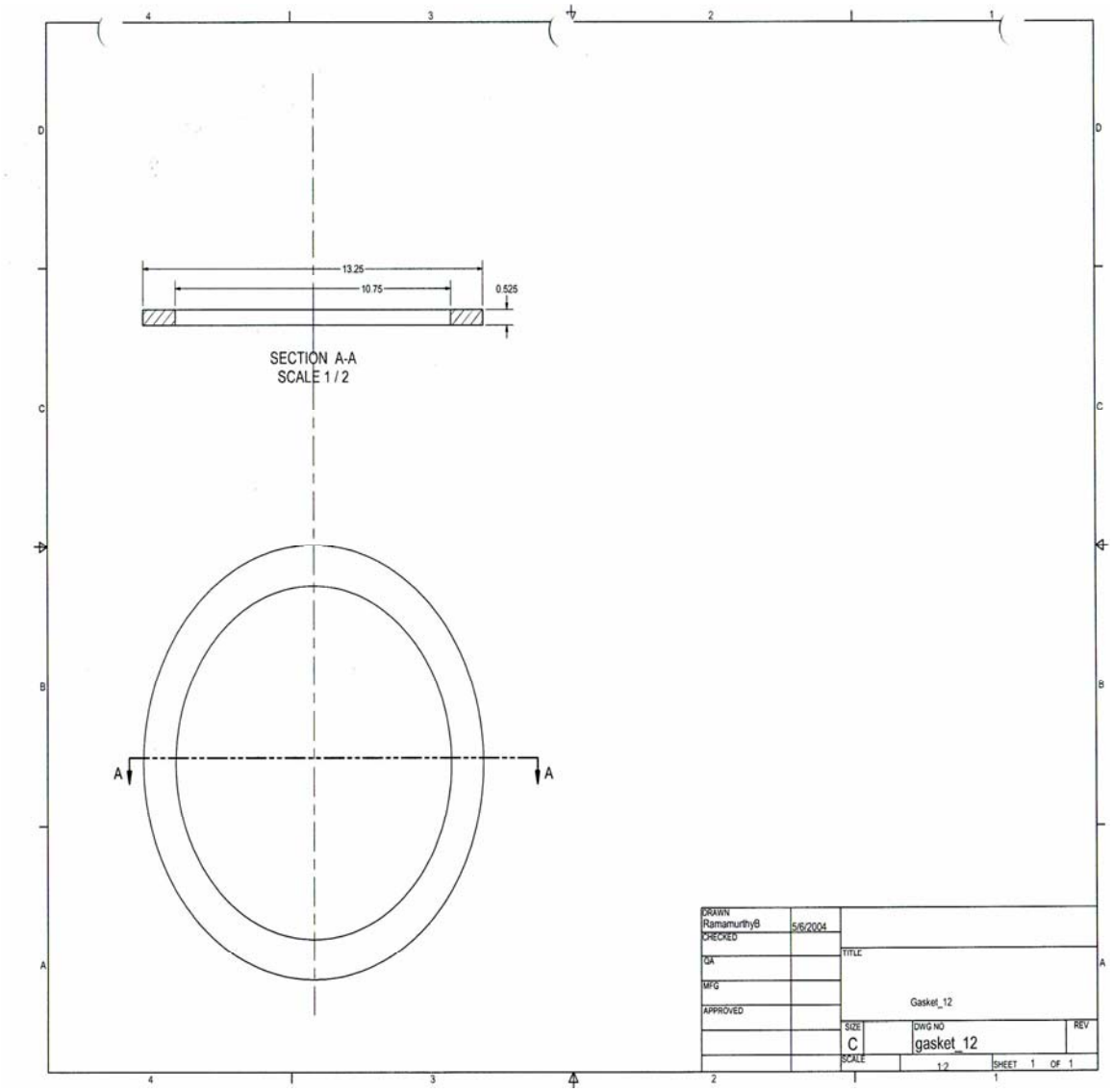


**Figure A-19 Sectional View of Stainless Steel Gasket**

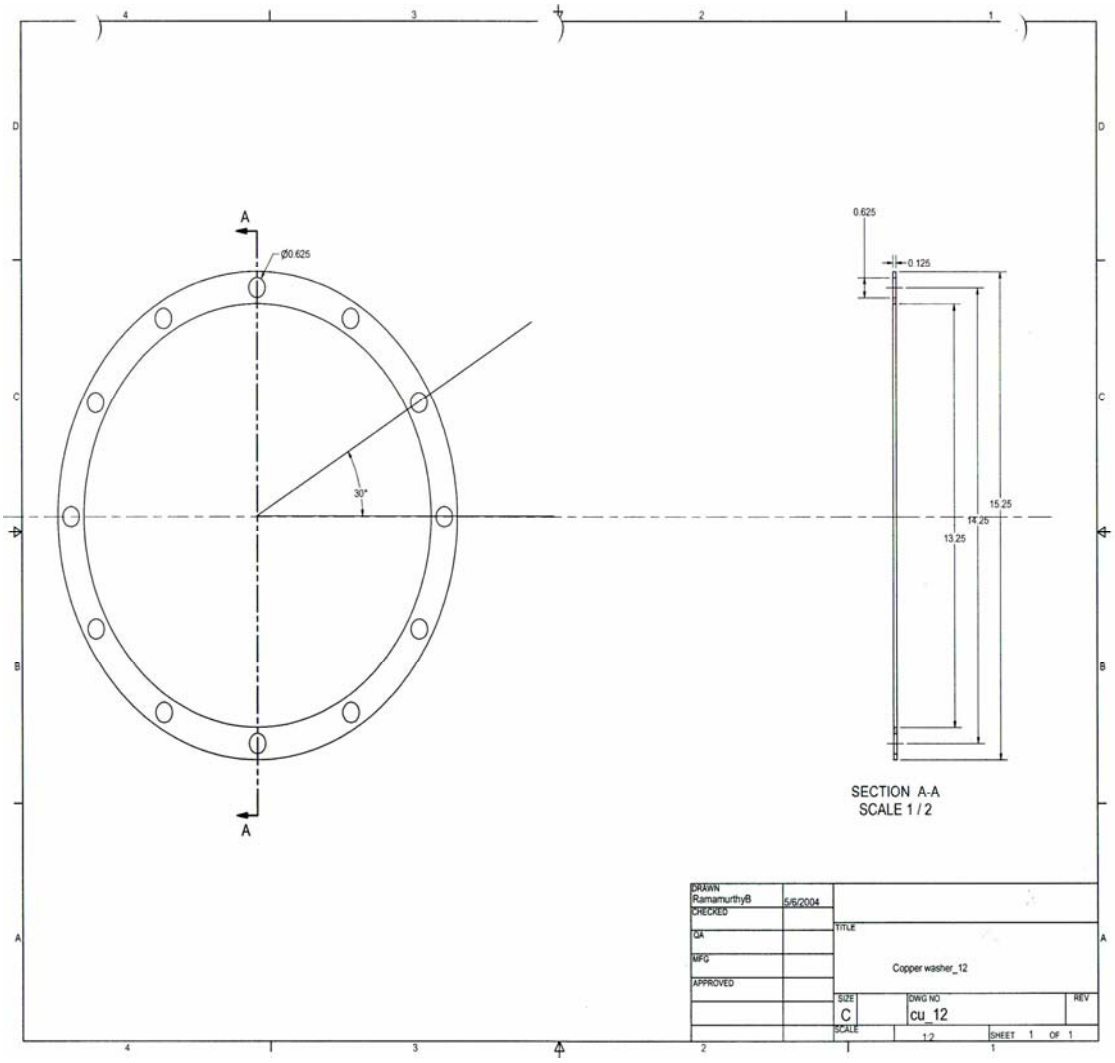


**Figure A-20 Sectional View of Copper Gasket**

# VITA

Balaji Ramamurthy was born in Madras, India, on February 15, 1980. After completing high school in 1997, he started doing his undergraduate in Mechanical Engineering, where he was introduced to the real math and science world. He gained a considerable amount of knowledge in his undergraduate program and completed his Bachelors in 2001. After graduating, he began working in an industry and got good practical exposure in Mechanical Engineering field. Then, he started pursuing his higher studies, Master of Science, in UT in Spring 2004. Since its inception he had been actively involved in his research under the guidance of Dr. David Irick and completed the requirements for the Master of Science in December 2005.